DESIGN OF ELECTROLYTIC DEWATERING SYSTEMS FOR PHOSPHATIC CLAY SUSPENSIONS

By

JAMES PATRICK MCKINNEY

A DISSERTATION PRESENTED TO THE GRADUATE SCHOOL
OF THE UNIVERSITY OF FLORIDA IN PARTIAL FULFILLMENT
OF THE REQUIREMENTS FOR THE DEGREE OF
DOCTOR OF PHILOSOPHY

UNIVERSITY OF FLORIDA

2010

To my parents, sister, and grandparents

ACKNOWLEDGMENTS

I thank my advisor, Professor Mark Orazem, for his support and guidance. He has shown me not only how to improve my abilities in research, but how to improve my abilities as a person. I would like to thank Charlotte Brittain of Mosaic Fertilizer LLC for her involvement in sponsoring this project. I appreciate Mrs. Brittain's willingness to be of help anytime that I had questions or needed assistance. She not only benefitted the project, but also benefitted my understanding in how this project fit into the scope of the phosphate mining business. I would also like to thank Charles Guan, Rick Grove, and Brandon Russell of Mosaic Fertilizer LLC for their support. I thank Professor Guerry McClellan, Professor David Bloomquist, and Professor Hassan El-Shall for their advisement on issues related to clays and clay dewatering. I would like to thank all of the students who have worked in Professor Orazem's research group during my time at the University of Florida. This includes Nelliann Perez-Garcia, Mei-Wen Huang, Michael Matlock, Sunil Roy, Shaoling Wu, Bryan Hirschorn, Erin Patrick, Daniel Rood, Rui Kong, and Rodney Del Rio. I would also like to thank the staff members in the Department of Chemical Engineering. This includes Shirley Kelly, Deborah Sandoval, Dennis Vince, Jim Hinnant, and Sean Poole. Finally, I would like to thank my parents, my sister, and my grandparents for their love and support throughout my life. I appreciate them instilling the value of education in me at an early age.

TABLE OF CONTENTS

LIST OF TABLES

LIST OF FIGURES

LIST OF SYMBOLS

Roman

A_c	cross-sectional area of bench-top experimental cell, cm^2
b_{aa}	kinetic parameter defined in equation (7–10), V^{-1}
b_{ac}	kinetic parameter defined in equation (7–11), V^{-1}
b_{ca}	kinetic parameter defined in equation (7–12), V^{-1}
b_{cc}	kinetic parameter defined in equation (7–13), V^{-1}
c_i	concentration of species i, mol/cm^3
D_i	diffusion coefficient of species i, cm^2/s
d	distance between electrodes, cm
E	electric field, V/cm
E_{Fe}	equilibrium potential for oxidation of iron, V
E_{H_2}	equilibrium potential for hydrogen evolution, V
E_{O_2}	equilibrium potential for oxygen reduction, V
E_{req}	energy requirement for removal of water, Wh/kg of water removed
F	Faraday's constant, $96,487$ C/equiv
I	current, A
i	current density, mA/cm^2
i_{lim,O_2}	mass transfer limiting current density for oxygen reduction, mA/cm^2
N_i	flux of species i, mol/cm^{2}s
q	charge, C/cm^2
R	resistance, Ωcm^2 or Ω ($1\Omega = 1\text{Vs/C}$)
R	universal gas constant, 8.314 J/molK
R_e	electrolyte or Ohmic resistance, Ω or Ωcm^2
R_i	rate of homogeneous production of species i, mol/cm^{3}s
T	temperature, K
t	experimental operating time, h
u_i	mobility of species i, related to diffusion coefficient by equation (8–4)
V	potential, V
v	velocity, cm/s

w_c solids content of the slurry, wt%

$w_{\max}$ maximum solids content of the slurry, wt%

z_i charge associated with species i

Greek

α symmetry factor used in electrode kinetics, dimensionless

β Tafel slope, V/decade of current

δ thickness, cm

ϵ permittivity, F/cm

ε_0 permittivity of vacuum, 8.8542×10^{-14} F/cm

ζ zeta potential, mV

η_a anodic overpotential, V

η_c cathodic overpotential, V

κ conductivity, S/cm

λ Debye length, nm

μ fluid viscosity, g/cms

ρ electrical resistivity, Ωcm^2

ρ_e electrolyte resistivity, Ωcm

Φ potential, V

Δw_c change in solids content of the slurry, wt%

Subscripts

i pertaining to chemical species i

Z_j pertaining to the imaginary part of the impedance

Z_r pertaining to the real part of the impedance

Abstract of Dissertation Presented to the Graduate School
of the University of Florida in Partial Fulfillment of the
Requirements for the Degree of Doctor of Philosophy

DESIGN OF ELECTROLYTIC DEWATERING SYSTEMS FOR PHOSPHATIC CLAY SUSPENSIONS

By

James Patrick McKinney

May 2010

Chair: Mark E. Orazem
Major: Chemical Engineering

Phosphatic clays arise as a waste product of the Florida phosphate mining industry. The clays exist initially as a 2-6 solids weight percent slurry which is pumped to large impoundment areas for natural settling. The clay settling process takes as long as 25 years to reach a value of 40% solids. The clay settling areas currently cover an area of over 100 square miles in Central Florida, representing 40 percent of the land that has been mined.

The Florida Institute of Phosphate Research (FIPR) has supported bench- and pilot-scale studies to determine the technical and economic feasibility of a variety of processes to speed the dewatering of clays associated with phosphate mining. The approaches considered included using a freeze-thaw cycle to remove water, adding sand layers to enhance drainage, and adding flocculants to enhance settling. While flocculants are used commercially, the other techniques have not been permanently implemented on a large scale, and settling to an acceptable solids content still requires as much as 25 years.

Application of an electric field provides an alternative approach for accelerating the removal of water from clay. In this concept, direct electrical current is applied to induce movement of either clay particles or water. In dilute suspensions, the electric field induces the movement of clay particles suspended in water which is known as electrophoresis. Upon formation of a solid matrix, the electric field further induces the movement of water in a process known as electro-osmosis.

The objective of this work was to use small-scale electrokinetic experiments to develop parameters that can be used for large-scale design. A bench-top Plexiglas cell was built to perform the experiments. Clay slurry samples were obtained from a phosphate mine located

in Central Florida. A set of experimental results were used to calculate scaling parameters to aid in predicting the solids content as a function of operating time and the electric field applied. This was done by scaling the change in solids content by the applied electric field. A linear relationship was found at short times while at longer times a maximum solids weight percent was reached as a function of the electric field. A constitutive relationship was established which relates the increase in solids content to time and the applied electric field.

A mathematical model previously developed at the University of Florida was used to model and evaluate varying electrode configurations in a one-square-mile clay settling area. The electrical current generated from the applied voltage was calculated to project electrical power and energy requirements for such a process. For a given electrode configuration, the associated electric field can also be calculated. The experimental work suggests a relationship between the solids content of the clays with the electric field. The model results can then be used to identify regions where the electric field is nonuniform, which indicates regions where the clays would have a nonuniform solids weight percent. Therefore, the model allows selection of an optimal electrode configuration based on electrical power requirements as well as the most uniform drying of the clays.

CHAPTER 1
INTRODUCTION

Electrokinetic dewatering takes place through interaction between fluid flow, electrical current, and charge adsorbed on the clay particles.[5] In order to apply an electric field there must be at least two electrodes immersed into the clay slurry or electrolyte. One electrode functions as the positively charged anode where oxidation reactions occur and the other functions as the negatively charged cathode where cathodic (or reduction) reactions occur. At the anode, the electrochemical reactions include oxygen evolution

$$2H_2O \rightarrow O_2 + 4H^+ + 4e^- \tag{1–1}$$

which creates an acidic environment near the electrode. A second possible reaction involves corrosion of the electrode

$$M \rightarrow M^{n+} + ne^- \tag{1–2}$$

At the cathode,

$$H_2O + e^- \rightarrow \frac{1}{2}H_2 + OH^- \tag{1–3}$$

creating a local basic environment. The water is driven from the anode to the cathode, creating a tendency to dry out the region close to the anode. Therefore, the water travels in the same direction as conventional current.[6] The solution pH is expected to increase rapidly to approximately 11 or 12 at the cathode and hydrogen will be generated, as shown by reaction (1–3). Cations are driven to the cathode by the electric potential gradient and can be reduced (the inverse of reaction (1–1)). A pH gradient will be generated across the soil as an overall result of the electrode reactions.

Electrophoresis and electro-osmosis methods of dewatering phosphate clays have been explored since the 1940s.[7–10] Although the basic technology was considered to have promise it was not considered commercially feasible. Significant progress has since been made in our understanding of the underlying electrokinetic and electro-osmotic processes and in the practical implementation of these techniques. For example, recently, electrokinetic methods have been demonstrated for dewatering of soil,[11] mine tailings,[4,12] sludge,[13] and clay,[14–16] including Florida phosphate clay.[17] The literature suggests electrokinetic methods can significantly decrease the

time required to dewater clay. Therefore, further research in this area is warranted due to the advances that have been made in the last two decades.

This work is presented in nine chapters. The background of the phosphate industry is discussed in Chapter 2. The phosphate production requirements which drive the phosphate industry are summarized. The locations of phosphate mines in the state of Florida are presented and the mineralogy of the phosphate reserves are discussed. The mining process and production of phosphate are described as well as the waste clay settling areas that exist as a result of phosphate production.

This work is motivated due to settling and consolidation issues that arise from clay settling areas; therefore, Chapter 3 provides detail on the characteristics of clays which includes their molecular structures. These features are used to explain why clays have such poor settling characteristics. However, discussion also involves how these features may aid settling or consolidation in the presence of an electric field.

Electrochemical engineering and electrokinetic phenomena are introduced in Chapter 4. The fundamentals of electrokinetic phenomena are introduced to provide a framework for how separations of clay suspensions occur. Polarization curves and impedance spectroscopy are introduced as techniques used to characterize electrochemical cells. Experimental results in the literature are presented in Chapter 5. A qualitative assessment of the literature was performed which discusses the feasibility of water removal from clays. Also discussed are items absent within the literature that provide the basis for the contributions of this work.

The experimental approach to this work is described in Chapter 6. Ex-situ studies were performed on the clay suspensions which were representative of samples used in bench-top experiments presented within this work. Particle size studies were performed to characterize the size distribution of the particles in suspension. X-Ray diffraction was performed to identify the types of clays present in the clay suspensions. Such analysis was warranted as the response to electrokinetics can vary due to the different surface properties of one clay mineral to another. Zeta potential measurements were also performed to help quantify the amount of charge on the clay particles in suspension. This chapter also introduces the bench-top apparatus (or electrochemical cell) and the instrumentation used to control the apparatus.

The bench-top experiments that were performed using an electric field to remove water from clay slurries are introduced in Chapter 7. The experimental results are given and discussed within this chapter. Constitutive relationships were developed, which relate the change in clay solids weight percent as a function of both the operating time and the electric field. Electrochemical techniques such as impedance spectroscopy and polarization curves were also implemented to characterize further the experimental work.

The simulation work performed to assess different electrode configurations in a simulated one-square-mile clay settling area is presented in Chapter 8. Relationships found in the experimental work were used to make assumptions regarding the development and results of the simulations. These relationships and assumptions supported the projections made for electric power requirements as well as the energy requirements of different electrode configurations. The simulations were performed using CP_3D, a mathematical model developed at the University of Florida.

The conclusions made from the experimental and simulation work are reviewed in Chapter 9. This discussion is followed by proposed work for the next steps of this project. Possible dewatering scale-up designs for future implementation are proposed and a new bench-top experimental design is introduced.

CHAPTER 2
THE PHOSPHATE INDUSTRY

The phosphate industry was started in the mid to late 19th century.[18] The industry was developed due to phosphate being invaluable as a key ingredient in fertilizers for food producing crops. It also contributes to the production of other items such as soft drinks, light bulbs, vitamins, shaving cream, tooth paste, and it can be used as a feed additive for livestock. However, in the state of Florida, about 90% of the phosphate mined is used as fertilizer for food producing crops.

Phosphate ore deposits are found all over the world in countries such as the United States, China, Morocco and Russia.[19] Phosphate is also mined in Canada, Australia, and Jordan. Overall, significant phosphate deposits exist on five continents and there are over 30 countries that mine phosphate. However, about 70% of the world's total production comes from the United States, Morocco and Russia.[20] In the state of Florida, the phosphate industry is the third largest industry behind tourism and agriculture. In 1982, it was reported that the phosphate industry injected 1.5 billion dollars into the Florida state economy annually.[1] In Central Florida alone, there are currently 4,000 employees working in the phosphate industry.

Phosphorus is considered as one of the three most essential plant nutrients.[21] It is a nutrient that is supplied through the soil along with nitrogen and potassium. Phosphate is the main source of phosphorus for organic fertilizers and it is a non-renewable resource.[1] It is required for all living cells in plants and animals as it allows cells to store energy from sunlight and food.[19] Plant growth is enhanced by soils that have been treated with phosphate fertilizers.

Once the phosphate rock has been mined and extracted through beneficiation, it is ground into a fine grain size and mixed with sulfuric acid. This process produces phosphoric acid and calcium sulfate. The calcium sulfate, also known as gypsum, can be removed through filtration. The resulting phosphoric acid is then reacted with ammonia to produce diammonium phosphate and monoammonium phosphate. Triple superphosphate is also created by adding phosphoric acid with the phosphate rock. These three products are combined together in most fertilizers and they exist as water-soluble granules to allow for absorption by the soil and plants. The conversion of insoluble phosphate rock to soluble phosphate fertilizer was first commercially

achieved in England in 1842.[22] In Germany, triple superphosphate was first commercially produced in 1870; however, it did not become an important fertilizer ingredient until 1950.[22]

2.1 Phosphate Mineralogy

Worldwide it is estimated that there are between 15 and 70 billion metric tons of phosphate reserves.[20] In the southeastern United States, there are phosphate reserves that exist in North Carolina, South Carolina, Georgia and as previously discussed, Florida. The deposits in Florida have been the most productive as one billion tons of phosphate were produced in the state of Florida from 1888 through 1990.[2] In 1982 it was reported that reserves in the state of Florida produced 80% of the phosphate used in the United States and 35 percent worldwide.[1] Ten years later, in 1992, another report credited the state of Florida with producing 85% of the phosphate used in the United States and 33% worldwide.[23] It appears that these percentages have been maintained through present day. However, the research director of the Florida Institute of Phosphate Research (FIPR) was quoted as predicting that the phosphate reserves will be depleted in the state of Florida by the year 2040.[19]

The phosphate deposits in Florida are dominated by the minerals carbonate-fluorapatite (also known as apatite or francolite), quartz, dolomite, and different clay minerals.[2] According to Bloomquist,[1] one sample taken from a specific reserve in Florida also included minerals such as wavelite, limonite and feldspar. Carbonate-fluorapatite is considered as the primary phosphate bearing mineral. Dolomite is calcium magnesium carbonate or can be written as $\mathrm{CaMg(CO_3)_2}$. Quartz has the molecular formula $\mathrm{SiO_2}$ and it is the second most abundant mineral in the earth's crust. The most abundant mineral in the earth's crust is feldspar, which is made up of a complex group of silicates. The mineral wavelite includes the element Phosphorus, while the mineral limonite does not.

The layout and locations of the Florida phosphate reserves are presented in Figures 2-1 and 2-2. Both figures illustrate the entire state of Florida, but each focuses on the region in Central Florida which represents the location where most of the phosphate mining occurs. A more specific depiction of phosphate reserves is presented in Figure 2-1 while additional regional descriptions in the state of Florida are identified in Figure 2-2 as well as specific mining locations.

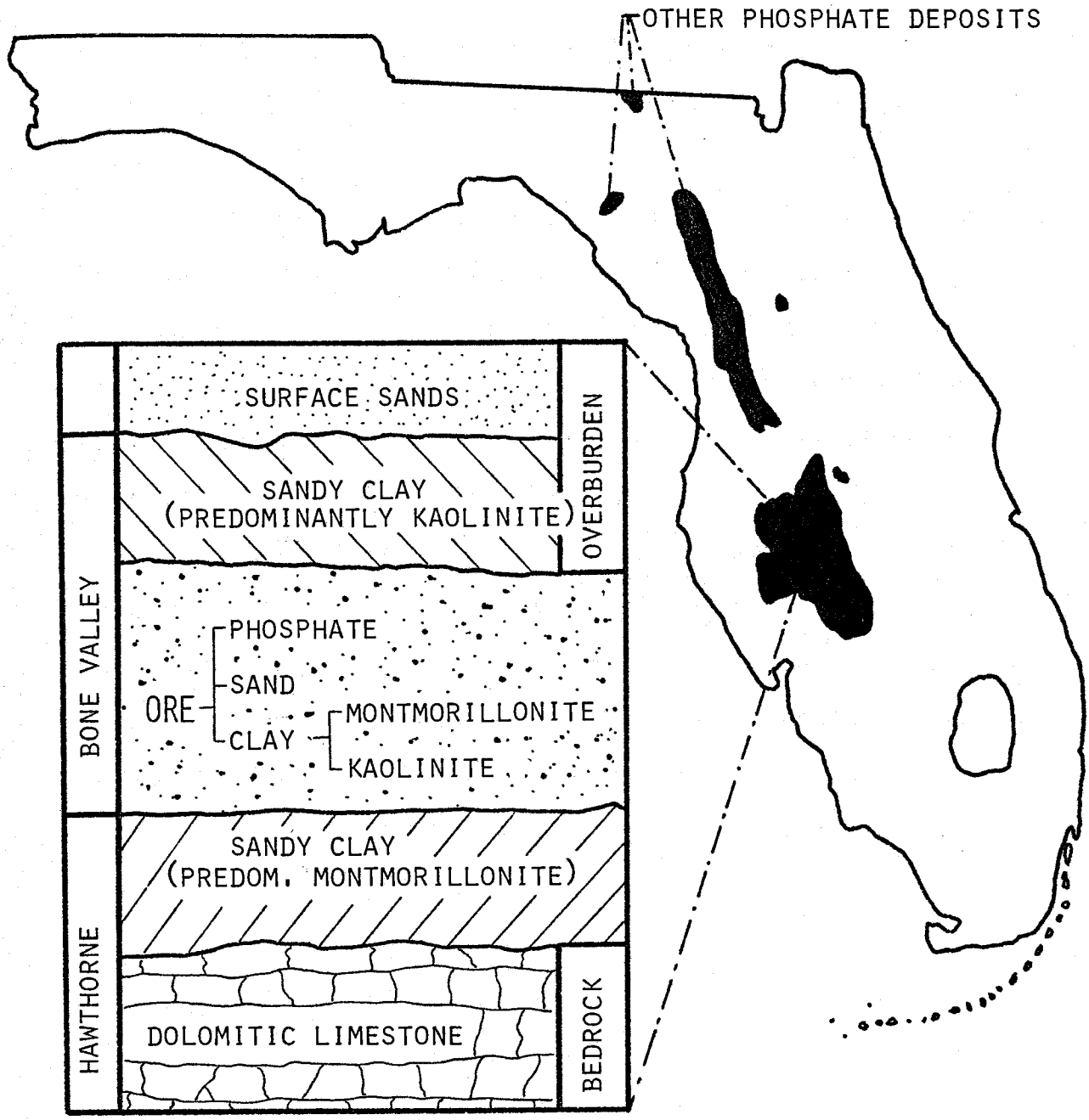

Figure 2-1. Regions (taken from Bloomquist[1]) of Florida phosphate deposits are identified. The inset presents a general view of the makeup of the Central Florida deposits with varying depth.

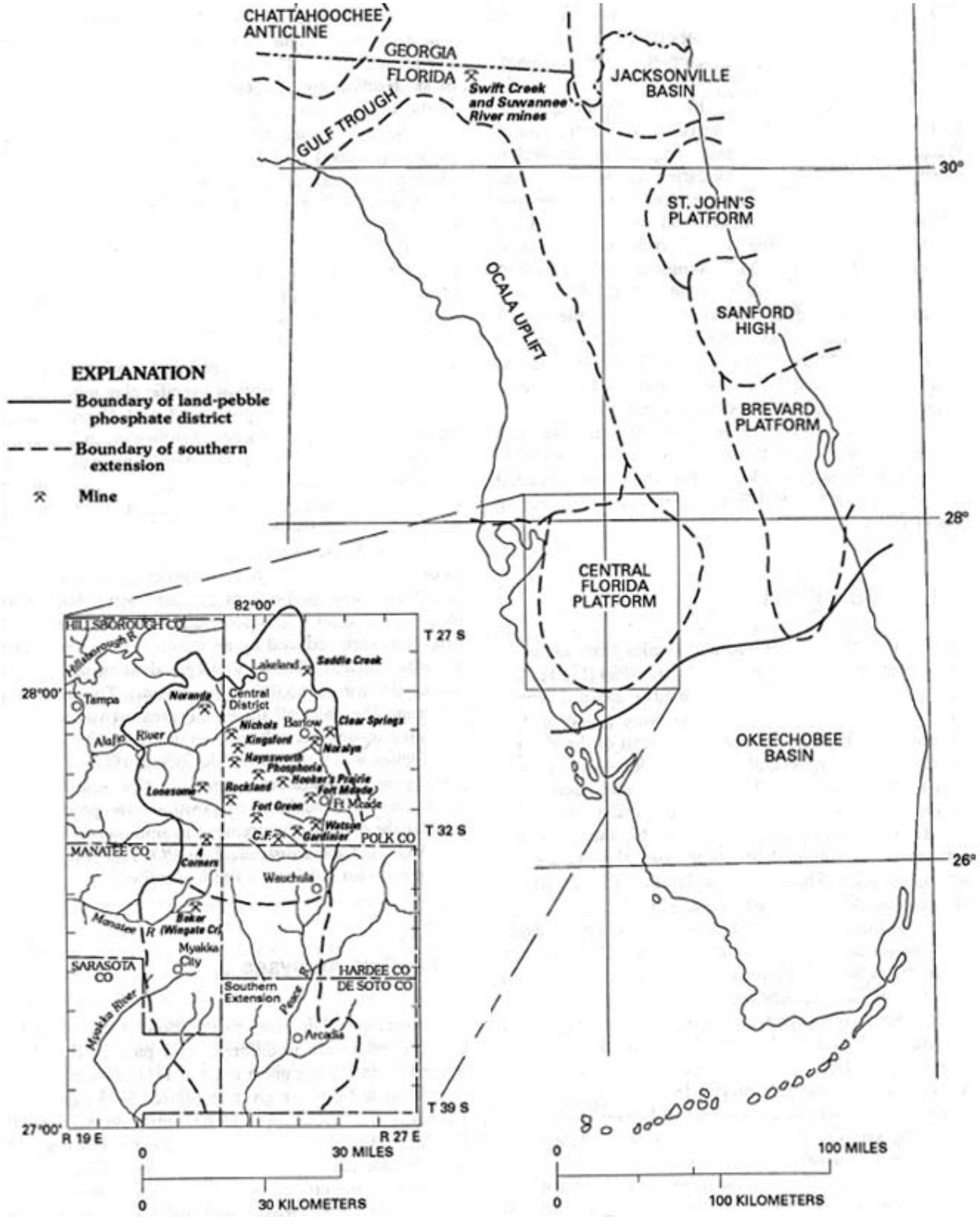

Figure 2-2. Land structural regions (taken from Kauwenbergh *et al.*[2] after USGS bulletin 1914) in Florida are indicated. The inset presents the locations of several phosphate mines in the Central Florida region. Each mine location is marked by the icon $\widehat{X}$.

Phosphate in the southeastern United States originates from rocks that were formed during the Miocene age.[2] The Miocene age can be described as the time period between roughly 5 to 23 million years ago. Much of the phosphate deposits were formed in the coastal waters surrounding Florida. The deposits have also been found to originate from the fossils of animal remains. The first discovery of phosphate in Florida occurred in 1881 in the Peace River, which is nearby the town of Fort Meade. The discovery was made by J. Francis LeBaron of the U.S. Army Corps of Engineers.[24]

2.2 Phosphate Beneficiation

Phosphate exists in a matrix of sand, clay and phosphate that lies underneath the ground. The matrix is made up of approximately one-third sand, one-third clay and one-third phosphate.[23,24] Above the matrix exists an overburden which is made of primarily sand and clay. The overburden lies from the surface of the ground to a depth of approximately 25 feet. Directly beneath the overburden lies the phosphate matrix. The phosphate matrix usually extends from a depth of 25 to 50 feet. An extremely large dragline excavation system is used to remove the overburden that lies on top of the phosphate matrix. The use of draglines for phosphate excavation began as early as the 1920s.[25] The draglines today can reach sizes over 3,500 tons with a reach larger than 300 feet. A photograph of a currently operated dragline mining phosphate is presented in Figure 2-3. Today's draglines, such as that pictured in Figure 2-3, can dig up to 15 acres a month.[19] Such large amounts are able to be excavated due to the huge bucket that extends from the dragline displacing large amounts of the matrix. A photograph of the bucket extending from the dragline pictured in Figure 2-3 is presented in Figure 2-4. These buckets are so large that at least 25 people could comfortably stand next to each other within the dimensions of the bucket.

Upon completion of the removal of the overburden, the dragline continues to excavate the phosphate matrix to an area that is more shallow. This shallower area, termed as a pit, is where the matrix is contacted with high pressure water which dissolves the matrix into a slurry. It is advantageous for the matrix to be in a slurry form such that it can be pumped through pipes away from the mining area and towards the phosphate beneficiation plant. At the beneficiation plant the phosphate, clay and sand are separated from each other. This is done through a series of washers and cyclones. The washers take advantage of the pebble size of the phosphate to

Figure 2-3. Photograph of electrically operated dragline shown mining the phosphate matrix (photograph by Mark Orazem, used with permission).

Figure 2-4. Photograph of bucket attached to the dragline used to displace the phosphate matrix (photograph by Mark Orazem, used with permission).

aid in its separation. The residual water tied up with the phosphate pebbles is easily removed through a series of dewatering tanks. The phosphate pebbles when dried are ready to be manufactured into water-soluble fertilizer. The separated sand is returned to the mine area to aid in refilling the original mine cut to expedite land reclamation.[22,26] The left over clays from the beneficiation process are then sent to large clay settling areas, also known as CSAs. The clays exist as a 2-6 solids weight percent slurry when they arrive at the CSAs. Typically, the slurry sent to the CSA contains particles finer than 150 microns in diameter.[1,23–25,27,28] This slurry includes 20 to 30% of the excavated phosphate not including the quartz and sand particles also present in the slurry.[23] It has not been determined whether improvements in the beneficiation process could be made to avoid such losses of phosphate. One source stated that approximately one third of the original $\mathrm{P_2O_5}$ in the phosphate matrix is usually lost to the clay slurries,[29] while another stated that 12 to 15% of the available phosphate is lost to the waste slurry.[30] The clay settling areas and the primary issues regarding them are discussed in greater detail in Section 2.3.

2.3 Clay Settling Areas (CSAs)

Disposal of the phosphatic clays has been one of the phosphate industry's most important challenges for several decades causing issues with regard to water consumption, water pollution, and land reclamation.[18] Issues associated with phosphatic clay disposal have stimulated research since the 1950s.[26,31] The clays are stored in large above-ground man-made dikes which typically reach 40 feet above ground level. These storage ponds are termed as clay settling areas (CSAs). The depth from the surface of the clays to the bottom of a CSA is usually between 30 to 40 feet. Clay settling areas occupy approximately 100 square miles of land in Central Florida as a result of phosphate mining. Each individual CSA is typically designed to have an area of one-square-mile. One report cited that Florida phosphate mines send 20,000 to 30,000 gallons per minute to clay settling areas;[32] while other reports have listed that 100,000 tons per day are generated in Florida .[28,33] Either way, it is clear that the volume of clay suspensions generated far exceed the void space created by mining which leads to major land storage issues.[34] To compound this problem, the poor settling characteristics of the clays means that it can take 10 years or longer to reach 25% solids by mass (or weight).[30]

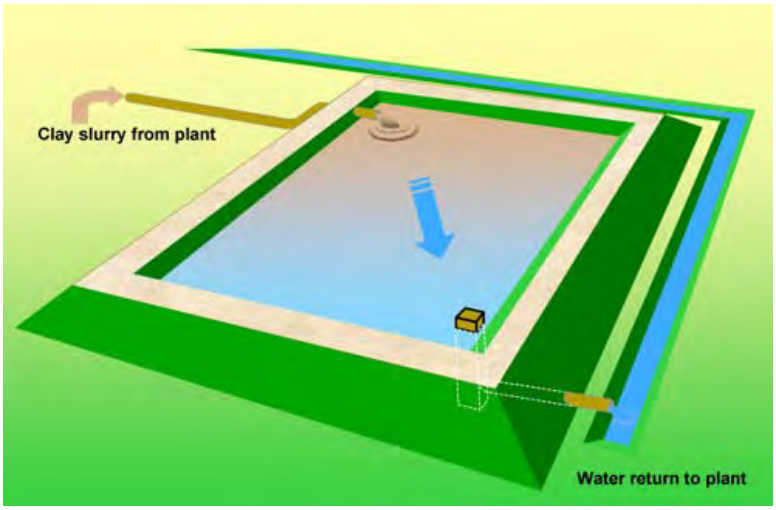

Figure 2-5. Illustration of clay settling area showing water migration towards one corner for recycling to the beneficiation plant (image accessed from Mosaic website).

The CSAs are considered to be of major environmental concern to environmental groups and nearby residents. From 1942 to 1971 there were twenty recorded dam failures that sent clays spilling into nearby rivers and streams.[18] This has led to the need to consolidate the clays more quickly and avoid building more CSAs. However, the clay settling areas have been known to serve three main functions. These include the recycling of water to the beneficiation plant, use as a reservoir system to conserve groundwater, and ultimate consolidation of waste clays.[24] Typically, the dilute clay slurry at 2 to 6% solids enters the clay settling area at one end of the pond while clear water forms at the other end of the pond as illustrated in Figure 2-5. This is further demonstrated in live photographs of clay settling areas in Central Florida presented in Figures 2-6 and 2-7. The separation pictured aids in recycling water to the beneficiation plant.

In the early to mid 1970s, the state of Florida began enforcing regulations that mined lands be reclaimed.[18,22,24] Generally, mined lands can be reclaimed to form housing developments, parks, orange groves, and golf courses. However, clay settling areas are not actually reclaimed. The settling areas are usually leased for cattle grazing once they reach an acceptable solids content (i.e., 40% solids). The above ground structures have poor aesthetic features according to nearby residents. Therefore, the goal is to avoid building more clay settling areas in order to allow more of the mined lands to be reclaimed.

A

B

Figure 2-6. Photographs of clay settling areas looking down from raised embankment; A) one end of the pond where clear water has surfaced to the top; and B) the other end of the pond where clay has not settled as well (photographs by Mark Orazem, used with permission).

A

B

Figure 2-7. Photographs of clay settling areas showing the interior sloped embankment; A) one corner of the pond where clear water has surfaced to the top; and B) another corner of the pond where clay has not settled as well (photographs by Mark Orazem, used with permission).

CHAPTER 3
STUDY OF CLAYS

Phosphatic clays consist of approximately one-third phosphate, one-third sand, and one-third clay. However, the clays fraction tends to dominate the overall dewatering behavior of the slurry. This is due to the clays representing the fine particle fraction which cause poor settling characteristics and when consolidated, have poor permeability properties. However, having a finer particle size also allows for a potentially favorable response to the application of an electric field.

The poor settling characteristics are partially due to some clay minerals being layered which means their internal surface area is huge while also having a very small apparent density. Metallurgist refer to phosphatic clays as slimes which are loosely defined as material that is too fine to dewater by beneficiation methods.[21] Typically, 98% of the particles contained in the phosphatic clay suspensions are less than 100 microns in diameter. The average specific gravity of the dry particles of the phosphatic clays is 2.7 with a range between 2.6 to 2.9. They consist of clay minerals such as smectite (or montmorillonite), palygorskite and kaolinite as well as non-clays such as carbonate-fluorapatite, quartz, wavelite and dolomite.

3.1 Clay Properties and Structures

Clay minerals are formed by chemical weathering of rocks into crystalline particles that typically have a diameter of 2 microns or less.[3] For example, kaolinite is formed from water and carbon dioxide breaking down felspar.[3] The general shape of most clay particles is a plate- or flat-like shape leading to a large ratio of surface area to mass.[3] This high specific surface area leads to hindered settling of clays. However, it also causes the surface properties of the clays to dominate which may be favorable for enhanced sedimentation due to an applied electric field.

Most clay minerals are made of a combination of silica and alumina sheets.[3] The silica sheet is made of silica tetrahedrons and the alumina sheet is made of alumina octahedrons which are presented in Figure 3-1. Different combinations of the silica and alumina sheets form different clay minerals. For example, kaolinite is made of a stack of sheets alternating between silica and alumina. Smectite, or montmorillonite, is composed of an alumina sheet sandwiched in between two silica sheets. The so called 'sandwiches' then stack consecutively together but with water molecules occupying the space between them. The amount of water adsorbed may

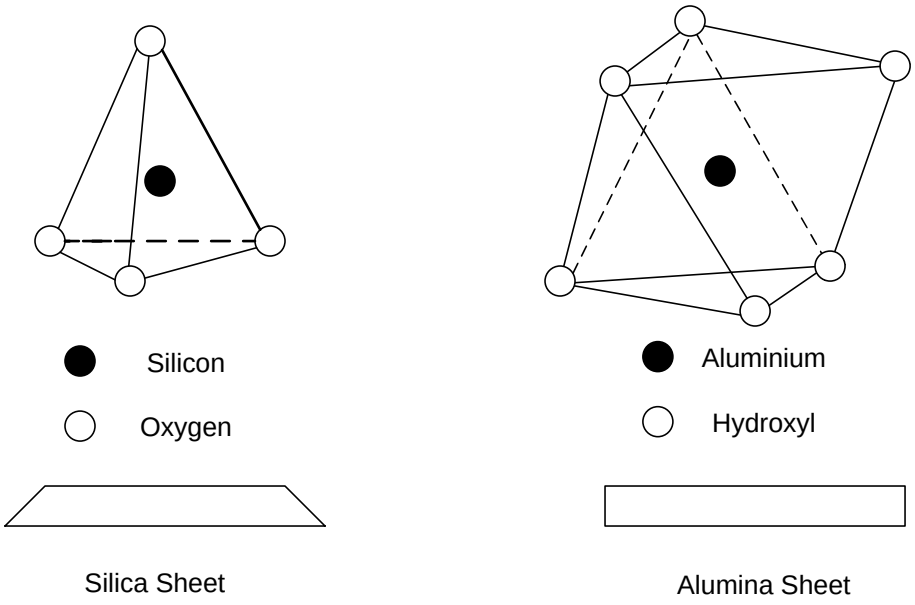

Figure 3-1. Molecular representations (reproduced from Craig[3]) of the basic structures of clay minerals. The molecular structures combine to form the depicted sheet structures.

increase causing the smectite particles to swell which increases their specific surface area and further hinders settling.

3.2 Charge on Clays

Typically, clay particles immersed in water have a negative surface charge. The negative surface charge can be due to several factors. One cause for this can be due to preferential specific adsorption of anions at the surface of the clays instead of cations. Another cause is due to isomorphic substitution, or lattice substitution,[35] which occurs when a silica or aluminium atom (shown in Figure 3-1) is replaced by an atom of lower valency. In other words, the positive charge on the central atom in a tetrahedron, for example, is reduced leading to a residual negative charge. Another cause of the negative charge is bond breaking at the surface of the clay particles. For example, the octahedron contains hydroxyl groups which can dissociate leaving negatively charged surface groups. The negative charge on the clays are naturally balanced by positive charges or cations in the adjacent water such that the overall clay-water interface is neutral. These cations predominate in a region approximately 1 to 10 nanometers from the surface of the clay. This overall interface is termed as the double layer which represents the clay-water (or solid-solution) interface with a net negative charge on the solid side and a net

positive charge on the solution side. Beyond approximately 10 nanometers from the clay-water interface the water becomes neutral as the concentration of cations decreases with increasing distance from the interface. This interface can be most simply modelled as a capacitor.

The characteristics of the double layer determine whether a given particle will respond favorably to an electric field. The magnitude of charge is usually expressed instead in terms of the zeta potential. The charge q is directly proportional to the zeta potential ζ as

$$q = -\frac{\epsilon\zeta}{\lambda} \tag{3–1}$$

where ϵ is the permittivity and λ is the Debye length which represents the thickness of the diffuse part of the double layer. The electrochemistry of this relationship will be discussed in more detail in Section 4.3. While the charge on the clay particles aids sedimentation when an electric field is applied, there is a counter force as the interaction of like charges between clay particles enhances dispersion. Additionally, there are short-range attractions between particles due to van der Waals forces which decrease with increasing distance between particles.[3] However, when no electric field is applied, the repulsion due to the like charges on the particles as well as their large specific surface area dominate in keeping the clays suspended in water and hindering settling.

3.3 Types of Clays

Three types of clays are known to occur within phosphatic clay suspensions. These are known as smectite, kaolinite, and palygorskite. The following sections discuss each of these clays in greater detail.

3.3.1 Smectite Clay

Smectite clay is often referred to as montmorillonite. It includes a combination of silica tetrahedral ($\mathrm{SiO_4}$) sheets and alumina octahedral ($\mathrm{Al(OH)_6}$) sheets.[3,36–38] Swelling of smectites easily occurs as water is adsorbed between the stacked arrangements of silica and alumina sheets. The bonding between the stacked sheets is weak leading to smaller particle sizes.[3,39] Magnesium and iron are known to substitute for aluminium in the alumina octahedrons in a process known as isomorphic substitution. Aluminium may also substitute for silica in the silica tetrahedrons. Smectites have a very high degree of isomorphic substitution in comparison to other clay minerals.[40]

3.3.2 Kaolinite Clay

Kaolinite clay is made up of alternating consecutive sheets of alumina and silica. An average kaolinite particle could consist of over one hundred stacks of combined alumina and silica sheets leading to larger particle sizes than smectites.[3] Kaolinite particles have a plate-like shape with a negative surface charge on its faces and a positive surface charge on its edges.[41–43] Kaolinite does not adsorb water easily and its stability is due to hydrogen bonding between silica and alumina sheets.[37] This increased stability also limits isomorphic substitution as it does not occur as readily in kaolinite.[3]

3.3.3 Palygorskite Clay

Palygorskite is a clay mineral whose make-up is more complex than smectites or kaolinites. Palygorskite is not simply composed of stacks of different structural combinations of silica and alumina sheets. Instead it is made of chain-length like structures leading to longer and thinner particles. The palygorskite clay particles are described as rod-shaped particles composed of length-wise fibers which vary from 0.01 to 5 microns in length.[44] Grim has classified palygorskite as a chain-structure type of clay mineral with “hornblende-like chains of silica tetrahedrons linked together by octahedral groups of oxygens and hydroxyls containing aluminum and magnesium atoms.”[39] The charge on palygorskite is much smaller than other clays and it has a higher surface area to mass ratio. Its minimal charge causes it to not respond favorably to an electric field and its high surface area to mass ratio does not allow it to settle well naturally either. Another commonly used name used for palygorskite is attapulgite.

CHAPTER 4
ELECTROCHEMICAL ENGINEERING AND ELECTROKINETIC THEORY

Electrochemical engineering is introduced as a discipline needed to meet the growing energy demands of the world. This discussion includes the introduction of different electrochemical techniques such as polarization curves and impedance spectroscopy. Electrokinetic theory is introduced, which is a subset of electrochemical engineering. The fundamental properties that drive electrokinetic phenomena are discussed in this chapter to provide a framework for how separations of clay suspensions occur.

4.1 Electrochemical Engineering Techniques

Electrochemical Engineering is a discipline with great potential for demand due to the growing energy needs of the earth. Electrochemical systems can be organized into two categories. The first is a system which uses spontaneous electrochemical reactions to produce electrical energy. These are often referred to as galvanic cells. Examples of this are batteries and fuel cells. The other category of electrochemical systems are those which need energy to drive electrochemical reactions to produce a specific product. This work involves the use of an electrolytic cell. Another application involving electrolytic cells is the chlor-alkili industry, which is introduced by Prentice,[45] yet described in much greater detail by Pletcher and Walsh.[46] This process uses electrical energy to drive several different electrochemical reactions to produce chlorine, hydrogen, and sodium hydroxide.[46] The advantage of electrochemical engineering is that it can be used to reduce the energy requirement needed to drive these reactions for a given amount of product produced. Electrochemical Impedance Spectroscopy (EIS) is a powerful tool that can be used to aid in the effort to reduce the energy requirement needed to drive these reactions. The contributions of EIS are highlighted by its ability to determine different electrochemical kinetic parameters.[47] EIS and polarization curves typically can aid in the characterization of electrochemical experiments and may help to describe the reactions or reaction mechanisms occurring. Detailed uses of EIS and its mathematical foundation are given by Orazem and Tribollet.[48] Other excellent sources on the concepts of electrochemistry are given by Bard and Faulkner,[49] and Bockris and Reddy.[50,51] However, Newman gives the most extensive detail on the mathematics of electrochemical engineering.[52]

4.2 Methods to Optimize Electrochemical Cells

Polarization curves and electrochemical impedance spectroscopy (EIS) are two measurement tools that can be used to obtain more information about a given electrochemical system. Polarization curves can provide open-circuit potentials, which represent the potential where there is no net current flow in the cell. Polarization curves can also be used to identify the mass-transfer-limited current for a given system, which represents the maximum current obtainable under a given set of operating conditions. EIS provides the magnitude of an electrochemical cell's resistance and allows identification of the dominating resistances in the cell. By taking impedance data at different points along the polarization curve, the roles of different kinetic, Ohmic, and mass-transfer phenomena can be distinguished.

The voltage losses for a given electrochemical cell can be investigated in order to create an optimal cell design. These losses can be due to kinetic, Ohmic, and mass-transfer limitations that are known to occur in electrochemical cells. They can be identified through use of EIS. Once the limitations in an electrochemical cell are determined from impedance data, different methods can be used to reduce the operating voltage of the cell. For example, the kinetic limitations are associated with the rate of the reaction that occurs on an electrode's surface. This can be improved by methods adding improved catalysts, increasing electrode size, and increasing operating temperatures. Ohmic limitations are based on the electrolyte's resistance to the flow of current through solution. An example of a method to decrease this resistance is to increase the concentration of the supporting electrolyte. The supporting electrolyte is a dissolved substance such as a salt that will reduce the resistance of the solution without participating in electrochemical reactions as it remains inert. Mass-transfer limitations involve the difficulty in delivering reactants to an electrode's surface. For example, at the mass-transfer-limited current, the concentration of the limiting reacting species at the electrode's surface is equal to zero. Two methods to improve this limitation are to stir the solution and to increase the concentration of the reacting species in the solution.

The overall impedance for a given cell can be measured by using the anode as a pseudo-reference electrode. In this case, no reference electrodes would be used for the impedance measurement. However, use of reference electrodes are often advantageous, especially in membrane cells. Additional EIS measurements involving reference electrodes can be performed to

identify the the dominant resistances present in an electrochemical cell by isolating their contributions. Such measurements provide the basis for identifying issues occurring in electrochemical cells.

4.3 Principles of Electrokinetics

Electrokinetic phenomena arise from the relationship and interaction between the electric field and the diffuse double layer at a solid-solution interface.[53] The existence of the diffuse double layer in the presence of an electric field leads to a hydrodynamic flow.[5,54] This represents the driving force for electrophoresis and electro-osmosis, which involve enhanced sedimentation and consolidation, respectively. In order to discuss the key principles which describe electrokinetic phenomena physically and mathematically, it is necessary to review first the concepts of the electrical or diffuse double layer.

4.3.1 Electrical Double Layer

A double layer naturally occurs when a solution (or electrolyte) is in contact with a solid. As ions are present in solution, some have a greater affinity for adsorption to the solid's surface than others. Generally, anions prefer to be closer to the solid surface than cations. Therefore, a separation of charge arises as anions adsorb to the surface forming the compact part of the double layer. The ions that are specifically adsorbed do not move freely because they are bound to the surface. In order to balance the negative charge adsorbed to the surface, a diffuse region of charge in the solution adjacent to the adsorbed ions forms, and this is termed the diffuse part of the double layer or simply as the diffuse layer.[55] The diffuse layer is not electrically neutral as, in this case, it is has a higher concentration of cations than anions. The cations in the diffuse layer are balanced between the electrostatic force pulling cations toward the oppositely charged surface and their tendency to diffuse away from the surface due to the concentration gradient from the diffuse layer into the bulk solution.[56] In the diffuse layer the ions are able freely move as they are not bound to the surface. The thickness of the diffuse layer is typically given as 1 to 10 nanometers;[5] although another source has reported the thickness to be as large as 100 nanometers.[57]

The physical description of the electrical double layer as described in this section is illustrated in Figure 4-1. Beyond the diffuse double layer, the solution is electrically neutral. The

length or thickness of the diffuse double layer is given by the Debye length,

$$\lambda = \sqrt{\frac{\epsilon RT}{F^2 \sum_{i=1}^{n} z_i^2 c_{i,\infty}}} \tag{4–1}$$

where R is the gas constant (8.314 J/molK), T is the temperature (in degrees Kelvin), z_i is the charge on ionic species i, F is Faraday's constant (96,487 C/equiv) and $c_{i,\infty}$ is the bulk concentration of ionic species i. The bulk concentration represents the concentration in solution away from the interface where the solution is electrically neutral and no concentration gradients are present. The inner Helmholtz plane (IHP) and the outer Helmholtz plane (OHP) are both indicated in Figure 4-1. The IHP (also referred to as the Stern surface[58]) represents the plane intersecting the centers of ions specifically adsorbed to the solid surface. The OHP represents the plane of closest approach to the solid surface for centers of freely moving ions.

If the solid itself becomes charged, then a redistribution of charge can occur in the double layer. The entire interface must be electrically neutral; therefore, the charge on the solid q_1 and the total charge of the all specifically adsorbed ions q_2 must balance the charge in the diffuse part of the double layer q_3 as

$$\mathrm{q_1 + q_2 + q_3 = 0} \tag{4–2}$$

Another treatment of the terms can involve combining the charge on the solid q_1 with the total charge of the specifically adsorbed ions q_2 as

$$\mathrm{q_1 + q_2 = q} \tag{4–3}$$

This is advantageous when considering particles in colloidal suspensions. As a particle moves, it carries with it the charge of the specifically adsorbed ions which are bound to its surface. Therefore, the charge can be combined as given by equation (4–3).

As the charge on the solid surface arises, a redistribution of charge in the diffuse double layer will occur to balance the total charge of the interface given by

$$\mathrm{q + q_3 = 0} \tag{4–4}$$

Changes in the bulk concentration will also affect the distribution of charge within the diffuse double layer. Equation (4-1) indicates that as the bulk concentration $c_{i,\infty}$ increases, the thickness

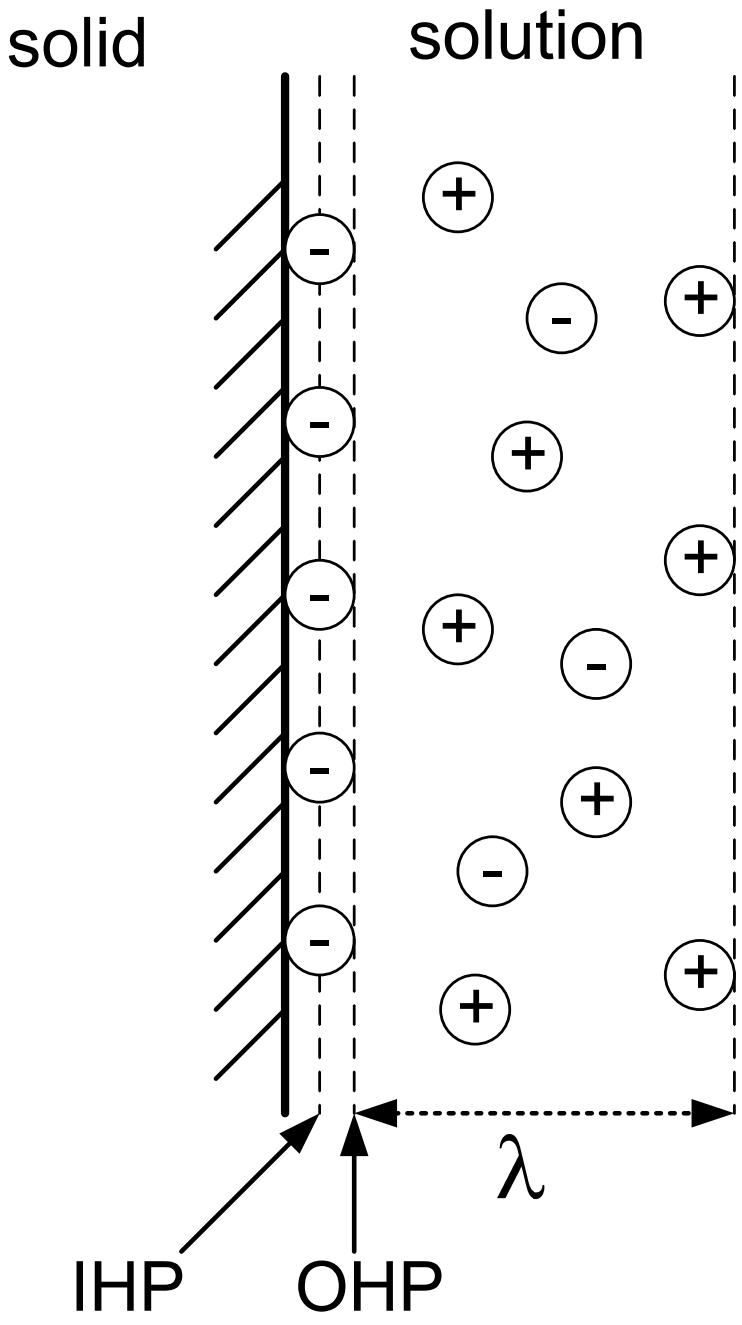

Figure 4-1. Schematic of electrical double layer indicating the inner Helmholtz plane (IHP), the outer Helmholtz plane (IHP), and the thickness of the diffuse part of the double layer λ. The positive circles indicate cations and the negative circles indicate anions.

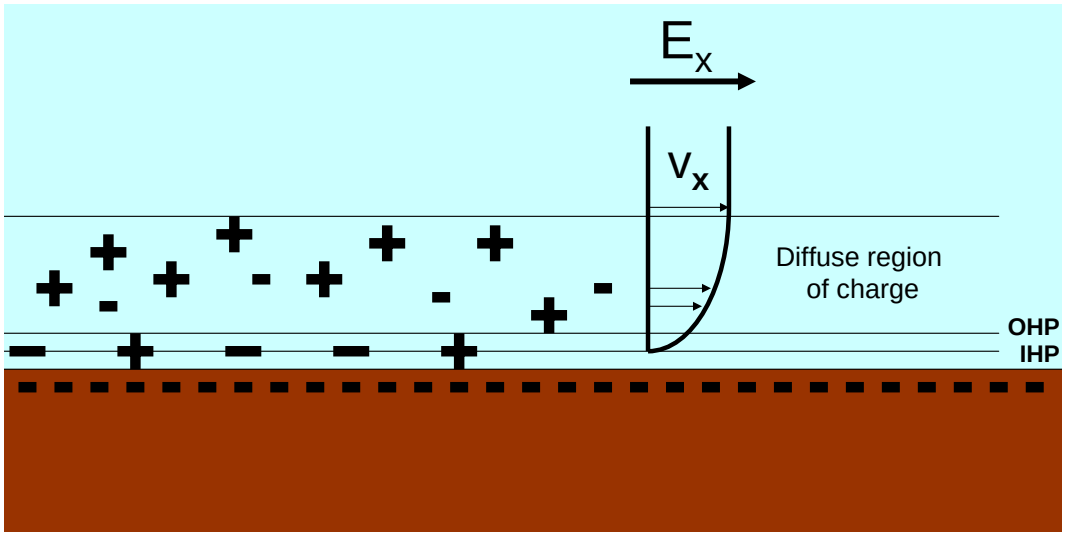

Figure 4-2. Schematic illustrating the direction of the electric field, the diffuse double layer, and the velocity profile that arises.

of double layer λ decreases. This affects the charge in the diffuse part of the double layer as

$$q_3 = -\frac{\epsilon\zeta}{\lambda} \tag{4–5}$$

By changing the charge in the diffuse double layer, the charge on the solid q must also change for equation (4–4) to hold.

4.3.2 Application of Electric Field

When an electric field is applied, a force acts on the freely moving ions in the diffuse part of the double layer. Cations respond to move in the direction of the electric field while anions move in the direction opposite of the electric field. If the diffuse layer is positively charged (i.e., contains more cations than anions), then the solution in the diffuse double layer will begin moving in the direction of the electric field.[59] If the solid is treated as a flat surface, then the direction of the electric field can be described as tangent to the surface as presented in Figure 4-2. A partial differential equation is developed by coupling the Navier-Stokes equation with Poisson's equation which relates the velocity of the solution v with the potential in solution Φ and the electric field E_x as

$$\mu\frac{\partial v}{\partial y} = \epsilon\frac{\partial \Phi}{\partial y}E_x \tag{4–6}$$

where μ represents the viscosity of the solution and y is the position into the solution which is normal to the solid surface.[5] The potential and velocity gradients are formed due to the presence

of a boundary layer at the solid-solution interface. The boundary conditions at the IHP are defined as v = 0 and Φ =Φ_0. The boundary conditions outside the diffuse double layer and towards the bulk solution are defined as v = v_x and Φ = Φ_∞. From integration and solving for the constants using the boundary conditions, equation (4–6) is simplified to

$$\mu(-v_x) = \epsilon(\Phi_0 - \Phi_\infty)E_x \tag{4–7}$$

The zeta potential ζ is defined as the potential drop through the diffuse part of the double layer as

$$\zeta = \Phi_0 - \Phi\infty \tag{4–8}$$

By substituting equation (4–8) into equation (4–7), the velocity of water v_x just outside the diffuse double layer can be obtained as

$$v_x = -\frac{\epsilon\zeta E_x}{\mu} \tag{4–9}$$

which yields an expression relating the velocity of the water as a function of the electric field. The velocity v_x can also be defined in terms of the charge in the diffuse layer q_3 or the charge on the particle q by substituting equation (4–5) into equation (4–9) to give

$$v_x = \frac{q\lambda E_x}{\mu} \tag{4–10}$$

Note that v_x represents the velocity of solution with respect to the particle or solid surface.

Further information on the principles of electrokinetics can be found in textbooks. Newman and Thomas-Alyea[5] give an extensive section on electrokinetic principles which includes the mathematical derivation of key phenomena such as the relationship of the electric field with the electric double layer. Hiemenz and Rajagopalan[58] also include a detailed section on electrokinetic phenomena and on the strong role of the double layer. Other related texts by Van Olphen[56] and Kruyt[60] primarily focus on colloidal systems yet have key information pertaining to double layer theory and its pertinence to electrokinetics.

CHAPTER 5
LITERATURE REVIEW

A review of the literature is presented ranging from small-scale to large-scale applications of electrokinetic dewatering. The applications presented are for removal of water from phosphatic clays as well as other materials. Other methods for water removal are also presented. An overall assessment of the accomplishments within the literature is discussed. This assessment also introduces items that are absent in the literature which motivate the contributions for this work.

5.1 Electrokinetic Dewatering

Numerous dewatering designs are presented in the literature. The following sections include descriptions of electrokinetic bench-top cells as well as large-scale applications. Although the focus is on the dewatering of clays, much can be learned from the electrokinetic dewatering of other materials. Some examples of electrokinetic dewatering applications other than clays include water removal of oily sludges,[13] harbor dredges,[61] contaminated river sediment,[62] waste sludge,[63] and activated sludge.[64]

5.1.1 Small-scale Bench-top Cells

Several bench-top cells are presented in the literature. A large portion of the bench-top cells studied are cylindrical in shape, vertically oriented, and made of Plexiglas or acrylic. Buckland *et al.*[62] developed a Plexiglas cylindrical cell for application of an electric field to remove water from contaminated river sediment. The cell had an inner diameter of 20 cm and a height of 100 cm. Electrodes were placed parallel to each other with the cathode at the top and the anode at the bottom. The parallel arrangement of the electrodes was used to ensure a uniform electric field along the length of the column. Reference electrode ports were installed along the length of cell to measure the electric field. Sampling ports were also installed which tapped into the cell such that the solids content could be determined at various locations while the experiment was still operating. A similarly designed cell was presented by Shang and Lo,[17] Lo,[65] and Shang,.[14] This bench-top cell had the same features as the cell reported by Buckland *et al.*[62] except that it was smaller, with a 9 cm diameter and a 20 cm height, it did not have sampling ports, and it was designed specifically for water removal from phosphatic clay suspensions. Shang[17] reported an increase in solids weight percent (wt%) of phosphate clay from 12.7 to 29 wt% in just 30

hours. Shang[17] reported a dewatering energy requirement of 7.6 kW-h/per cubic meter of clay suspension.

Ho and Chen[66] also developed a vertically oriented cylindrical cell which was used for removal of water from clay suspensions. This cell featured a rotational anode placed at the top of the cell. By increasing the rotations per minute (RPMs) the rate of dewatering increased as the higher number of rotations forced the caked clays to fall off of the anode. Disadvantages of this design were that the electrode gap could not be adjusted and the rotating anode could not operate properly if the solids weight percent became too large. Ho and Chen[66] reported an increase in solids content from 9.1 to 24.6 wt% in just 4 hours.

Reddy *et al.*[61] also produced a vertically oriented acrylic cell. This cell included a weight on the top electrode to maintain electrical contact with the sediment being dewatered. The use of the weight was also designed to ensure uniform consolidation. Reddy*et al.*[61] reported a range of dewatering energy requirements between 280 to 1022 W-h/per cubic meter of sediment treated.

Jin *et al.*[67] developed a cell horizontally oriented to remove water from a fermentation broth. This cell was rectangular in shape. One advantage of this type of cell is that it allowed for efficient venting of the gases generated at the electrodes. Other designs by Maini *et al.*[68] and Paczkowska[15] also used horizontally oriented bench-top cells for electrokinetic removal of water.

5.1.2 Large-scale Field Applications

Several outdoor tests have been performed to remove water through application of an electric field on waste clays or mine tailings. Some of these implementations involved building above ground storage tanks to perform tests and others either built experimental clay ponds or applied electrokinetic instrumentation to pre-existing clay ponds. Fourie *et al.*[4,12] built and operated an above ground tank to dewater mine tailings. The design involved vertically oriented electrodes inserted into the tailings. Such an arrangement of electrodes is expected to be more feasible because it may be difficult or impossible to insert horizontally oriented electrodes at the bottom of an already existing clay settling area (CSA). Vertically oriented electrodes could be much easier to install as they can be thrust (i.e., as a stake) downward and implanted into such settling ponds. From the raw numbers reported by Fourie *et al.*,[4] a dewatering energy requirement of 1.25 W-h/kg of water removed was determined. This energy requirement was based upon an increase in solids content from 39 to 57 wt%.

McLean[69] reported a large-scale clay dewatering experiment which was performed on settling ponds specifically designed and built for such tests. This involved the use of draglines to prepare trenches which were subsequently filled with dilute clay suspensions. Such experimental preparation would be beneficial for installation of horizontally oriented electrodes at the bottom of the pits before they are filled with suspensions (or slurries). Large-scale designs reported in the literature may be beneficial when considering issues that may arise from any scale-up design based on bench-top results.

5.2 Other Dewatering Methods

The Tennessee Valley Authority investigated numerous methods to enhance water removal of slurries that feed or already exist in clay settling areas.[21] Techniques that were listed include flocculants, filtration, high temperature drying, electrophoresis, centrifugal applications, magnetically induced current, controlled stirring and others. The Florida Institute of Phosphate Research (FIPR) has published numerous dewatering methods that do not include electrokinetic field applications. Pittmann reported and summarized several methods such as a freeze-thaw technique, use of movable screens, crust development, and a sand-clay sandwhich process.[25]

5.2.1 Flocculation

Flocculation can be defined in various ways as it involves several different types of mechanisms. In the most general sense, flocculation is defined as the formation of flocs or flakes that occur as colloidal particles come out of suspension. In phosphatic clay suspensions, flocculants are used to increase the settling rate which aids the recycling of water back to the phosphate beneficiation plant.[70] The dilute suspension fed directly from the beneficiation plant is treated with flocculant which increases the solids content from 2 to 10 weight percent within minutes, possibly even seconds.

The flocculants are made of polymeric materials.[71] The polymer used is charged and termed as either anionic or cationic. Its associated charge attracts and attaches to suspended clay particles forming condensed bundles of the particles. Some flocculants reported in the literature include polyethylene oxide[72] and polyacrylamide.[1,70] Polyacrylamide has worked with great success, but is not widely used due to its high expense. Although most flocculants (i.e., polyacrylamide) used are organic, inorganic flocculants also exist.[1] Inorganic flocculants actually

had a larger sales volume in the 1970s but were overtaken shortly after once synthetic organic polymers arrived on the market.[1]

Rahman[70] describes the flocculation mechanism in two stages with the first stage involving the adsorption of the polymer reagent onto a single clay particle's surface. The second stage involves the aggregate flocs that are subsequently formed. The polymer molecules are described as long string-like chains which absorb to several locations on an individual particle. Slack exists in the string-like flocculant as it attaches from location to another on the particle's surface. Loops then form which extend outward from the surface. These loops collide and attach with other clay particles forming a bridge from one particle to another.[70] As the collisions continue to occur the aggregate flocs form. As the aggregates form, the specific surface area of the clays decrease and gravitational forces dominate over any repelling surface charges of the clays which promotes the clays to commence settling.[1]

Another mechanism which can be termed as flocculation involves compressing the size of the double-layer that exists at the clay-solution interface. The presence of the double-layer on all clay particles leads to a repulsive force due to the like charges on the clay particles. By increasing the concentration of ions in the electrolyte, the thickness of the double layer decreases as described by equation (4–1). The compression of the double layer leads to a reduction in the repulsive forces between particles.[1] This allows the particles to begin to aggregate. Other mechanisms also exist which involve different adsorption techniques specific to certain types of flocculants (or polymers).

5.2.2 Large-scale Field Application

The Florida Institute of Phosphate Research (FIPR) has published a large number of reports on the dewatering of clays that do not include the use of electrokinetics. Carrier[73] reported a field test including the use of a plastic, prefabricated geodrain system that was installed on a pre-existing clay settling area to decrease the overall reclamation period by one or two years. The geodrain cover was placed such that it laid on an embankment that sloped down into the CSA. As the CSA was filled, the slurry would contact the geodrain cover, which adsorbed water from the slurry decreasing the solids content of that entering the CSA. Small-scale tests had previously been performed which indicated that the geodrain material would be effective on a large-scale. The adsorbed water was released from the geodrain by a pipeline connected to the

geodrain material. This test ultimately failed because the pipeline was not installed properly as it was incapable of withstanding the changes in height level of the CSA over time. However, the shear strength of the clays near the geodrain was 30% higher than at areas where the geodrain was not used. Therefore, the recommendation of this project was to repeat the project with an improved installation of the drainage pipes.

5.3 Additional Electrokinetic Application

Cellular particles have been previously treated with electrokinetic phenomena in order to separate, manipulate, or analyze such particles.[74] Typically, such cellular particles are one micron in diameter or larger. However, Hughes[74] has proposed applying AC electrokinetics to particles on the nanometer-scale. This type of study involves dielectrophoresis, which is the application of a nonuniform electric field which induces a dipole on particles that are subject to the electric field.[14,17,75,76] The nonuniform electric field coincides with an alternating current (AC). It was initially believed that particles on the nano-meter scale would be controlled by Brownian motion instead of the dielectrophoretic force.[74] However, microfabricated electrodes were used which provided control over such small particles.[77] Advancement of such an application could have large effects in expanding or developing nanotechnology in its attempts to become mainstream.

5.4 Electrokinetic Parameters

Experimental issues reported within the literature which involve application of an electric field to remove water from waste clay or other types of suspensions are discussed here.

The objectives of this work center on the application of an electric field to dewater clay suspensions. However, application of an electric field to remove water from other materials is also relevant in terms of studying electrokinetic phenomena. Several issues such as the selection of electrodes, pH of suspension, zeta potential of particles, particle size, evolution of gases, and current pausing can greatly effect the power requirement of an electrokinetic dewatering process. The reported energy requirements in the literature range from 0.6 to 880 kW-hr/dry metric ton.[4] Most early studies used voltage drops as large as 70 V. The associated large currents result in drying of the soil around the anode, which causes large parasitic potential drops. The large currents also create significant gradients in pH, which can change the clay properties and can increase parasitic losses. Issues that arise due to changes in pH are

discussed in more detail in Section 5.4.2. The effects of changes in pH and parasitic potential drops can be mitigated by reversing polarity or by pausing the current to allow natural diffusion to relax the concentration profiles. Using intermittent current or current pausing is discussed further in Section 5.4.3. Operating at a smaller electric field can also reduce issues associated with corrosion of electrodes and parasitic voltage drops. A smaller electric field should also reduce the power required per unit of clay processed.

5.4.1 Selection and Design of Electrodes

The selection and design of electrodes is often dependent on the cell design or the objectives of the experiment. If it is desired to filter or remove water through the electrodes, then mesh or porous electrodes should be beneficial. These electrodes would also be useful if there is concern with ventilation of gases evolved due to electrochemical reactions occurring at the electrode surfaces. Some electrodes can be machined in order ensure that the electrodes are porous enough such that gases do not get trapped.[62] If the electrodes are oriented vertically, then gases evolved should not get trapped underneath the electrodes as they often may with horizontally oriented electrodes. Therefore, vertically oriented electrodes may not need to be porous for gas ventilation.

Corrosion is also a big issue in determining selection of electrodes. Due to the large voltages applied in early electrokinetic studies, metal electrodes corroded and needed replacement on a regular basis. Alternative electrodes such as the dimensionally stable anodes used for cathodic protection may provide a cost-effective alternative.[6] Fourie has reported excellent results for dewatering of mine tailings by using electrokinetic geosynthetic electrodes, which comprise a charged porous felt cloth wrapped around a carbon-doped plastic mesh.[4,11,12] The electrokinetic geosynthetic electrodes also appear to resolve the problems with electrode stability or degradation. Graphite electrodes have also been used to mitigate issues involving corrosion.[62]

5.4.2 pH and Zeta Potential

Changes in pH will occur due to electrochemical reactions producing hydrogen ions at the anode and hydroxide ions at the cathode which are generated from reactions (1–1) and (1–3). Such changes in pH are significant due to its effect on the charge of clay particles. The level of pH can also affect the stability of electrodes as corrosion or degradation of electrodes can occur at low pH. Often in the literature, instead of quantifying the charge on clays in terms of

Coulombs, the zeta potential is used to characterize clay particles which are usually on the order of 10 to 50 milli-Volts (mV). Several studies in the literature measure the zeta potential as a function of the pH. The zeta potential is critical to electrokinetic processes as given by equation (4–9).

Several studies have involved pH and zeta potentials and how they affect various electrokinetic processes. Bjelopavlic *et al.*[78] reports that changes in pH can affect the surface charge of clay particles due to the specific adsorption of ions onto particles. As the pH increases, the hydroxyl groups added to the suspension are known to adsorb to the surface of the particles changing their charge. The charge on the particle q is directly proportional to the zeta potential as given by equation (4–5). Other effects of pH changes can involve further contamination of clay suspensions. Cabrera-Guzman[79] reports that at low pH values, hydrogen ions can promote ion exchange effects which can release metal contaminants that were bonded to the clay particles. This could lead to further issues in terms of managing the hazards associated with land storage of the clays.

Dixit *et al.*[80] measured the mobility of clay particles as a function of pH. These results found that as pH increased, the mobility increased. This was attributed primarily to dissociation of hydroxyl groups at the edges of the clay particles which is known to occur at larger pH values. The bond between the oxygen atom and the hydrogen atom breaks leaving a more negative charge on the clay particle as the positively charged hydrogen ion diffuses away. As the charge on the clay becomes more negative, the absolute value of the zeta potential increases leading to improved mobility at larger pH values. Such a relationship was verified experimentally by Gopalakrishnan *et al.*[81] as the zeta potentials were measured as a function of pH for two types of clay slurries. The absolute value of the zeta potential increased with increasing pH for both clays.

5.4.3 Use of Intermittent Current

Intermittent current or voltage (or current) pausing is often employed in electrokinetic cells to rehydrate dried areas which can reduce parasitic voltage drops and relax pH or concentration gradients. Reducing areas where parasitic voltage drops occur can aid in reducing the resistance to the flow of current through a given electrochemical cell. Shang and Lo[17] implemented

the use of an intermittent current interval to determine the most efficient on-off cycle for electrokinetic water removal of clays. An on-off cycle of 15 minutes on and 5 minutes off was reported as the most efficient for removal of water. Another study was performed by Gopalakrishnan *et al.*[81] to determine an optimal on-off time for current pausing. Their results indicated an optimal on-off time of 30 seconds on and 0.1 seconds off. The discrepancy between the optimum ratios of the two papers could be due to the difference in time scales used for each ratio. Another discrepancy could be due to differences in the clays used from one study to the other.

5.4.4 Particle Size

Particle size has been reported to have an effect on the rate of sedimentation of clays which is contact with an applied electric field. Shang's[14] experimental results compared two types of clays against each other which had different particle size. One clay was termed as the brown clay and the other was termed as a grey clay. The brown clay had a finer average particle size and achieved better dewatering results from the application of the electric field. However, Shang also performed control tests with gravity only, where the grey clay achieved better settling results. Therefore, these results indicated that finer particle size adversely affects the sedimentation behavior when no electric field is applied but enhances sedimentation when under the force of an electric field. Reasons for this can be attributed to surface properties of the particles. For finer size particles, the surface properties are expected to dominate which allow them to respond to an electric field. However, when no electric field is applied, these surface properties may aid in dispersing the particles due to like charges on the clay particles causing their repulsion of each other.

5.5 Assessment of the Literature

The literature has presented many examples of electrokinetic dewatering of clays and other materials. These include small- and large-scale studies which consistently demonstrate that the application of an electric field can be used to remove a significant amount of water from clays and\or other materials. However, the results of bench-top experiments presented in the literature have not been used to develop parameters for large-scale design of a water removal system. Constitutive relationships linking the electric field with operating time and the amount of water removed have not yet been presented within the literature. Such relationships are needed in combination with a mathematical model to project the energy requirements for a large-scale

water removal system to assess its feasibility in terms of large-scale treatment of clay settling areas.

CHAPTER 6
EXPERIMENTAL APPROACH

Ex-situ characterization of clay samples as well as the bench-top experimental set-up are presented in this chapter. The ex-situ studies included X-Ray diffraction, particle size distribution measurements and zeta potential measurements. The ex-situ measurements were performed to verify properties of the clay which could affect the results and reproducibility of the bench-top experiments. The introduction of the bench-top experimental set-up includes the description of the instrumentation used and the design of the bench-top cell.

6.1 Ex-situ Analysis of Clay Suspensions

Characterization of clay suspensions was desired to verify its physical properties which may affect the ability of an electric field to remove water from the clays. This also allowed for determination of whether variations existed between the various clay suspension samples provided by Mosaic Fertilizer LLC.

6.1.1 X-Ray Diffraction

X-Ray Diffraction (XRD) patterns were generated at the Major Analytical Instrumentation Center (MAIC) at the University of Florida using the XRD APD 3720 instrument. XRD was performed on phosphatic clay samples in order to determine the identity of the clay minerals contained within the slurries. It has been reported that mineralogical variations do exist throughout clay settling areas.[18] These mineralogical variations could cause significant changes in the electrokinetic dewatering results on phosphatic clays. For example, a sample that has a high content of palygorskite may not respond well to electrokinetic treatment due to palygorskite's small surface charge.[7,61,66,82] Sedimentation of palygorskite is also difficult due to its low density and small particle size. Bromwell reported that as the concentration of palygorskite in clay slurries increases, the rate of settling decreases.[18] While it is likely that the clay samples from Mosaic do not contain large amounts of palygorskite, the possibility of larger quantities presents the need for a composition study such as XRD.

X-ray diffraction was performed on selected samples provided by Mosaic. Some samples had been treated with Mosaic's proprietary flocculant while other samples had not. One of the most critical issues for generating a useful XRD diffraction pattern is to prepare the sample for analysis properly. A properly dried form of the clays must be prepared. Using an oven to

dry samples represents an improper drying technique. In oven or natural drying, as the water evaporates, the surface tension of the water molecules pushes the clay particles together. This leaves the clay samples in a cohesive phase that can not be examined properly by XRD. The proper preparation method is called the Peel technique which involves the preparation of an oriented aggregate mount of the clay onto a Millipore filter using a vacuum pump. This forces the clay mineral particles to lie flat, which enhances the ability of the XRD beam to produce useful results.

An X-ray diffraction pattern generated from a flocculated clay sample is presented in Figure 6-1 with the y-axis representing intensity counts in arbitrary units while the x-axis is the angle of the X-ray diffraction beam in degrees. The peaks in Figure 6-1 were identified using published diffraction pattern data representing the locations for each mineral type. The presence of smectite, palygorskite, and quartz was identified. Palygorskite existed in trace amounts which is favorable for electrokinetic experiments.

An X-ray diffraction pattern on a sample that was not treated with flocculant showed no significant difference from Figure 6-1. In fact, several other samples (with or without flocculant) yielded similar XRD results and it was concluded that each sample contained no significant variation of clay minerals. Therefore, all samples provided by Mosaic are expected to behave similarly in the presence of an electric field. This provided confidence in the reproducibility of the electrokinetic experiments presented within this work. Methods to determine the identity of phosphate bearing minerals were not performed as the XRD sample preparation excluded the larger sized particles that typically contain phosphate bearing minerals. The larger particles were excluded because they limit the ability to prepare a good mount and also clay minerals are expected to provide the primary limitations to natural settling as well as to the effectiveness of electrokinetic methods. For further information regarding the study of XRD and its use on clays, Cullity[83] provides in-depth description and analysis on XRD while Grim[39] discusses how XRD can be used to study and identify the mineralogy of clay samples.

6.1.2 Particle Size Distribution

The instrumentation used to determine particle size distribution was provided by the Department of Geological Sciences at the University of Florida. Results indicated that approximately 90% of particles from the phosphatic clay suspensions were finer than 60 microns in diameter

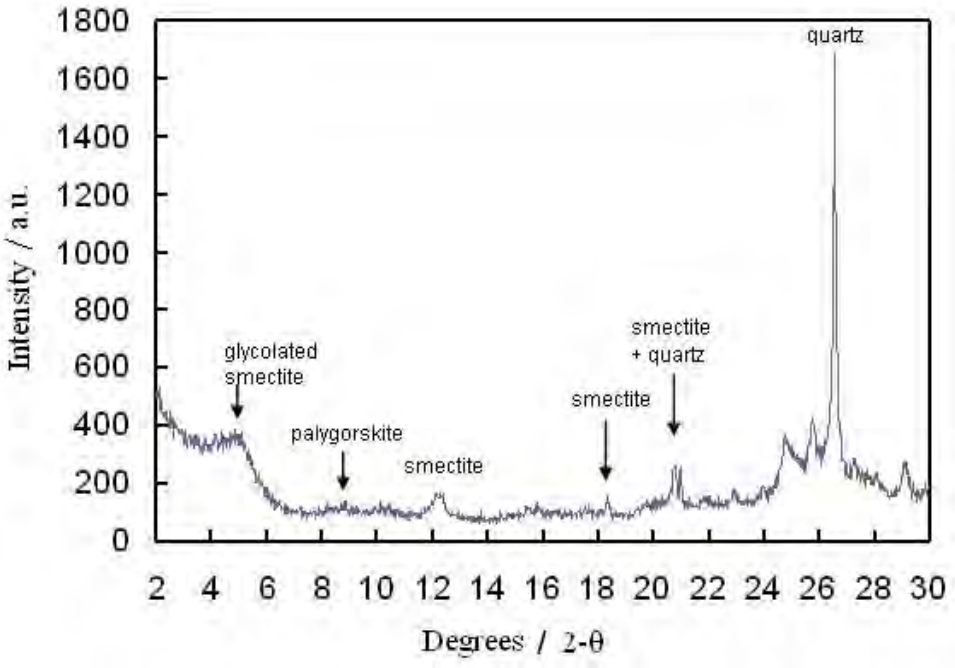

Figure 6-1. X-ray diffraction pattern generated from an oriented aggregate mount of a phosphatic clay sample. Peaks are identified with their associated clay or sand mineral.

and approximately 65% were finer than 2 microns in diameter. These results were generated using a sedigraph which measures settling velocities. Using Stoke's Law, the settling velocities were converted into characteristic diameters or sizes. These results were the same for both flocculated and unflocculated clay samples.

Particle size distribution measurements and calculations were also performed using optical methods in terms of the real and imaginary refractive indices of clay particles. The distributions were determined in terms of number distribution and volume distribution. However, this method is only accurate for homogenous suspensions, which does not include phosphatic clays. Therefore, these results were not useful and are not presented in this work.

6.1.3 Zeta Potential Measurements

Instrumentation used to perform zeta potential measurements was provided by Particle and Engineering Research Center at the University of Florida. The results were generated by the PALS Zeta Potential Analyzer. The instrumentation experimentally determined the average zeta potential of suspensions containing a flocculant and separately determined the average zeta potential for suspensions not containing a flocculant. The difference between the averaged zeta potential between flocculated and unflocculated samples was not significant. The

flocculated clay suspension had an average zeta potential of -20.1 mV and the unflocculated clay suspension had an average value of -19.9 mV. This result indicates that both types of clays should respond equally to an equivalent electric field as the velocity of water is a function of the zeta potential as given in equation (4–9).

6.2 Electrokinetic Studies

Bench-top experiments were performed to remove water from clay suspensions. The instrumentation used to perform experiments and the experimental apparatus used are presented. Information regarding the clay samples used in experiments are described as well as the methods used for performing experiments.

6.2.1 Experimental Instrumentation

The instrumentation used for potentiostatic or galvanostatic modulation involved the use of a potentiostat (i.e., Solartron 1286 Electrochemical Interface or EG&G Princeton Applied Research (PAR) Potentiostat/Galvanostat Model 273A). The potentiostat was used to apply a constant potential or a constant current. The potentiostat also had the capability of generating polarization curves. The potentiostat was operated through use of CorrWare software (Scribner Associates, Inc.). In order to generate electrochemical impedance spectroscopy data, an impedance frequency response analyzer (i.e., Solartron 1250 Frequency Response Analyzer or the Solartron SI 1260 Impedance/Gain-Phase Analyzer) works in combination with a potentiostat. This type of measurement involved the use of Z-Plot software (Scribner Associates, Inc.).

6.2.2 Bench-top Cell

A cylindrical Plexiglas cell was designed and constructed for bench-top experiments. The advantage of using a cylindrical cell is that its geometry provides a uniform potential drop along the length of the cylinder. The dimensions of the cell were 30 cm in length with an inner diameter of 9 cm. The cell was modified to include Ag/AgCl reference electrodes such that the voltage drop through the clay slurry could be measured. This allowed for determination of the electric field force acting on the slurry as the reference electrodes measured only the Ohmic potential drop. This was required because the potential difference between the cathode and anode (i.e., cell potential) does not only include the contribution of the Ohmic potential drop, but also includes the potential drop due to reaction kinetic limitations at the electrodes. A schematic of the cell is presented in Figure 6-2. The design was adapted from the description of the

experimental cell presented by Shang,[14] Shang and Lo,[17] and Lo.[65] All experiments began with the electrodes placed 19 cm or 20 cm apart. Initially, only two reference electrodes were installed to measure the voltage gradient. They were fixed to be 10 cm apart. After an initial matrix of experiments, the cell was further modified to include a total of four reference electrodes. This allowed for additional measurements for situations where the electrode gap was reduced and the original two reference electrodes did not both physically remain in contact with the consolidated clay. Such a scenario would occur when decanting the supernatant water after the experiment had operated for some length of time.

For all experiments, the cell was oriented vertically with the cathode placed at the top of the cell and the anode placed at the bottom of the cell. The electrodes were configured in this way such that the electric field would work with gravity and not against it. Under this configuration, the electric field applied a downward force on the negatively charged clay particles towards the positively charged anode while simultaneously attracting the water upwards to the cathode. Although natural settling due to gravity is not expected to achieve beyond 15 weight percent solids slurry over short and intermediate times, it was still desired to have an electric field that operated consistently with gravity. Mesh electrodes were used for both the cathode and anode. Both were dimensionally stable anodes made of titanium with a ruthenium oxide coating. They were machined and fit to work with movable plungers within the cell such that the electrode gap could be shortened or adjusted as supernatant water was removed.

All bench-top dewatering experiments included an on-off cycle of 30 minutes on and 2 minutes off. This cycle was included to allow concentration and hydraulic gradients to relax to reduce the resistance to the flow of electric current through the cell. Experiments operated at longer times were controlled to operate for 12 hours on and then 12 hours off each day. During the 12 hours of on-time the experiment continued to maintain the on-off cycle of 30 minutes on and 2 minutes off. Upon completion of each dewatering experiment, the contents within the cell were removed and immediately weighed. The treated clay samples were then placed in an oven to dry completely and were then re-weighed when dried to determine the solids weight percent upon completion of each experiment.

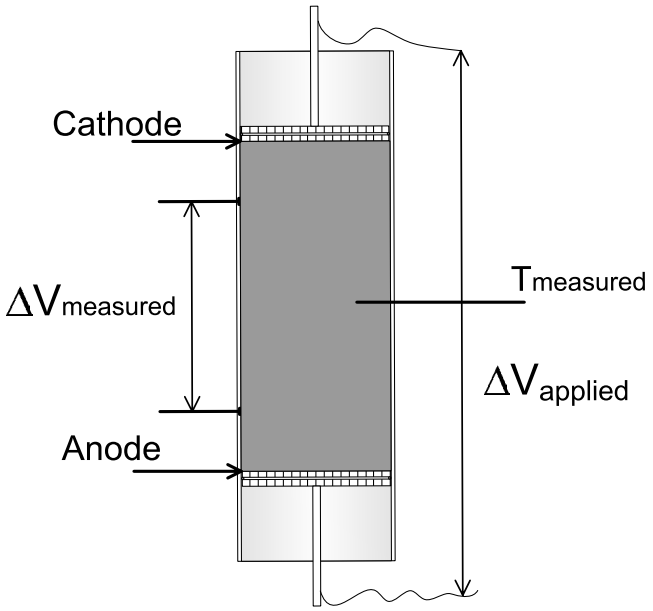

Figure 6-2. Schematic of bench-top cell with labeled locations of the electrodes and the temperature and voltage measurements. Darker shaded area within the cell represents where clay slurry is loaded for experiments.

6.2.3 Experimental Operation

One of the initial objectives of the bench-top experiments was to study the fundamental properties of the clay and water and their associated response to an applied electric field. The small-scale electrokinetic cell was not intended as a proto-type model for large-scale dewatering. However, the experiments were expected to aid in determining the feasibility of a large scale design for implementation in an already existing clay settling area (CSA). All experiments were performed using the phosphatic clay suspension samples provided by the project sponsor, Mosaic Fertilizer LLC. The samples provided varied from 2 to 12% solids by mass (or weight). Samples that initially existed in the 2 to 4 weight percent solids range had not yet been treated with a proprietary flocculant while other samples initially 8 to 12 weight percent solids had been treated with the flocculant. Additional electrokinetic experiments performed without flocculant showed that the use of a flocculant did not affect the electrokinetic results.

The solids content of the clay suspensions was determined by weighing the slurry sample and then weighing it again after the sample was dried in an oven such that all moisture was removed. 15 weight percent solids was the highest content achieved through natural settling in

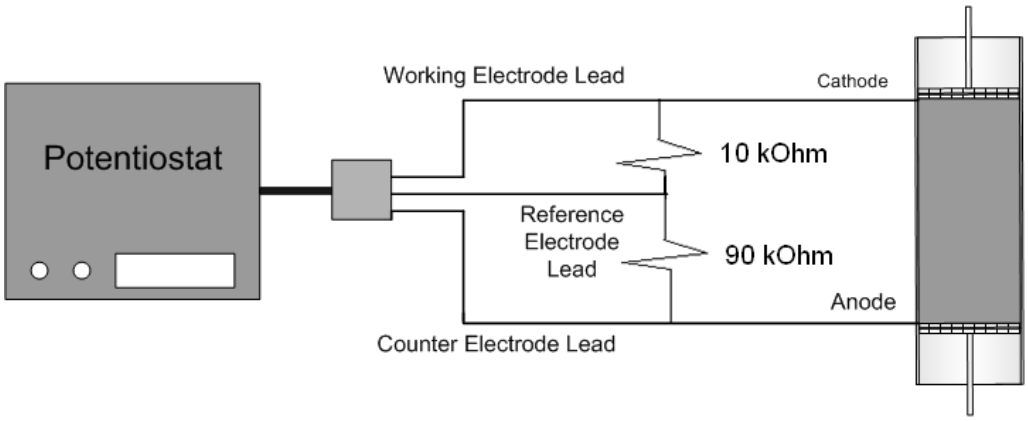

Figure 6-3. Schematic illustrating connections and use of resistors between potentiostat and bench-top cell. Resistors are included to amplify the applied potential to the cell.

combination with pre-treatment of flocculant. From the current thickening operation at Mosaic, the solids content quickly reaches 8 to 12 weight percent solids. Therefore, the experimental cell was typically loaded with a solids slurry content within the 8 to 12 weight percent range.

Initially, all experiments were operated under potentiostatic modulation and the electric current was measured as a response variable. However, issues developed when attempting to operate at small cell potentials in the range of 1.5 to 2 Volts. Under such operating conditions the electrodes did not remain polarized and the resulting electric field was effectively equal to zero. Such behavior was likely due to kinetic limitations dominating the potential drop the cell was attempting to apply. In order to remedy this issue, the potentiostat was switched to operate under galvanostatic modulation. A constant electric current was applied with the cell potential measured as a response variable. The applied current was operated as low as 2 to 4 milliamps (mA). The matrix of experiments presented in this work was operated in either potentiostatic or galvanostatic modulation. There was no evidence that the type of modulation affected the dewatering results as long as it provided a stable electric field.

One variation between galvanostatic and potentiostatic modulation occurred when adjusting the distance between the cathode and anode. If operating in potentiostatic mode, reducing the electrode gap required the reduction of the cell potential in order to maintain the same electric field. For galvanostatic mode, this distance had no effect on the electric field as long as the conductivity of the suspension did not change. Another experimental variation for potentiostatic modulation occurred when attempting to apply a cell potential beyond 10 V. The CorrWare

software prohibits applied potentials beyond 10 V. However, the potentiostat operated included a 100 V power supply. A schematic of a potentiostat with working, reference and counter electrode leads is presented in Figure 6-3. The working electrode was connected to the cathode and the counter electrode was connected to anode. The reference electrode lead, for the purposes of the bench-top experiments, was connected to the anode such that the anode acts as a pseudo-reference electrode. However, if the counter and reference leads are not shorted together and instead have a large resistor between them as well as a resistor between the working and reference (as shown in Figure 6-3) then a cell potential beyond 10 V can be generated. The potentiostat controls the potential between the working lead and the reference lead; however, the working electrode draws electric current from the counter electrode. Larger resistors are used to avoid a significant leakage current. The cell potential could be multiplied by a factor of 10 if the resistance between the working and reference leads is 10% of the resistance between the working and counter leads. Therefore, up to a 100 V cell potential can be reached by applying just 10 V between the working and reference under such conditions presented in Figure 6-3. If it is desired to double the cell potential then both resistors in Figure 6-3 would need to be equal. For galvanostatic modulation, the absolute current applied is controlled between the cathode and anode in such a way that there is no multiplier capability. However, this did not cause any issues under galvanostatic mode because the bench-top experiment always operated well below the software's maximum set-point for electric current.

CHAPTER 7
EXPERIMENTAL RESULTS AND DISCUSSION

The development and results of the bench-top experiments are discussed in this chapter. The bench-top experiments involve the application of an electric field to remove water from clay suspensions. A matrix of experiments were performed varying operating time and the electric field. Constitutive equations were developed and presented here, which give the change in solids weight percent of the clay as a function of operating time and the electric field. Electrochemical techniques such as impedance spectroscopy and polarization curves were used to characterize aspects of the bench-top experiments.

7.1 Proof of Concept with Bench-top Cell

Experimental results demonstrating a proof of concept are presented in Figure 7-1 for an experiment operated for 9 hours at a cell potential of 80 V. Figure 7-1A represents the Plexiglas cell loaded with the clay suspension before the electric field is applied. The composition of the clay suspension was initially 9 weight percent (wt%) solids. Upon completion of the experiment, the existence of a thickened clay mass formed which is presented in Figure 7-1B. Supernatant water that formed towards the top of the cell was removed before the photograph illustrated in Figure 7-1B was taken. The remaining thickened clay in Figure 7-1B had a solids content of 33.5 wt%. In the absence of an electric field, it normally takes 25 years for the clay suspension to reach a solids content of 40 wt%. From this experiment alone, the application of an electric field yielded a solids content approaching 35 wt% after just 9 hours of cell operation. Therefore, the application of an electric field is demonstrated as a method that can enhance removal of water from clay and a proof of concept is established.[84] Note that the solids content of the slurry in units of wt% is defined within this work as

$$w_c = \frac{m_c}{m_c + m_w} 100\% \tag{7–1}$$

with m_c representing the mass of dry clay and m_w representing the mass of water present.

7.2 Constitutive Relationship at Short Times

A matrix of bench-top experiments were performed varying operating time and the electric field. A relationship was desired to predict the time required to remove water as a function of the electric field. Upon completion of each experiment, the change in solids weight percent

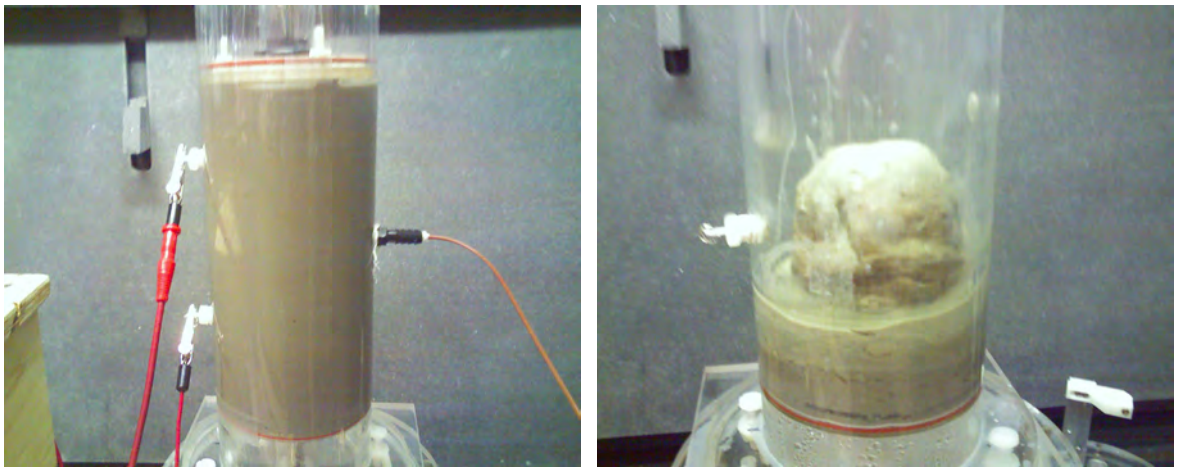

A B

Figure 7-1. Photographs of the bench-top Plexiglas shown: A) Before experiment was started the cell was loaded initially with a 9 wt% solids suspension, and B) after the experiment ended the cell was occupied by a thickened lump of clay consisting of 33.5 wt% solids.

was measured. The results of the entire matrix of experiments are presented in Figure 7-2. No evident relationship was found relating the change in solids content with operating time based upon the results presented in Figure 7-2. However, by scaling the change in solids weight percent by the applied electric field (in V/cm), the data superimpose to form a linear relationship as presented in Figure 7-3. A trend line was included to fit the data presented in Figure 7-3. The equation of the line was used to suggest a relationship between the change in solids weight percent Δw_c and the electric field E (in V/cm) as

$$\frac{\Delta w_c}{E} = 0.72t \tag{7–2}$$

with t representing the operating time (in hours). Equation (7–2) suggests that a prediction can be made for the time required to achieve a certain solids weight percent at a given electric field. This indicates that the time required to achieve a desired separation is inversely related to the electric field applied. Therefore, the size of the electric field corresponds to a specific solids weight percent of the clay meaning that a nonuniform electric field should result in nonuniform water removal. While the bench-top cell was designed for a uniform electric field, this result could be relevant to a large-scale dewatering system where the electric field will likely be nonuniform in some locations. The relationship given as equation (7–2) does not apply for operating times

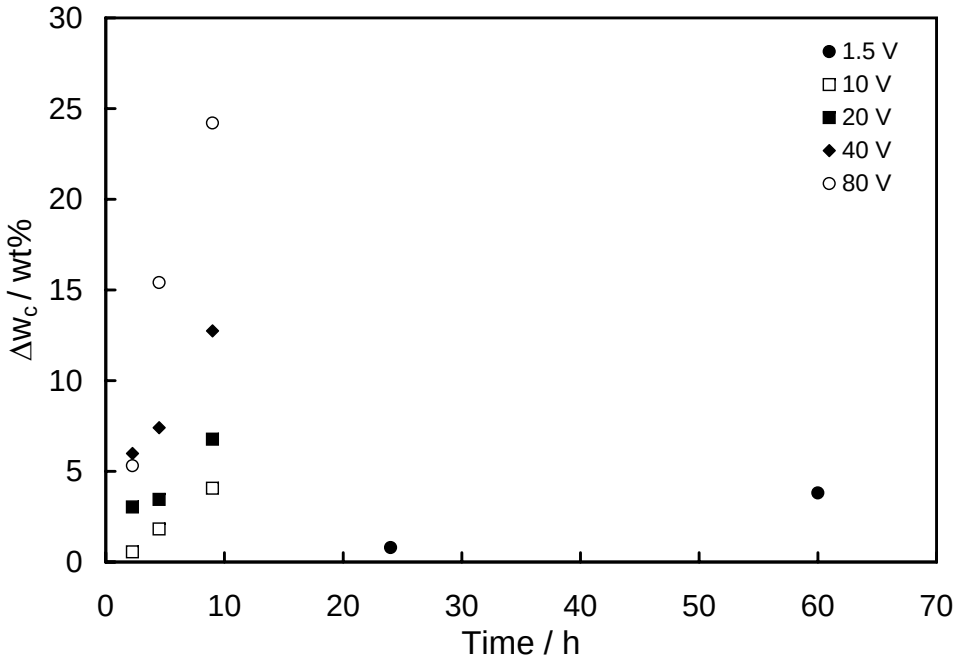

Figure 7-2. Results of bench-top dewatering experiments illustrating the change in solids weight percent as a function of operating time with applied potential as a parameter. The data marked 1.5 V were controlled galvanostatically to yield a constant electric field.

beyond the range of values presented in Figure 7-3 and is described as a valid relationship only at short times.

7.3 Uniformity of Water Removal

The matrix of experiments presented in Section 7.2 were analyzed in greater detail to examine the level of uniform dewatering within the cell. Sampling at various locations within the cell was performed to determine the extent of dewatering by position. The results are presented in Figures 7-4 - 7-8 which give the solids weight percent as a function of time. Each plot represents a specific applied cell potential. The extent of dewatering was found to be non-uniform for all results presented in Figures 7-4 - 7-8.

As shown in Figures 7-4 - 7-8, higher solids content was achieved by operating at larger potentials and for longer times. For an applied cell potential of 10 V, the highest solids weight percent was located near the anode and the next highest solids content was adjacent to the clay-supernatant interface (zones C and D) as presented in Figure 7-4. The center of the clay suspension in terms of height (zone B) was still the consistency of the original suspension at short times. For larger potentials (i.e., see Figure 7-7)) the middle region behaved differently

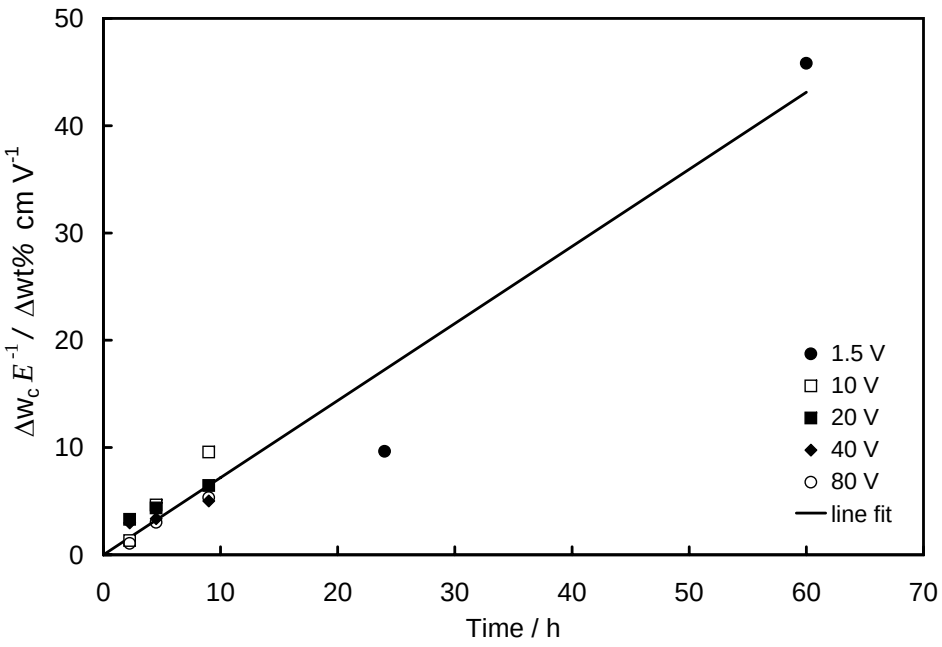

Figure 7-3. Solids weight percent results from Figure 7-2 are scaled by the applied electric field E. A trend line fit to the data suggests a linear relationship which is given as equation (7–2).

such that a solid core developed containing the highest solids weight percent. This behavior was previously presented in Figure 7-1B. This experiment illustrated the effects of gas evolution at the anode. The large rate of gas evolution forced the suspension to become dilute around the perimeter of the thickened clay mass located in the center. Additional experiments identified that lower current densities which decreased the rate of gas evolution helped alleviate such nonuniform behavior.

A much longer experiment at 20 volts was operated to determine the degree of nonuniform behavior of the clay over longer times. The results presented in Figure 7-8 indicate that at longer times the clay dewatering becomes more uniform. Physical observations also found that the transparency of the supernatant water was much improved which is attributed to allowing the cell to sit overnight for 12 hours without any applied potential. This behavior is indicated in Figure 7-9 (on left). In fact, the supernatant water from this experiment is much clearer when compared to the supernatant water formed by only gravitational settling in a one liter cylinder pictured in Figure 7-9 (on right). The experiment photographed in Figure 7-9 was also very

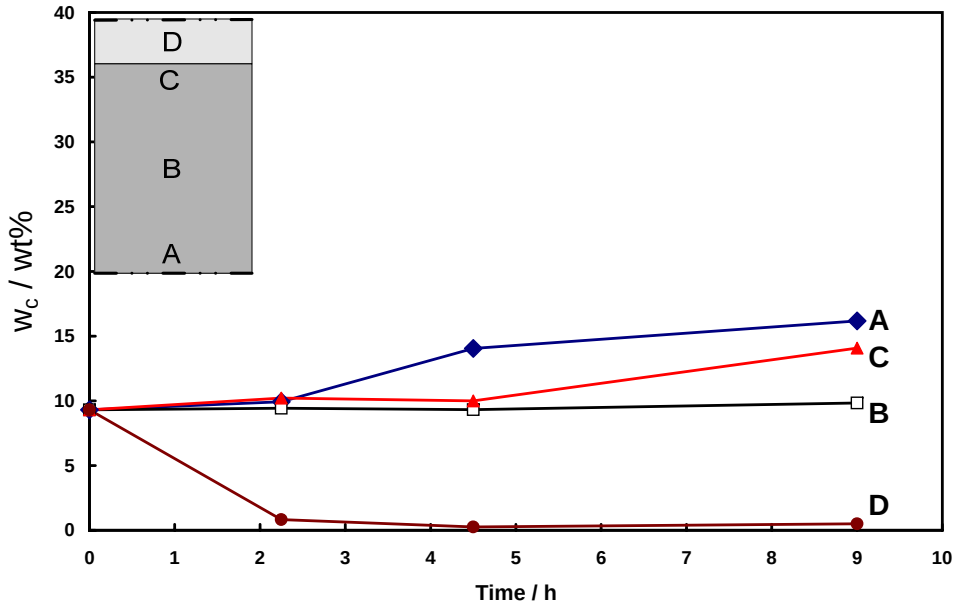

Figure 7-4. Cell potential of 10 V was applied for the duration of the experiment. The inset represents a schematic of the vertically oriented cell with zone D at the top of the cell representing the location of the supernatant water separated from the bulk clay.

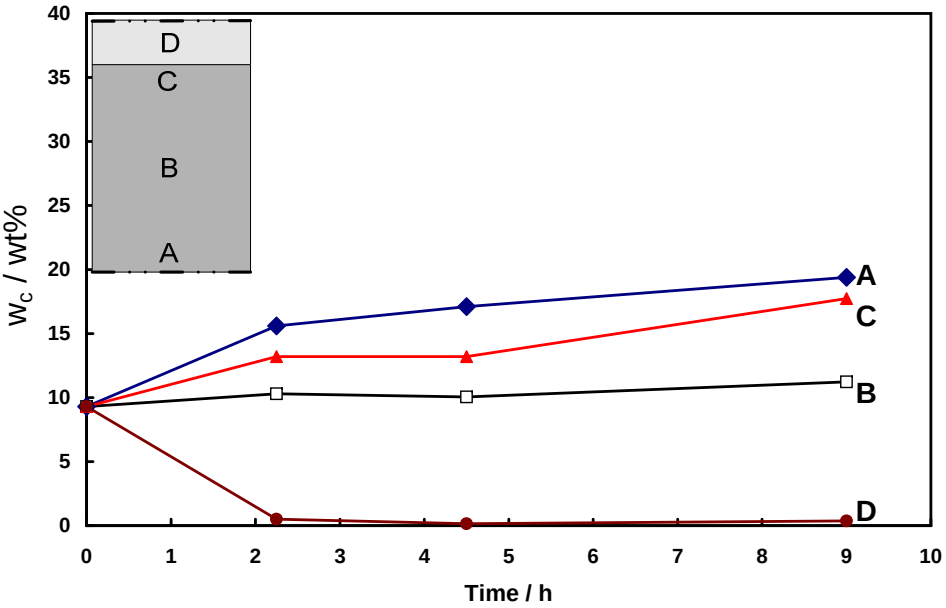

Figure 7-5. Cell potential of 20 V was applied for the duration of the experiment. The inset represents a schematic of the vertically oriented cell with zone D at the top of the cell representing the location of the supernatant water separated from the bulk clay.

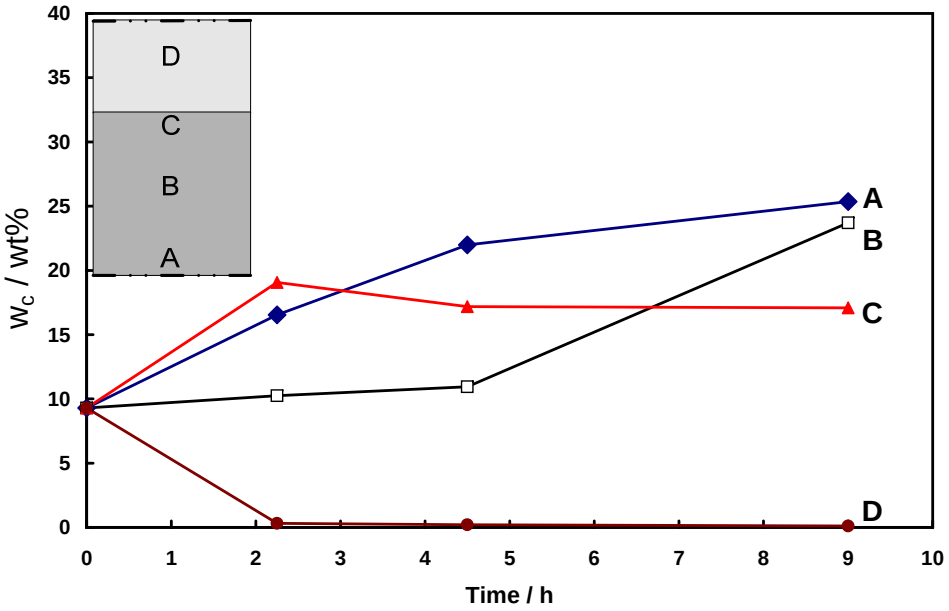

Figure 7-6. Cell potential of 40 V was applied for the duration of the experiment. The inset represents a schematic of the vertically oriented cell with zone D at the top of the cell representing the location of the supernatant water separated from the bulk clay.

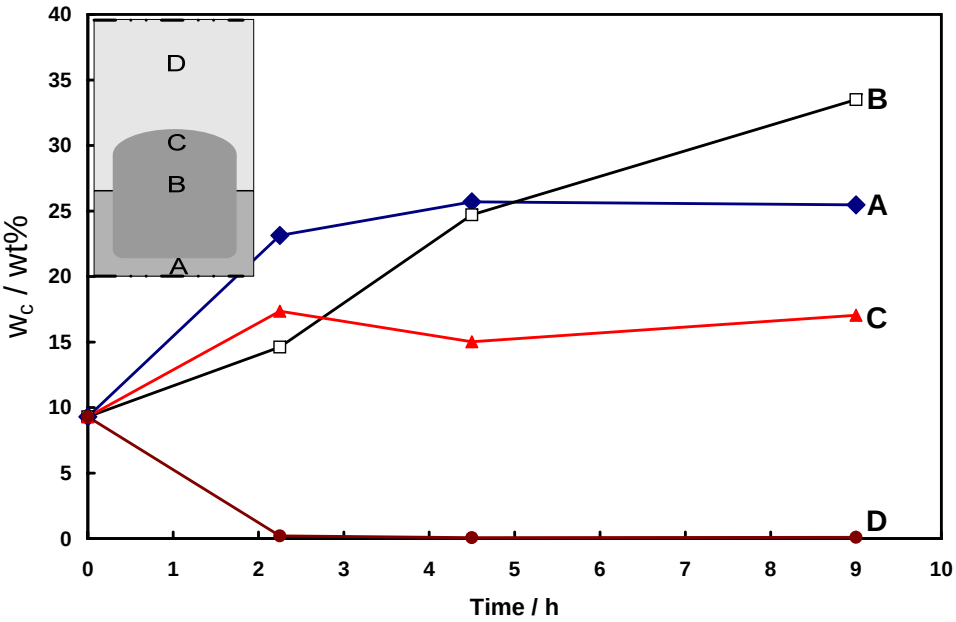

Figure 7-7. Cell potential of 80 V was applied for the duration of the experiment. The inset represents a schematic of the vertically oriented cell with zone D at the top of the cell representing the location of the supernatant water separated from the bulk clay.

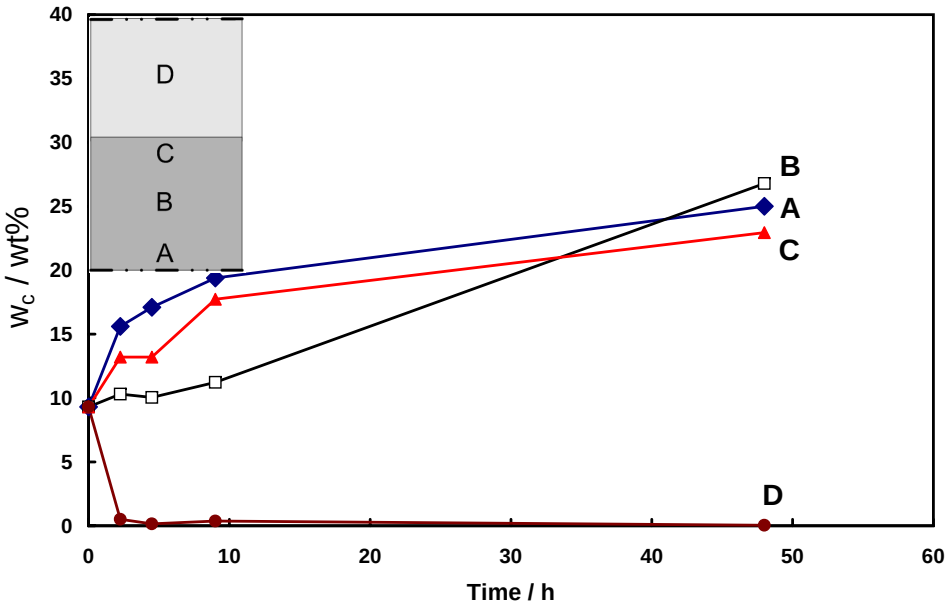

Figure 7-8. Cell potential of 20 V was applied for the duration of the experiment. The data in Figure 7-5 are reproduced here in addition to an experiment operating for 48 hours.

promising in terms of the amount of water removed from the consolidated clays portion of the cell as presented in Figure 7-8.

Other observations from the 20 V experiment at long times indicated electrokinetic treatment actually re-suspends some clay particles due to gas evolution at the anode. This was indicated by having clearer supernatant water after the experiment had been turned off overnight for 12 hours than after the experiment was operated during the day for 12 hours. This suggests that possible future designs may need a better path way for gas bubbles to vent instead of upwards through the cell column. This also suggests that the supernatant water should be removed after some time to avoid re-suspending clay particles into the water. For the experiments presented in this section, the gap between the electrodes was maintained at the same distance throughout the entire experiments to avoid changing the potential gradient (in V/cm) in the cell. In order to maintain these conditions the supernatant water was not removed allowing the electrodes to remain in electrical contact with the clay slurry without adjustments.

The results of this section demonstrate trends which indicate that the solids weight percent increased as the cell (or applied) potential increased. The results also indicated the solids weight percent of the clays increased with increased operating time. However, the purpose of presenting the results in terms of Figures 7-4 - 7-8 was to study the uniformity of the clay

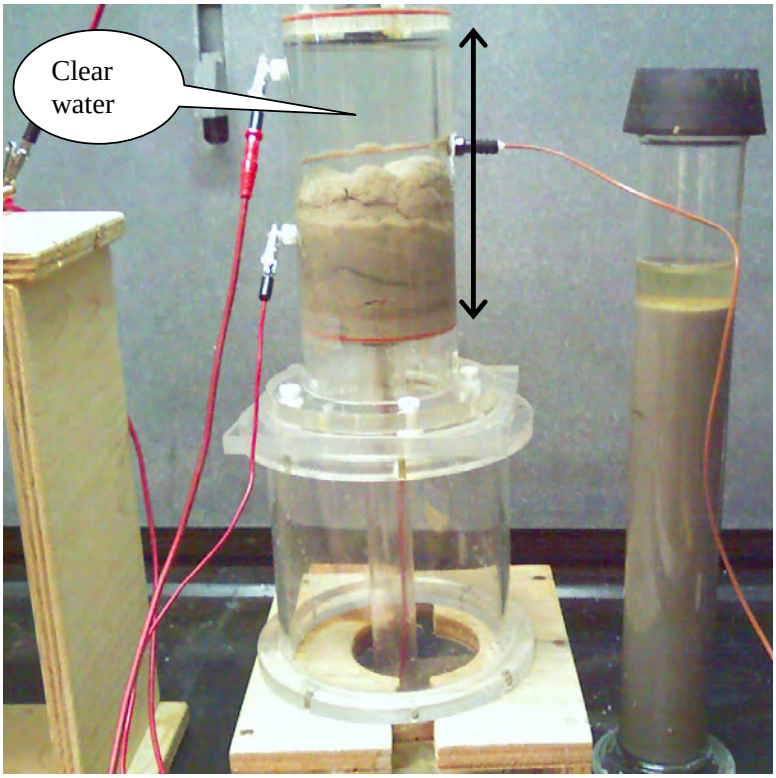

Figure 7-9. Photograph of cell after the completion of a 4 day, 20 V experiment and its comparison to the settling of a control (on right) sample in the absence of an electric field. The cell potential was applied for 12 hours each day. The arrow indicates the distance between electrodes. A clear layer of water is indicated above the clay.

suspensions. The experiments revealed that lower cell potentials or current densities could improve the uniformity of clay dewatering by decreasing the rate of gas evolution. Longer operating times were found to improve the uniformity of dewatering as illustrated by Figure 7-8. This may be meaningful for a large-scale water removal system that would be expected to require many days of operation to treat an area as large as a one-square-mile clay settling area.

7.4 Constitutive Relationship at Long Times

Bench-top experiments were performed at longer operating times to determine the validity of equation (7–2) beyond the range of parameters presented in Section 7.2. Upon completion of a new set of experiments, the associated data points were added to the data in Figure 7-3 to give Figure 7-10. The experiments performed at longer operating times showed that, even when supernatant water was periodically removed, a limiting value for solids weight percent was reached. The value of the maximum solids content achievable was found to be a function of the applied electric field as the solids maximum increased with increasing electric field strength. The

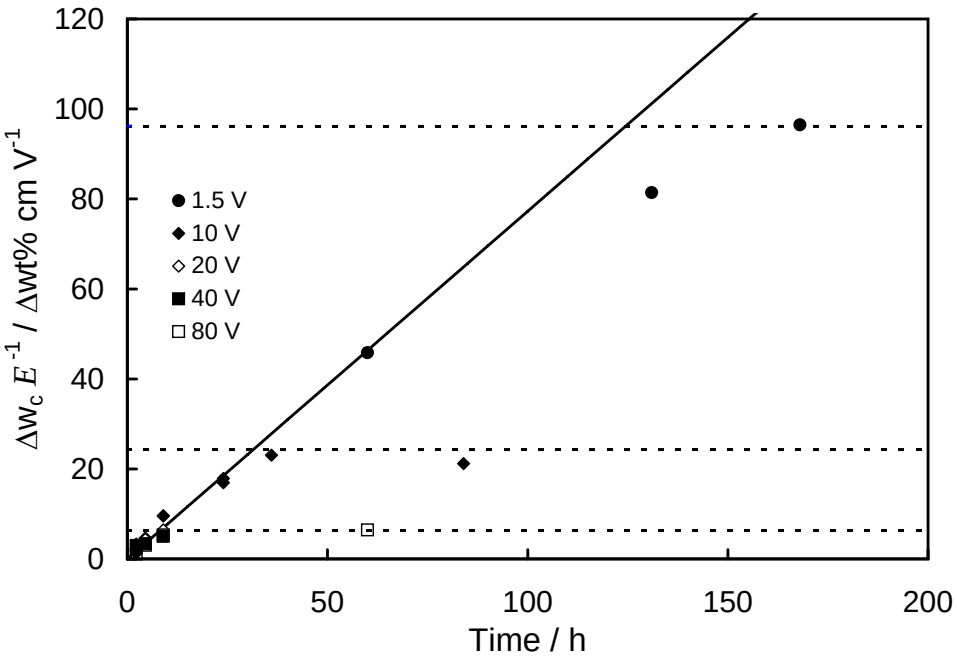

Figure 7-10. Additional data at longer times and larger solids weight percent are included with the data presented in Figure 7-3. The horizontal dashed lines represent the suggested plateau reached at three different electric field sizes.

data points that converge towards the horizontally dashed lines in Figure 7-10 were concluded to have reached their maximum solids weight percent. For such data, the maximum change in solids weight percent was given as a function of the electric field in Figure 7-11. The equation of the line was used to suggest a relationship between the maximum change in solids weight percent and the electric field as

$$\Delta w_c = 7.1 Log_{10}(E) + 16.5 \tag{7–3}$$

An interpolation model equation was developed to incorporate the linear behavior at short times (i.e., equation (7–2)) giving a constitutive relationship for short and long times as

$$\Delta w_c = [(0.72tE)^{-n} + (7.1 Log_{10}(E) + 16.5)^{-n}]^{-1/n} \tag{7–4}$$

where n is a dimensionless parameter that controls the transition from short-time to long-time behavior, E has units of V/cm and t has units of hours. The comparison of equation (7–4) for n = 5 to the experimental data for three different applied electric fields are presented in Figures 7-12 and 7-13B. The result is presented in the form of $\Delta w_c/E$ in Figure 7-12 and as Δw_c in Figure

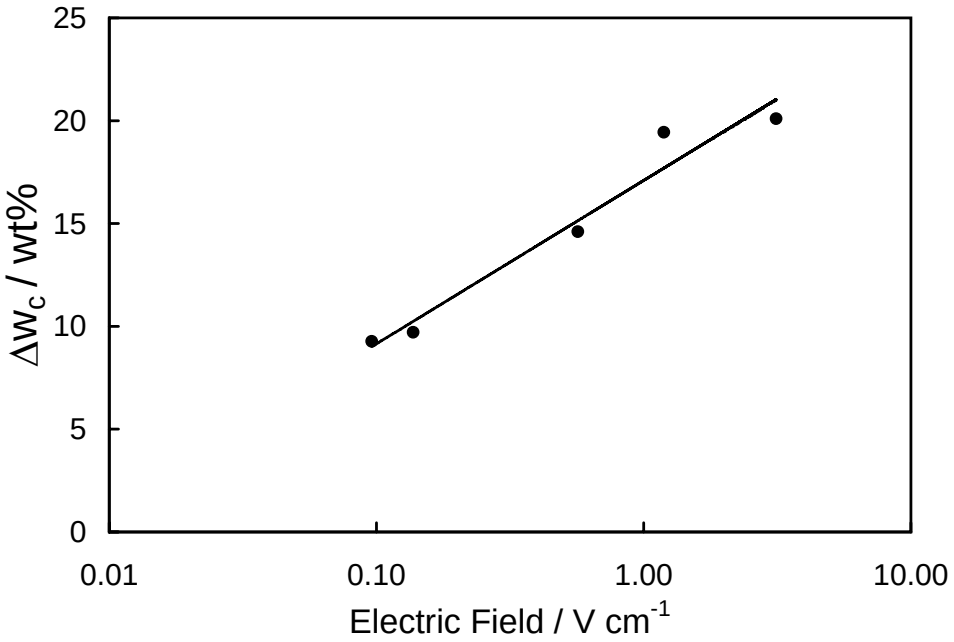

Figure 7-11. Maximum change in solids content plotted as a function of the electric field. The relationship developed from the linear trend line is given by equation (7–3).

7-13. The agreement with experimental data suggests that the change in solids weight percent can be determined at a known electric field and for a large range of operating times.

The interpolation model results using equation (7–4) were plotted for a range of electric fields as presented in Figures 7-14 and 7-15. The results indicate that at larger electric fields the transition from the short-time behavior to long-time behavior occurred much earlier. At very small electric fields, this transition appears to take much longer, and it is difficult to determine when the transition occurs based upon the time scales presented in Figures 7-14 and 7-15.

The interpolation model given as equation (7–4) was selected after consideration of other simpler models. The models considered were

$$\Delta w_c = \frac{w_{\max} t}{k + t} \tag{7–5}$$

and

$$\Delta w_c = w_{\max}(1 - exp(-kt)) \tag{7–6}$$

where $w_{\max}$ is given as

$$w_{\max} = 7.1 Log_{10}(E) + 16.5 \tag{7–7}$$

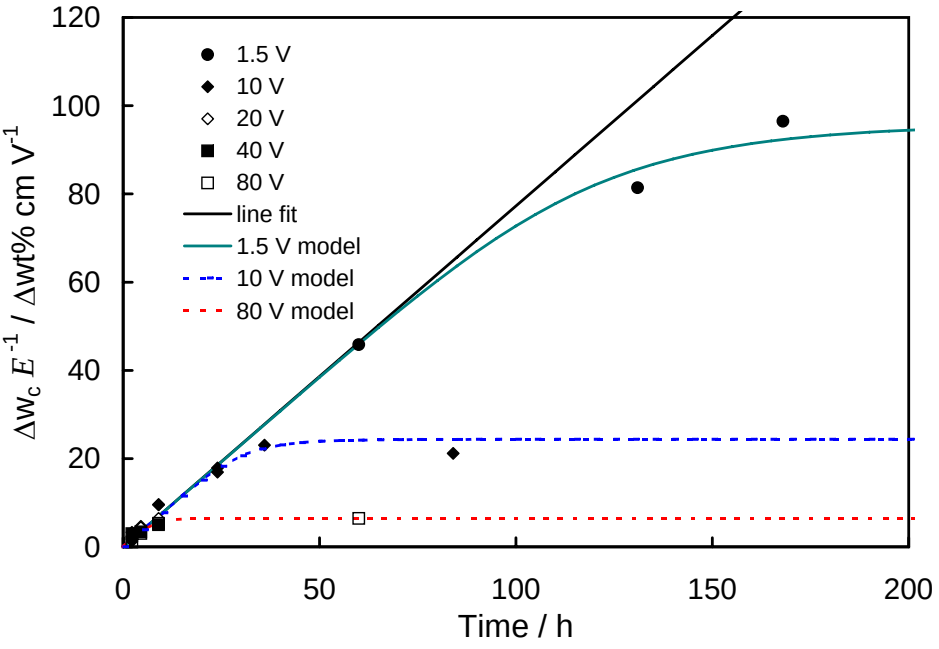

Figure 7-12. Data from Figure 7-10 with the constitutive relationship for long-times (eq. (7–4)) fit to the data for three different electric field sizes.

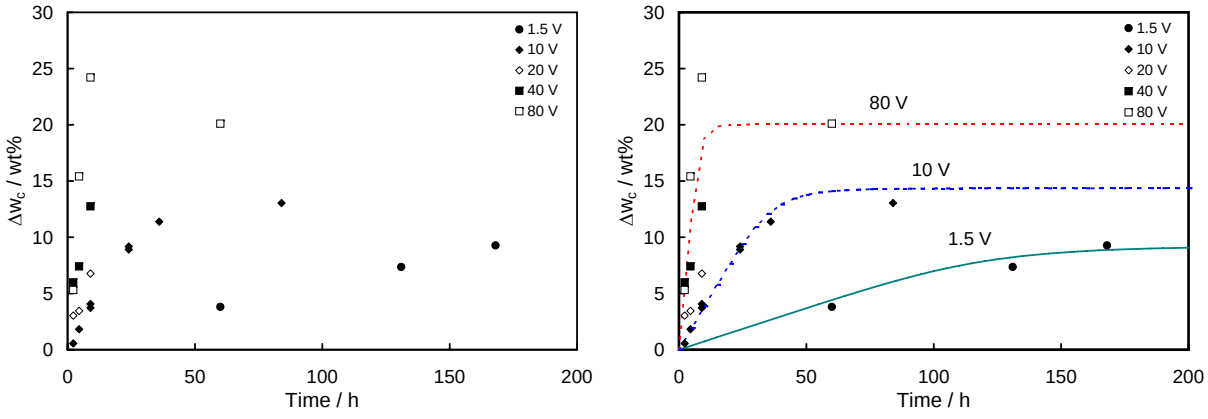

Figure 7-13. Data included in both Figures 7-10 and 7-12 are presented without scaling by the electric field. In B), the constitutive relationship for long times (eq. (7–4)) is fit to the data at three electric field sizes.

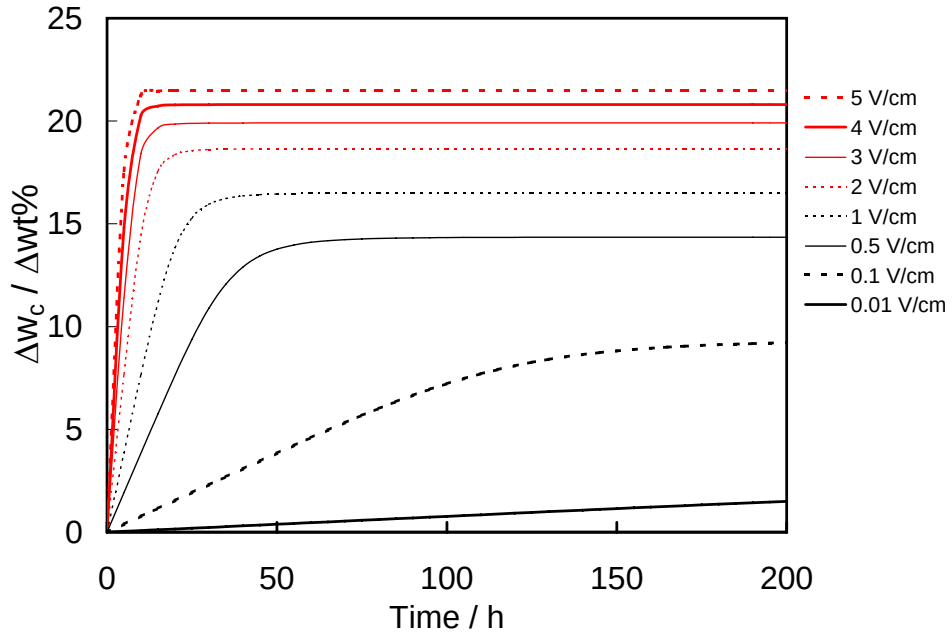

Figure 7-14. Constitutive relationship for long times (eq. (7–4)) plotted for several electric field sizes.

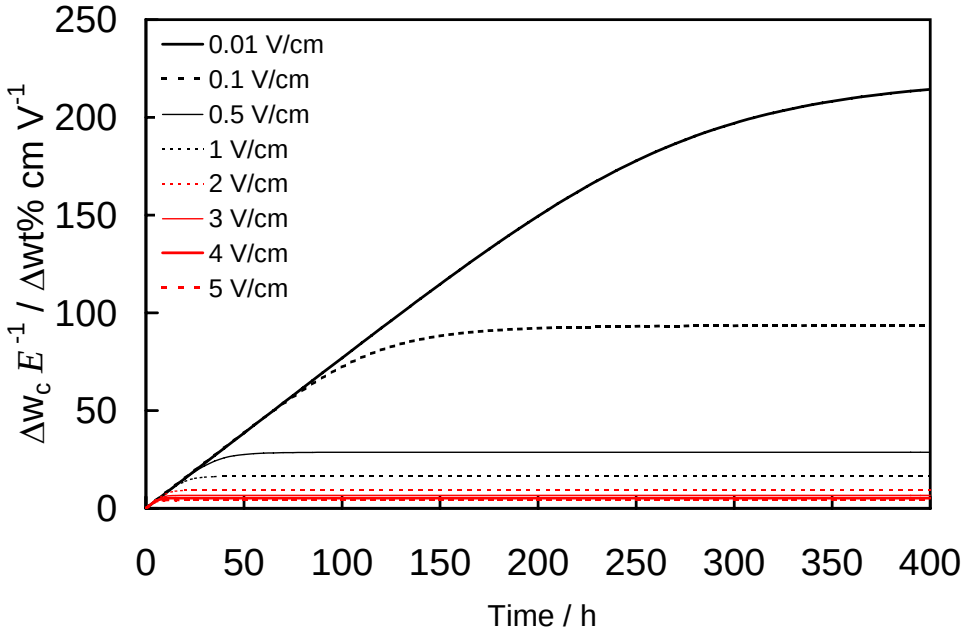

Figure 7-15. Constitutive relationship for long times (eq. (7–4)) plotted for several electric field sizes with the change in solids weight percent scaled by the electric field.

Equation (7–7) is the expression for the maximum solids content given in equation (7–4). The parameter k is dimensionless and is adjusted separately to fit the data for both equations (7–5) and (7–6), and t is operating time with units of hours. These models were fit to the data presented in Figure 7-10. The fit provided by equations (7–5) and 7–6 were less satisfactory than the fit provided by equation (7–4). The behavior of equations (7–5) and (7–6) were non-linear at short times and failed to accurately transition from short-time to long-time behavior. As equation (7–4) was found to provide the best fit to the data, it is introduced within this work as the model that best characterizes the behavior of the bench-top clay dewatering cell.

7.5 Energy Usage Model

The energy requirement (in W-h/kg water removed) for water removal was determined for the bench-top experiments presented in previous sections within this chapter. The values were calculated by multiplying the cell potential V_{cell} by the product of the operating current I and operating time t and then dividing by the mass of water removed during a given experiment. Experimental requirements were determined from a group of bench-top experiments and are presented in Figure 7-16. All values lie within the range of energy requirements reported in the literature. From the raw numbers reported by Fourie *et al.*,[4] an energy requirement of 1.25 W-h/kg of water removed was calculated, while Larue *et al.*[16] reported 700 W-h/kg of water removed. According to the experimental results presented in Figure 7-16, the energy requirement increases with increasing electric field strength. This trend provides insight for the management of operating costs for a large-scale water removal system as the experimental results indicate that operating at smaller electric fields would yield smaller energy costs.

The experimental energy requirements presented in Figure 7-16 were modeled based upon fundamental electrochemical engineering equations in combination with the constitutive relationship for long times (given as equation (7–4)). The results of the model are compared to the experimental data in Figure 7-17. Favorable agreement is found, verifying the electrochemical parameters used for the model and the use of equation (7–4).

The energy requirements of the experimental results from Figures 7-16 and 7-17 were calculated by multiplying the cell potential V_{cell} by the product of the operating current I and operating time t and then dividing by the mass of water removed during a given bench-top

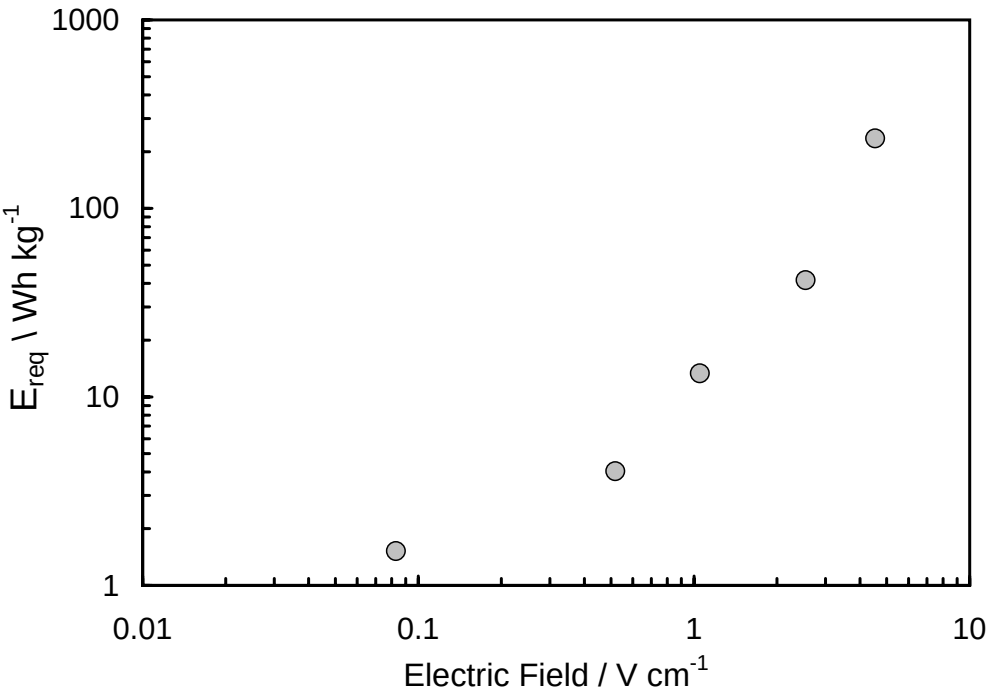

Figure 7-16. Energy required per mass of water removed is given as a function of the electric field.

experiment. As indicated from Figures 7-16 and 7-17, the energy requirements were adversely affected as the electric field increased.

The development of the model presented in Figure 7-17 included the calculation of the cell potential V_{cell} as a function of operating current density i. The relationship between the cell potential V_{cell} and the operating current density i is given as

$$V_{\text{cell}} = 1.23 + \eta_a - \eta_c - iR_e \tag{7–8}$$

where η_a represents the anodic overpotential, η_c represents the cathodic overpotential and R_e represents the Ohmic resistance of the clay suspension. The value of 1.23 (Volts) is the minimum potential required to promote the hydrolysis of water. The operating current I, or current density i, was controlled as an input with the cell potential V_{cell} calculated as a response variable. The values of η_a, η_c, and R_e were then calculated in order to determine V_{cell} at a given operating current density i.

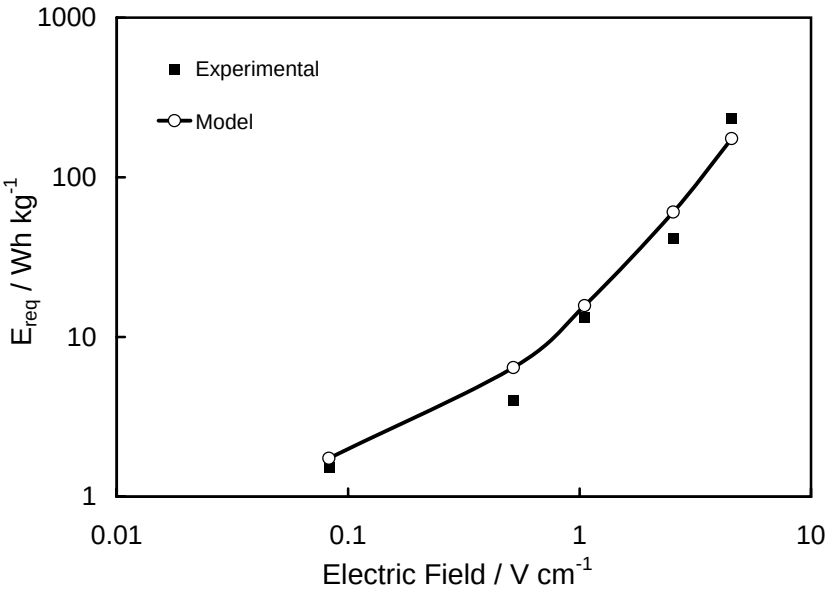

Figure 7-17. Data presented in Figure 7-16 compared with a modeled energy requirement curve. Energy required per mass of water removed is given as a function of the electric field.

To calculate η_a, the Butler-Volmer equation

$$i = i_o(exp(\eta_a b_{aa}) - exp(-\eta_a b_{ac})) \tag{7–9}$$

was used where

$$b_{aa} = \frac{\alpha F}{RT} \tag{7–10}$$

and

$$b_{ac} = \frac{(1-\alpha)F}{RT} \tag{7–11}$$

with α being the dimensionless symmetry factor. The Butler-Volmer equation (given by equation (7–9)) is written for a reversible reaction with both an anodic and cathodic contribution. At large and positive overpotentials, the anodic contribution dominates and the cathodic contribution can be neglected simplifying equation (7–9) to

$$i = i_o exp(\eta_a b_{ca}) \tag{7–12}$$

Conversely, when operating at large and negative overpotentials, the cathodic contribution dominates and the anodic contribution can be neglected. This allows equation (7–9) to be

simplified to

$$i = -i_o exp(-\eta_a b_{cc}) \tag{7–13}$$

However, in order to solve for η_a, an iterative method was performed as the Butler-Volmer equation (given by equation (7–9)) is rearranged to give

$$\eta_{a,n+1} = \frac{ln(\frac{i}{i_o} + exp(-\eta_{a,n} b_{ac}))}{b_{aa}} \tag{7–14}$$

where $\eta_{a,n}$ represents the initial guess for the anodic overpotential. The initial guess was approximated by the linear form of the Butler-Volmer equation

$$i = i_o(b_{aa} + b_{ac})\eta_a \tag{7–15}$$

which is rearranged to

$$\eta_{a,n} = \frac{i}{i_o(b_{aa} + b_{ac})} \tag{7–16}$$

The linear form of the Butler-Volmer equation is valid only at very small overpotentials where neither anodic or cathodic contributions can be completely neglected. A spreadsheet program was used to perform the iterations. Each calculation of $\eta_{a,n+1}$ was used as the subsequent input value for $\eta_{a,n}$ which was continuously plugged back into equation (7–14) until the resulting value of $\eta_{a,n+1}$ no longer and the solution converged.

A similar iterative method was used to determine the cathodic overpotential η_c. The Butler-Volmer equation

$$i = i_o(exp(\eta_c b_{ca}) - exp(-\eta_c b_{cc})) \tag{7–17}$$

was again used where

$$b_{ca} = \frac{\alpha F}{RT} \tag{7–18}$$

and

$$b_{cc} = \frac{(1-\alpha)F}{RT} \tag{7–19}$$

The Butler-Volmer equation is rearranged as

$$\eta_{c,n+1} = \frac{-ln(-\frac{i}{i_o} + exp(\eta_{c,n} b_{ca}))}{b_{cc}} \tag{7–20}$$

where $\eta_{c,n}$ represents the initial guess used. The initial guess, was again approximated by the linear form of the Butler-Volmer equation

$$i = i_o(b_{aa} + b_{ac})\eta_c \tag{7–21}$$

which is rearranged to

$$\eta_{c,n} = \frac{i}{i_o(b_{aa} + b_{ac})} \tag{7–22}$$

In order to calculate V_{cell}, the Ohmic resistance of the electrolyte R_e must also be calculated. The methods to calculate the Ohmic resistance R_e experimentally are described in Section 7.6.

Upon determination of V_{cell} for a given set of operating conditions, the energy requirement (in W-h/kg of water removed) was calculated as a function of operating time t for a range of electric field values. The objective of this section was to model the experimental data presented in Figure 7-16 based upon the use of fundamental electrochemical engineering relationships and the constitutive relationship for long times (given as equation (7–4)). Therefore, the operating current density i was controlled to yield the same range of electric field values for comparison with the experimental results presented in Figure 7-16. In order to model the energy requirement, the amount of water removed was calculated as a function of time for a given electric field using the constitutive relationship for long times (given as equation (7–4)). As equation (7–4) incorporates the operating time, the energy requirement can be plotted as a function of operating time at a specified electric field. This was performed separately at different electric field values to develop the modeled energy requirement curve presented in Figure 7-17. The values calculated to develop the energy requirement curve are presented in Table 7-1. The parameters used for the Butler-Volmer equation and the expression for the cell potential V_{cell} are given in Table 7-2. Note that the electrolyte resistance R_e and the electrolyte resistivity ρ_e are related as

$$R_e = \frac{\rho A_c}{d} \tag{7–23}$$

where A_c represents the cross-sectional area of the cell, which corresponds to the nominal area of both the anode and cathode, and d represents the distance between the electrodes.

An example of the energy requirement given as a function of operating time at a specified electric field is presented in Figure 7-18. The model in Figure 7-17 was calculated for the same

Table 7-1. Results of calculations used to model the energy requirements presented in Figure 7-17.

E / $\mathrm{Vcm^{-1}}$	$V_{\mathrm{cell}} \times I$ / W	water removed / kg	t / h	energy requirement / $\mathrm{Whkg^{-1}}$
0.08	0.01	0.34	60	1.7
0.52	0.24	0.34	9	6.4
1.05	0.95	0.54	9	15.7
2.54	5.34	0.79	9	60.6
4.54	16.90	0.87	9	174.8

Table 7-2. Values of parameters and variables used in energy usage model.

parameter	numerical value
ρ / Ωcm	1500
b_{aa},b_{ac},b_{ca},b_{cc} / $\mathrm{V^{-1}}$	10
α	0.5
i_o / $\mathrm{mAcm^{-2}}$	1.0
A_c / $\mathrm{cm^2}$	63.6
d / cm	20

operating time as the experimental data. However, a terminal operating time was identified in Figure 7-18 where the data transitions from nonlinear behavior to linear behavior. Once the linear behavior dominates, the solids weight percent has reached its maximum based upon the constitutive relationship for long times (given as equation (7–4)). Therefore, as indicated in Figure 7-18B, the transition from nonlinear to linear behavior can be determined which is defined as the terminal operating time to achieve maximum removal of water. This behavior was observed at a range of electric field values, with each yielding a different terminal operating time. At the terminal operating time, the corresponding energy requirement can be identified from the data as presented in Figure 7-18. The model was calculated separately based upon the terminal operating time identified at each electric field. This result is presented in Figure 7-19. Both models are compared together with the experimental data as presented in Figure 7-20. The discrepancies in the two models are concluded to be based upon the use of different operating times as this was the only parameter changed. The difference in operating times are included in Figure 7-21. The modeled energy requirements are found to vary as a function of operating time as presented in Figure 7-20. For future energy usage models, it is suggested that the operating time should be the same as that of experiments to obtain favorable agreement.

The agreement of the model with the experimental data suggests that the constitutive relationships for long times (given as equation (7–4)) in combination with electrochemical

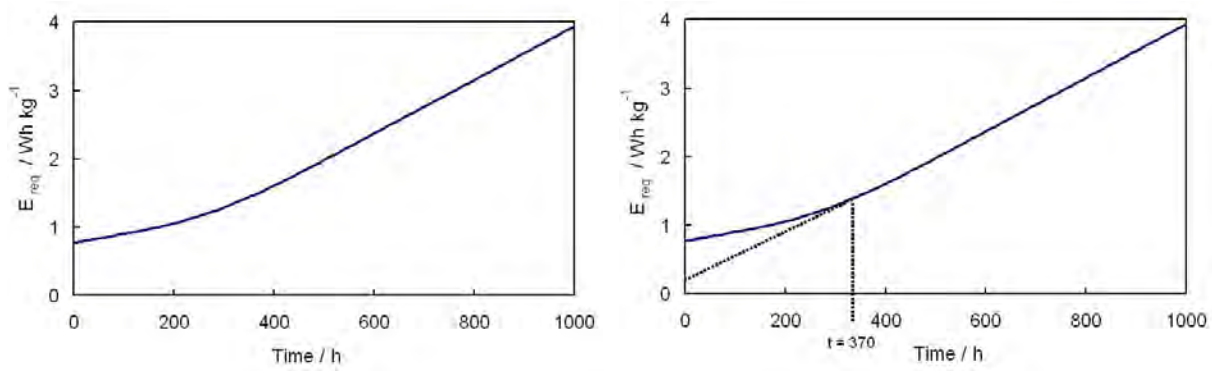

Figure 7-18. Energy requirement is given as a function of operating time. In B), the transition from linear to nonlinear behavior is indicated.

relationships can be used to effectively project energy requirements. This further validates the ability of the constitutive relationship (given as equation (7–4)) to characterize the water removal from clay using the bench-top experiment.

7.6 Electrochemical Characterization

A manually generated polarization curve is presented in Figure 7-22. Each data point was generated individually from separate experiments within the matrix discussed in Section 7.3. After each potential was applied, the current was recorded after reaching steady state. In some cases polarization curves can be used to identify electrochemical reactions or mechanisms within the cell; however, for the work presented in this section the objective was to determine whether the dominant resistance in the cell was controlled by kinetic, Ohmic, or mass transfer limitations. The linear behavior presented in Figure 7-22 indicates that the dominant resistance in the bench-top experimental cell was the Ohmic resistance. This suggests that for operating conditions of the experimental data presented in Figure 7-22 that no adverse issues occurred regarding the electrodes used for the experiments.

An electrochemical impedance spectroscopy (EIS) scan was also performed on the bench-top experiment. The impedance scan is presented in Figure 7-23. The vertical dashed line represents the high frequency asymptote. The high frequency asymptote gives the Ohmic resistance which is 152.5 Ohms. A re-scaled view of Figure 7-23 is presented in Figure 7-24 which includes the frequency range used for the impedance scan. The impedance results also suggest that the Ohmic resistance is the dominant resistance of the cell as the magnitude of the

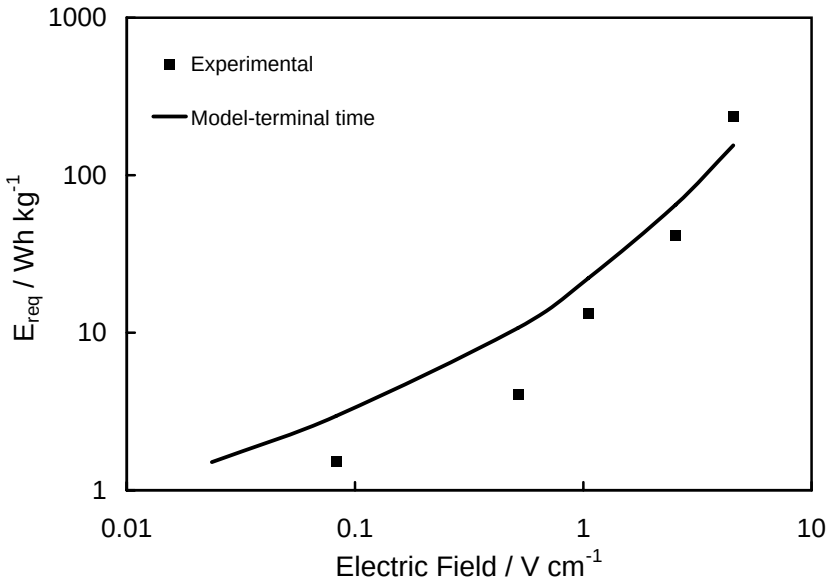

Figure 7-19. Energy requirement as a function of the electric field for the maximum separation achievable at the applied electric field E. Values were determined using the terminal operating time indicated by the method presented in Figure 7-18A.

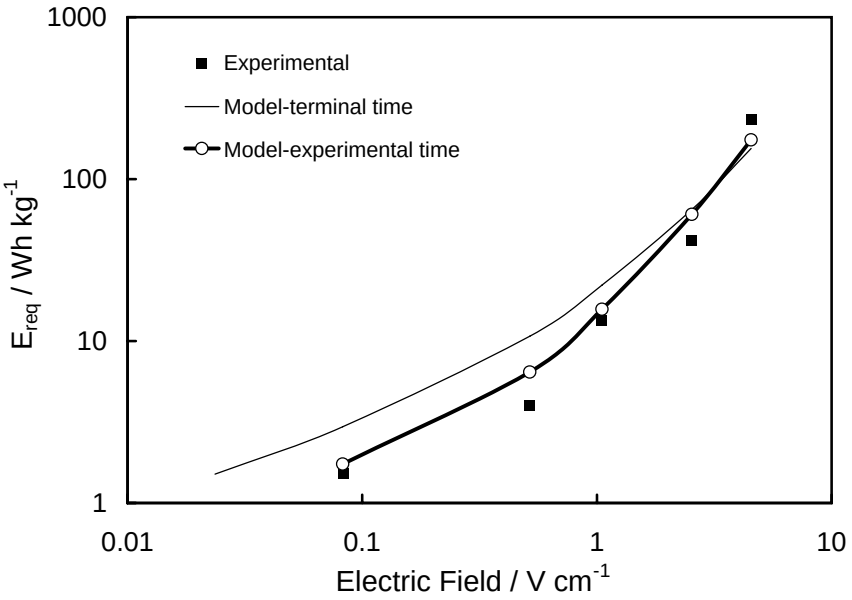

Figure 7-20. Data presented in Figure 7-17 are included for comparison to the model based upon the terminal operating time.

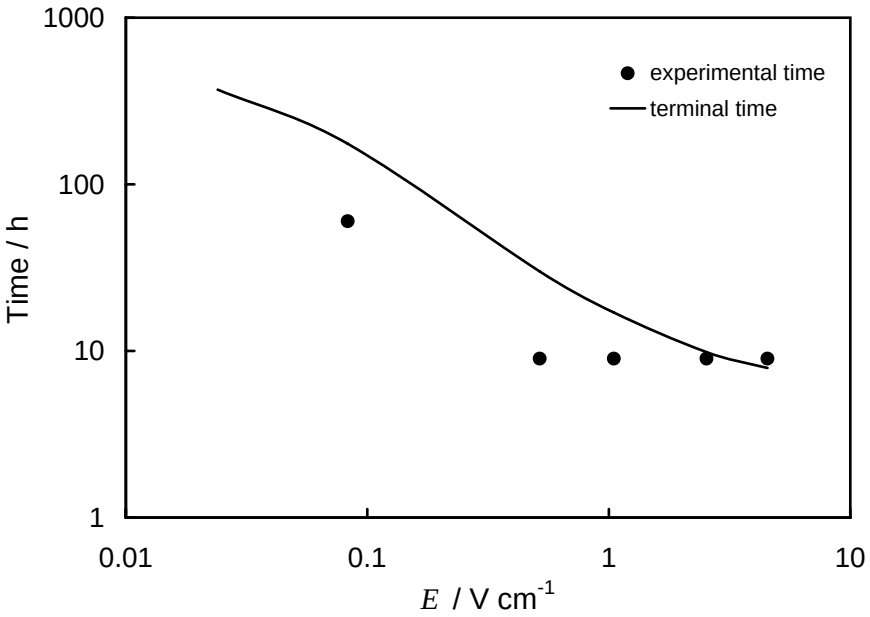

Figure 7-21. Two sets of operating times used for the model are given as a function of the electric field.

impedance is very small compared to the absolute value of the Ohmic resistance. Therefore, the qualitative observations from the impedance scan were consistent with that from the polarization curve.

The Ohmic resistance of the cell is used to determine the conductivity of clay suspension. The clay suspension was approximately 10% solids by mass (or weight) when both polarization and impedance plots were generated. By including the calculated Ohmic resistance (R_e) as well as the bench-top cell dimensions, the conductivity (κ) can be calculated as

$$\kappa = \frac{d}{R_e A_c} \tag{7–24}$$

where d is distance between electrodes (in cm) and A_c is the cross sectional area of the cell (in cm^2). From equation (7–24) the conductivity was calculated as 700 microSiemens per centimeter ($\mu S/cm$). The conductivity was also calculated for the exact same clay sample using a DC (direct current) measurement. The Ohmic resistance was calculated by taking the potential drop measured between two Ag/AgCl reference electrodes within the cell and dividing it by the current flowing through the cell. From this method, the conductivity was calculated as 682 $\mu S/cm$ using equation (7–24) with d representing the distance between the two reference electrodes.

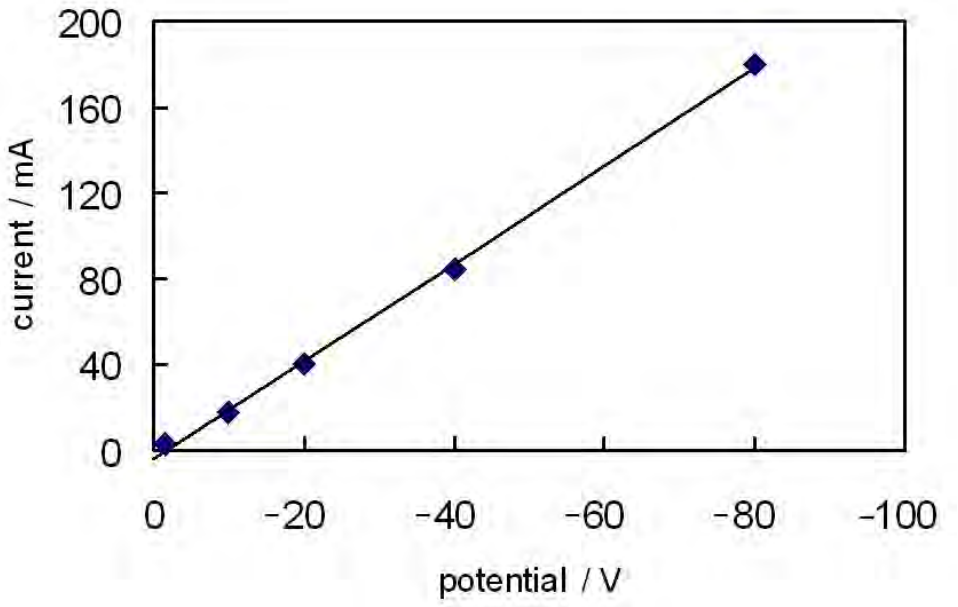

Figure 7-22. Polarization curve generated from bench-top cell loaded with clay suspension. Each data point was individually measured from separate experiments for each applied potential.

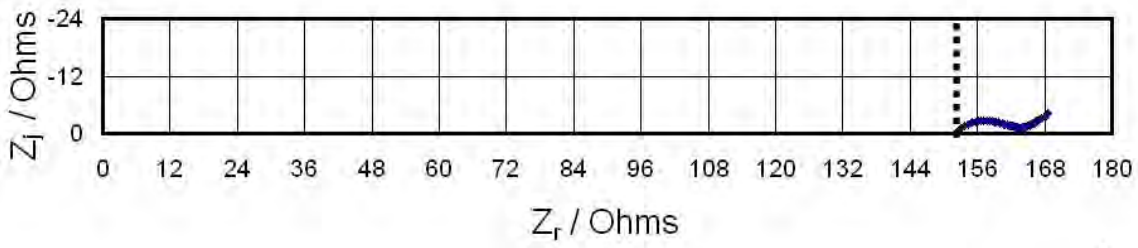

Figure 7-23. Impedance scan generated at open circuit potential on bench-top cell loaded with clay suspension.

Therefore, no significant difference in the calculated conductivity was found, regardless of the different techniques used. This further indicates that either method should be valid for calculating conductivity. These values are compared to reported conductivities of different clay suspensions from the literature as presented in Table 7-3.

The polarization curve and the impedance scan presented in this section were used to characterize further the bench-top experiments presented in this chapter. Both methods were used to determine the dominating resistance within the bench-top cell. Both methods indicated that the Ohmic resistance was the dominating resistance of the cell. This meant that any kinetic limitations due to electrochemical reactions occurring at the electrode surfaces was negligible

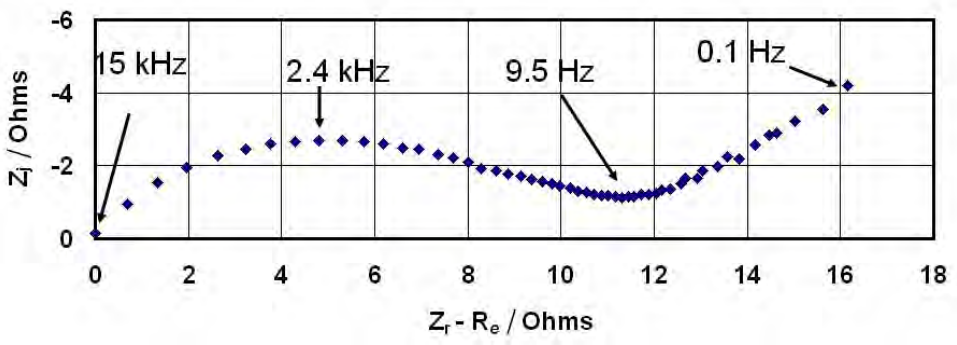

Figure 7-24. Re-scaled perspective of impedance scan presented in Figure 7-23 with the axis for the real impedance subtracted by the Ohmic resistance R_e.

Table 7-3. Conductivities of clay suspensions from this work are compared with those reported in the literature. EIS and DC were the methods used to experimentally determine the conductivity of clay suspensions used within this work.

Source	Clay type	conductivity / $\mu\mathrm{Scm}^{-1}$
EIS	Mosaic phosphatic clay	701
DC	Mosaic phosphatic clay	682
McLean[69]	Florida phosphatic clay	700
Shang[14]	Ontario, Canada natural soil clay	410
Shang *et al.*[85]	Ottawa, Canada natural soil clay	256-2520

in comparison to the Ohmic resistance of the cell. The conductivity of the clay suspension was determined from potentiostatic experiments and compared to the conductivity found from the impedance results. Very good agreement was found for the conductivities calculated from both methods as presented and compared with other results in the literature in Table 7-3.

CHAPTER 8
SIMULATIONS FOR LARGE-SCALE DEWATERING SYSTEMS

Simulations were performed to assess different electrode configurations in a simulated one-square-mile clay settling area (CSA). CP_3D, a mathematical model developed at the University of Florida, was used to perform the simulations. The background for the mathematical framework of the model is presented which is based upon its primary application involving cathodic protection of buried pipelines. The application of the model can be easily fit to simulate cathodes and anodes in a clay settling pond. The relationships discovered in the experimental work from Chapter 7 were used to make assumptions regarding the development and results of the simulations.

8.1 Introduction to CP_3D and Application for Cathodic Protection

CP_3D is a computer program developed by Professor Mark Orazem's electrochemical engineering research group to model cathodic protection of buried pipelines.[86,87] It allows for the creation of a visualized three-dimensional cathodic protection system of buried structures. This program was developed as a tool to improve the ability to assess pipeline conditions. There are several parameters that can be used and varied in the calculations performed by the mathematical model. Some of these include coating flaw (or holiday) size, soil resistivity, cathodic protection level, coating condition, depth of cover, and pipeline thickness. In order to replicate above-ground survey techniques within CP_3D, a soil surface is created and utilized within the program. The soil surface is made up of nodes where on- and off-potentials are calculated by the model at each node's exact location. The on-potential represents the potential measured or calculated when the cathodic protection (CP) current is turned on or energized. The off-potential represents the potential when the CP current is off. In order to study the details of interest, soil surfaces are typically placed above the anode and also above the coating flaw located on the pipeline. The soil surfaces are located in proximity of the anode and coating flaw because these locations represent areas where a useful distribution of on- and off-potentials are found. Figure 8-1 is an image of the three dimensional environment of CP_3D showing the arrangement of the soil surface in respect to the pipeline and the coating flaw. The soil surface must be limited in size to avoid putting a strain on the resources of the program. However, in a real-life field survey, measurements may include the entire length of the pipeline in order

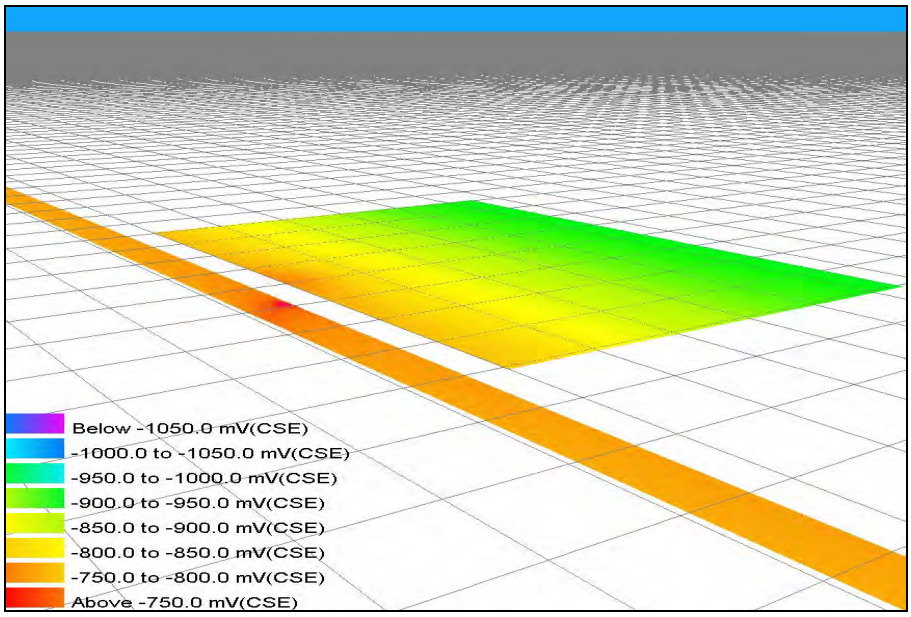

Figure 8-1. CP_3D image showing the physical orientation of the soil surface with respect to the pipeline. The darker area on the pipeline represents the coating flaw or holiday.

to inspect its overall integrity. Since the area of interest (i.e., location of the coating flaw) is specified within CP_3D, a soil surface that covers the entire pipeline is not necessary. A matrix of simulations were performed in another study using CP_3D to develop design equations which incorporate pipeline and soil parameters in the assessment of survey indications to predict coating flaw size.[88] This study has major implications on how pipeline survey data should be interpreted to assess pipeline integrity.

8.1.1 Mathematical Development

The governing equations for the CP_3D model work as a basis for all calculations made by the program. For protection of underground pipelines, the model accounts for the current flow through the soil, the pipeline (or cathode), and through the circuitry back to the anode. There are two different domains which are governed separately in the model. One is the outer domain which is represented by the soil. The other is the inner domain which represents the pipeline, the anode, and the electrical wiring that connects them.

The first of the governing equations for the outer domain is the material balance of a solute species

$$\frac{\partial c_i}{\partial t} = -(\nabla \cdot \boldsymbol{N}_i) + R_i \tag{8–1}$$

where c_i is the concentration of a species $\boldsymbol{i}$, N_i is the net flux vector for species $\boldsymbol{i}$, and R_i represents the rate of generation of species $\boldsymbol{i}$ due to homogeneous reactions. Homogeneous reactions are defined as the reactions which occur in the electrolyte and not at the electrode surfaces, which in this system are either the anode or the pipeline. Equation (8–1) must be coupled with the equation of electroneutrality in order to account for the concentrations and potentials that are present in the soil. The equation for electroneutrality is given as

$$\sum_i z_i c_i = 0 \tag{8–2}$$

where z_i represents the charge associated with species $\boldsymbol{i}$. For a dilute electrolyte, the flux of a given species can be given based on its contributions from convection, diffusion, and migration as

$$\boldsymbol{N}_i = v c_i - D_i \nabla c_i - z_i u_i F c_i \nabla \Phi \tag{8–3}$$

where v is the fluid velocity, D_i is the diffusion coefficient for species i, u_i is the mobility, F is Faraday's constant and Φ represents the distribution of potential in the domain. The diffusion coefficient is related to the mobility by the Nernst-Einstein equation as

$$\boldsymbol{D}_i = RTu_i \tag{8–4}$$

where R is the gas constant and T is the temperature. The equation for current density is based on the contribution of the movement of each ionic species and is given as

$$i = F \sum_i z_i N_i \tag{8–5}$$

If the concentration of ions in the electrolyte are uniform and steady state is assumed the equation for current density can be written as Ohm's law. Therefore,

$$i = -\kappa \nabla \Phi \tag{8–6}$$

where κ represents the conductivity of the electrolyte. The conductivity is given by

$$\kappa = F^2 \sum_i z_i^2 u_i c_i \tag{8–7}$$

and it is uniform because the concentration is uniform. Due to uniform concentration, the potential is governed by Laplace's equation which is given as

$$\nabla^2 \Phi = 0 \tag{8–8}$$

Laplace's equation can be derived by first multiplying equation (8–1) by $z_i F$ and summing over all ionic species which gives

$$\frac{\partial}{\partial t} F \sum_i z_i c_i = -\nabla \cdot F \sum_i z_i N_i + F \sum_i z_i R_i \tag{8–9}$$

From electroneutrality and from the assumption that R_i is zero because it represents reactions in the bulk, equation (8–9) reduces to

$$\nabla \cdot i = 0 \tag{8–10}$$

By substituting Ohm's law into equation (8–10) and by the assumption of constant conductivity, Laplace's equation is obtained as equation (8–8).

Since it is assumed that there are no concentration gradients in the soil or electrolyte, the concentration gradients due to reactions at the surface of the anode and pipeline are treated so that they lie in a thin layer adjacent to the electrode surfaces.[86] The concentration gradients in this thin layer are incorporated into the boundary condition which is based on electrochemical reactions.

For the inner domain, there are also some assumptions that must be made. For example, this model treats the potential through the pipeline as nonuniform. Previously, pipelines of shorter lengths have neglected the potential drop along the pipeline steel.[89] However, it has been proven that for long pipelines this potential drop can not be neglected.[90–92]

Laplace's equation also governs the flow of current through the pipe steel, anode, and the connecting wires. It is given as

$$\nabla \cdot (\kappa \nabla V) = 0 \tag{8–11}$$

where κ is the conductivity of either the pipeline steel, the anode, or the electrical wires and V is the drop in potential of the metal from a uniform value. The conductivity of the inner domain is not constant because it is not the same for the anode, pipeline, or the copper connecting wires.

Laplace's equation can be simplified as

$$\Delta V = IR = I\rho\frac{L}{A} \tag{8–12}$$

which accounts for the potential drop along the copper connecting wires. For this equation, R represents the resistance of the wire, ρ represents the electrical resistivity of the wire, L is the length, and A is the cross-sectional area of the connecting wire.

The two domains are coupled through boundary conditions. The boundary conditions develop a relationship between the local values of potential and the current density on the metal surface.[86] This relationship varies depending on whether the type of surface is the bare metal pipeline, the coated pipeline, a sacrificial anode, or an impressed current anode.

8.1.2 Bare Steel

For a non-coated pipeline, bare steel is exposed to the soil. Bare steel can also be exposed in places where a coated pipeline has scratches or flaws on it. There are three different electrochemical reactions that can take place at the surface of the bare steel. These reactions include the oxidation of iron, reduction of oxygen, and hydrogen evolution. Hydrogen evolution can occur if the metal is polarized to very negative potentials. The current contribution of each of these reactions can be included in the relationship between local current density i, the potential of the steel V, and the potential of the soil next to the steel Φ. The following equation[93,94] represents the boundary condition of the bare metal pipeline and the adjacent soil and is given as

$$i = 10^{\frac{(V-\Phi-E_{Fe})}{\beta_{Fe}}} - (\frac{1}{i_{lim,O_2}} + 10^{\frac{(V-\Phi-E_{O_2})}{\beta_{O_2}}})^{-1} - 10^{\frac{-(V-\Phi-E_{H_2})}{\beta_{H_2}}} \tag{8–13}$$

The term E_{Fe} represents the equilibrium potential for the oxidation of iron and this term is written similarly for the reactions of oxygen reduction and hydrogen evolution. The β term is given for each reaction and it represents the tafel slope of the corresponding reaction. The i_{lim,O_2} term represents the mass transfer limiting current density of oxygen reduction at the metal surface. Therefore, the current contribution of oxygen reduction can not be larger than the value of i_{lim,O_2}.

8.1.3 Coated Steel

For coated pipelines, treatment of the reactions at the pipeline-soil interface must be different than that of bare steel. The purpose of the coating is to provide resistance for the transport of reducing species to the metal surface. It also reduces the amount of CP current that

is needed to protect a given pipeline. There are two main types of coating behavior and these are both modeled differently. One model of coating behavior is where the transport of species is uniform through the coating. The electrochemical reactions take place once the transported species reach the coating-metal interface. These reactions are driven by the difference in potential V of the metal and the potential Φ_{in} just underneath the coating but still above the metal or steel.

The other type of model involves the presence of pores which allow for the transport of solute species to take place. It has been shown that the pore structure will expand after it has been contacted with water and that the conductivity of the coating increases with time after its exposure to water.[95] The resistivity of the coating with pores is a function of the number of pores per unit area. The electrochemical reactions also take place at the coating-metal interface for this model and these reactions are also driven by the potential difference between V and Φ_{in}.

It has been shown that the non-porous coated steel forms a diffusion barrier when put in aqueous environments. As the water is adsorbed by the coating, the steel can be polarized slightly even if the coating is disbonded.[96–99] Equation (8–13) can be modified based on either model of transport through the coating.[100,101] The current density can be written as a function of the potential drop through the coating as

$$i = \frac{\Phi - \Phi_{in}}{\rho\delta} \tag{8–14}$$

where Φ is the potential of the soil adjacent to the coating, ρ is the resistivity of the coating, and δ is the thickness of the coating. By writing the current density in terms of electrochemical reactions it is also given as

$$i = \frac{A_{pore}}{A}[10^{\frac{(V-\Phi_{in}-E_{Fe})}{\beta_{Fe}}} - (\frac{1}{(1-\alpha_{blk})i_{lim,O_2}} + 10^{\frac{(V-\Phi_{in}-E_{O_2})}{\beta_{O_2}}})^{-1} - 10^{-\frac{(V-\Phi_{in}-E_{H_2})}{\beta_{O_2}}}] \tag{8–15}$$

where $\frac{A_{pore}}{A}$ is the effective surface area available for reactions to occur and α_{block} is the reduction of the transport of oxygen through the diffusion barrier. In order to determine the values for the current density (i) and Φ_{in}, both equation (8–14) and equation (8–15) are solved simultaneously by the Newton-Ralphson method.

8.1.4 Sacrificial and Impressed Current Anodes

The reactions at the surface of a sacrificial anode typically include oxygen reduction and the corrosion of the anode. The current density expression is treated similarly as that of the bare steel except that the hydrogen evolution reaction is neglected. The expression is given as

$$i = i_{lim,O_2}(10^{\frac{V-\Phi-E_{corr}}{\beta_{anode}}} - 1) \tag{8–16}$$

where E_{corr} is the corrosion potential at the anode and β_{anode} is the corresponding Tafel slope for the anodic corrosion reaction.

The current density model equation for impressed current anodes is similar to that of the galvanic or sacrificial anode. The only difference is the inclusion of the rectifier potential setting. This equation is given as

$$i = i_{lim,O_2}(10^{\frac{V-\Phi-\Delta V_{rect}-E_{corr}}{\beta_{anode}}} - 1) \tag{8–17}$$

This equation must be modified if there are chloride ions present in the soil.

8.2 Application for Clay Dewatering

CP_3D was used to develop different electrode configurations to simulate the design of a large scale water removal system in a clay settling area. Simulations specified all electrodes as constant potential surfaces. The pipelines within the software program are considered, and more appropriately referred to, as cathodes in this section. The governing equation through the electrolyte or clay slurry is Laplace's equation given as equation (8–8). In solving for Laplace's equation, one of the key assumptions is that there are no concentration gradients. Therefore, since the concentration is uniform, the conductivity must also be uniform.

8.2.1 Large-scale Simulations

Two different electrode configurations were explored. The first configuration included cylindrical electrodes that were 6 inches in diameter and placed 3 feet apart. The electrodes were horizontally oriented and one mile long to be consistent with a one-square-mile clay settling area. They were equally spaced for the entire length of one mile. An illustration is given in Figure 8-2 showing cylindrical cathodes placed near the surface of the simulated clay settling area (CSA) and cylindrical anodes placed near the bottom. The depth of the CSA is simulated as 40 feet. The electrode configuration yielded a uniform electric field as shown by the

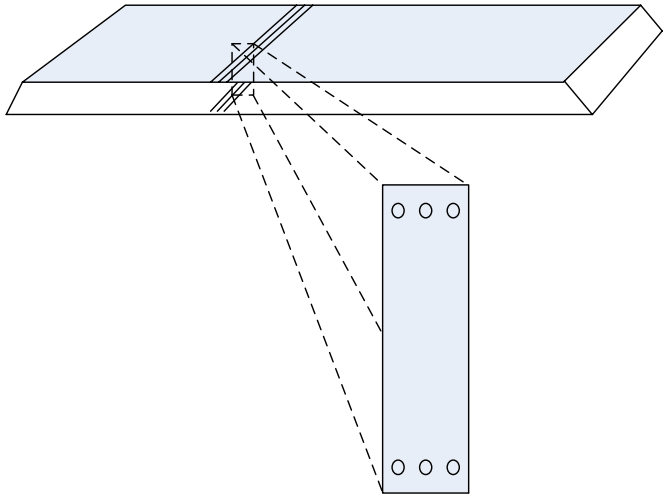

Figure 8-2. Representation of a large clay settling area with one mile long cylindrical electrodes spaced equally along top and bottom surfaces. The zoomed in portion represents a cross-section of the cylindrical electrodes. Although only rows of three cylinders are shown, the simulation was scaled for rows that extend to a distance of one mile.

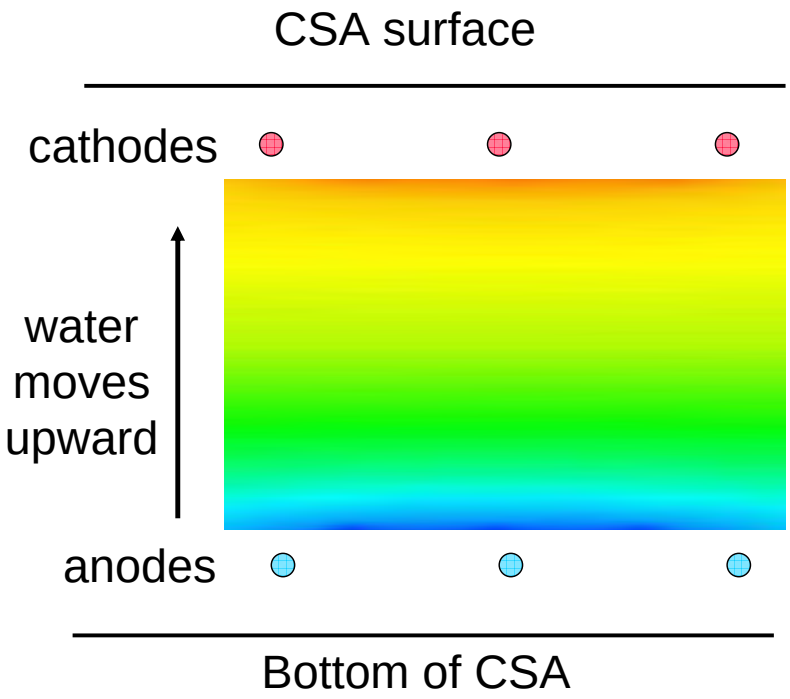

Figure 8-3. Illustration of horizontally oriented electrode configuration presented in Figure 8-2 with the calculated potential distribution from CP_3D presented as a false-color image.

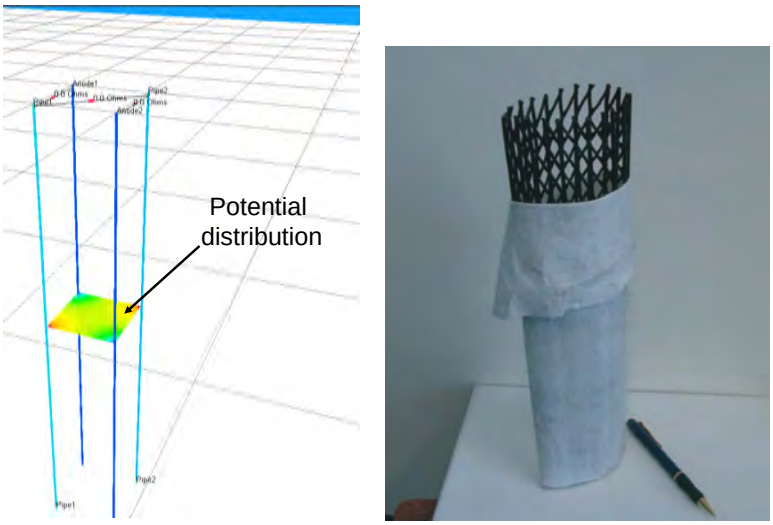

A B

Figure 8-4. Vertically oriented electrodes are presented: A) CP_3D image of vertically oriented electrode configuration; and B) photograph of a geosynthetic electrode covered with a filter cloth required as a separator for removal of water using a vertically oriented cathode (taken from Fourie *et al.*,[4] Copyright © 2008 NRC Canada or its licensors and reproduced with permission).

potential distribution calculated by CP_3D presented in Figure 8-3. The uniform change in color with respect to the position between the top row of cathodes and the bottom row of anodes is representative of a uniform potential distribution. This behavior was due to the close spacing of the electrodes and by having only cathodes in the row near the surface and only anodes in the row at the bottom.

The second configuration explored is represented in Figure 8-4A. For this simulation, the electrodes were oriented vertically, with cathodes and anodes placed diagonally from one another. The average electric field was calculated, and the applied potential was adjusted such that the average electric field was the same for the two different configurations (i.e., horizontal and vertical). The visualization in Figure 8-4A represents a unit cell that is scaled up by adding additional electrodes to cover an entire square mile. A separator or filter cloth is required for vertically oriented cathodes such that the clay is filtered from the water entering the inner diameter of the cathode as pictured in Figure 8-4B. The electric field corresponding to the potential distribution shown in Figure 8-4A is presented in Figure 8-5. The location near the center where the electric field is flat represents a region where the electric field tends toward

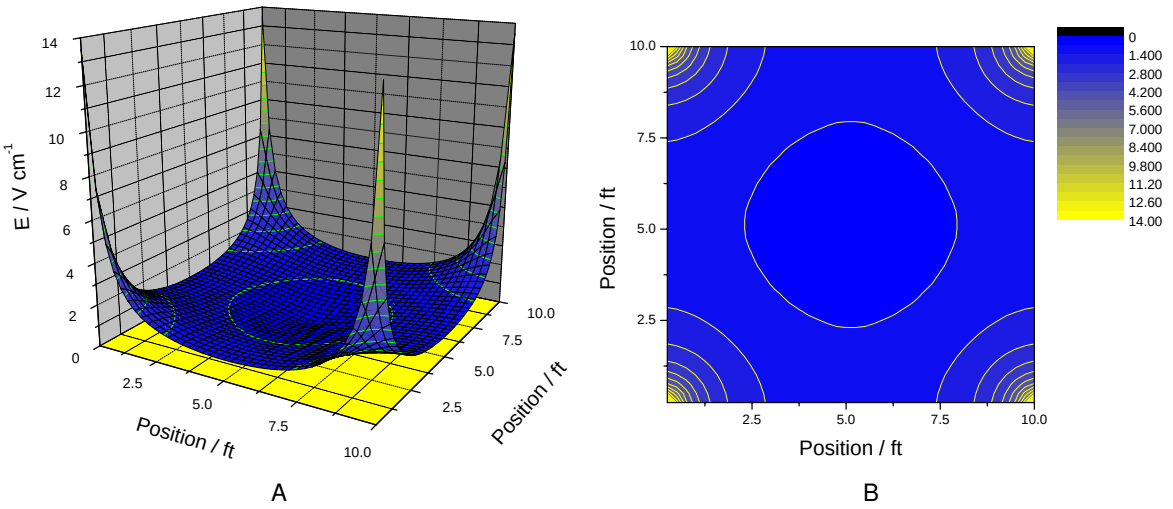

Figure 8-5. Illustration of the electric field calculated from the simulation presented in Figure 8-4A: A) three dimensional representation, and B) two dimensional representation.

zero. The peaks shown at the corners represent areas where the electric field is much stronger. The experimental work demonstrated a relationship between the size of the electric field and the solids content (or solids weight percent) for a given operating time. Therefore, the nonuniform electric field would have nonuniform drying with locations located in proximity of the electrodes (i.e., the four corners in Figure 8-4) having a strong change in solids content and the locations away from the electrodes (i.e., at the center in Figure 8-4) maintaining the consistency of the original content of the suspension.

Time and power requirements are presented in Tables 8-1 and 8-2 based on simulation results for the two different electrode configurations. The simulation result for the vertical configuration reported in Table 8-1 was represented in Figure 8-4. A comparison with a bench-top experimental result is also included in each table. For the bench-top experimental results presented in Tables 8-1 and 8-2, the electric field and energy requirement values were reported directly from the experiment. The time required was determined using equation (7–4) presented in Section 7.4. The power and energy calculations for these experimental results were based on a hypothetical scale-up to a one-square-mile clay settling area. These values do not represent the bench-top experimental cell's actual operating power and energy requirements. The values in Table 8-1 are based on a solids content increase from 10 to 25 wt% for a one-square-mile clay settling area and Table 8-2 is based on an increase from 10 to 20 wt%. The energy requirement

Table 8-1. Results of power and energy calculations for dewatering of simulated one-square-mile clay settling area. Solids weight percent was increased from 10 to 25 wt%.

Configuration	Horizontal Simulation	Vertical Simulation	Bench-top Experiment
Average Electric Field / $\mathrm{Vcm^{-1}}$	1.2	1.2	1.1
Time Required / days	0.8	1.3	1.0
Power Required / kW	4.4E+7	3.5E+7	1.2E+7
Energy / kWh	8.5E+8	1.1E+9	2.8E+8
Energy Requirement / $\mathrm{Whkg^{-1}}$	43.6	53.7	13.9

Table 8-2. Results of power and energy calculations for dewatering of simulated one-square-mile clay settling area. Solids weight percent was increased from 10 to 20 wt%.

Configuration	Horizontal Simulation	Vertical Simulation	Bench-top Experiment
Average Electric Field / $\mathrm{Vcm^{-1}}$	0.1	0.1	0.08
Time Required / days	8.8	12.9	9.6
Power Required / kW	3.5E+5	2.8E+5	1.0E+5
Energy / kWh	7.4E+7	8.8E+7	2.4E+5
Energy Requirement / $\mathrm{Whkg^{-1}}$	4.4	5.2	1.5

results (in W-h/kg water removed) presented in Tables 8-1 and 8-2 are included along with additional bench-top experimental energy requirements in Figure 8-6. All data lie between the two different energy requirements reported in the literature. From the raw data reported by Fourie *et al.*,[4] an energy requirement of 1.25 W-h/kg of water removed was calculated; whereas, Larue *et al.*[16] reported an energy requirement of 700 W-h/kg of water removed.

8.2.2 Economic Implications

Power and energy requirements were calculated for electrokinetic dewatering of a one-square-mile clay settling area in Section 8.2.1. The values were achieved through use of the mathematical model, CP_3D, in combination with the constitutive relationships developed to characterize the experimental work. The power and energy requirements for achieving a solids content up to 25 wt% for a one-square-mile clay settling area were as large as 10^7 kW and 10^9 kW-h, respectively. Such large power and energy requirements suggest that the remediation of an entire large-scale clay settling area may require a modified approach for implementation. A power requirement of 10^7 kW would exceed the capabilities of most power plants, which typically do not generate above 1,000 MW. In order to avoid such large power requirements, the volume could be reduced by treating only a portion of a clay settling area for a given time. Such a modification is presented in Figure 8-7. This modification would involve isolating a portion of the CSA and pumping the slurry from other locations within the CSA into the isolated area

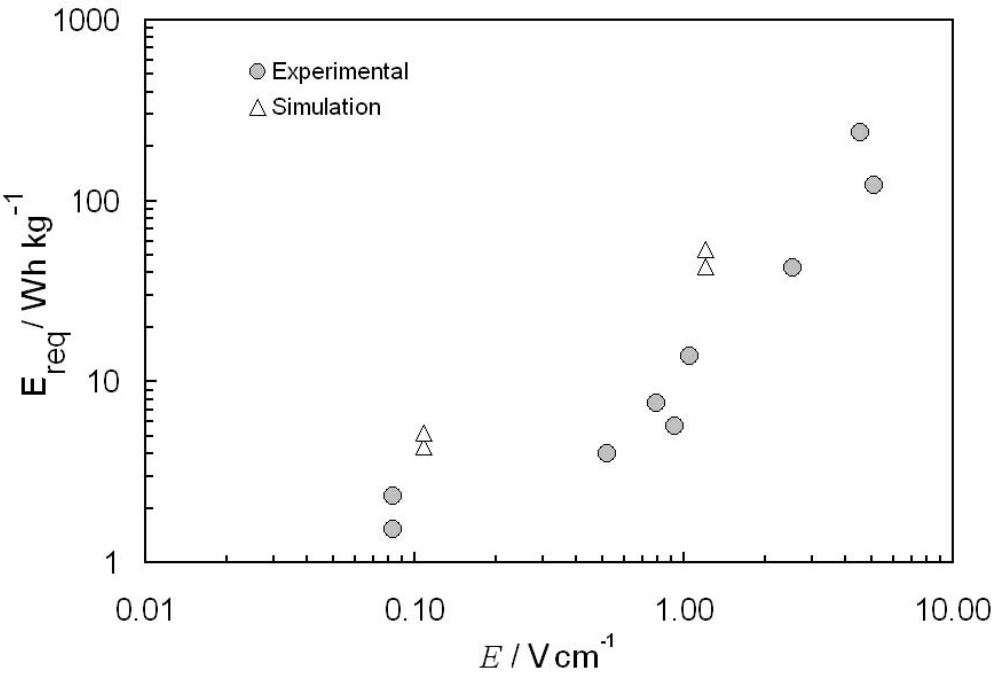

Figure 8-6. Energy requirement for water removal is given as a function of the electric field. Experimental data presented in Figure 7-16 are included with both simulation and additional experimental data.

for electrokinetic treatment. This would allow the gap between electrodes to be smaller and the electric field to be larger with reduced power requirements. Once the area has reached an acceptable solids content, this treatment could be moved to another section of the CSA. The penalty for such a modification would be that the time required to dewater the entire CSA would be increased. However, such a modification would only be made if the benefits of decreased power consumption outweighed costs associated with increased operating time.

Another alternative could be to modify an existing in-line process dewatering unit such as a thickener presented in Figure 8-8. For this type of implementation, the bottom of the thickener could serve as an anode and the rotating vane could serve as a cathode. The applied electric field would enhance the separation of solids typically achieved through the thickener. This type of implementation could be attractive because it would involve modifications to the newly designed thickener operation on-site at Mosaic. The operation would be continuous, with a solids-rich stream leaving from the bottom of the thickener and a decanted stream leaving from the overflow. Other thickener schematics can be found in Geankopolis,[102] McCabe *et al.*,[103] Perry and Chilton,[104] and Kos.[105]

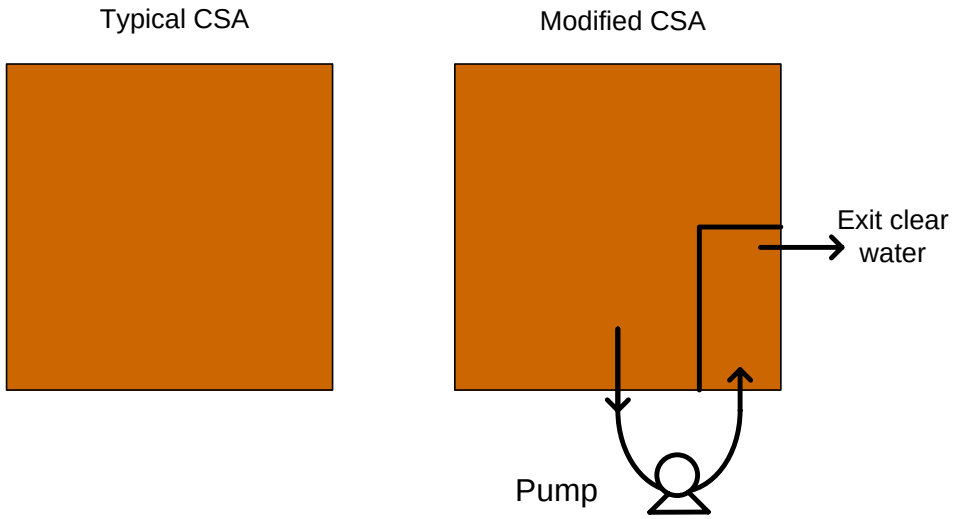

Figure 8-7. A top view of two different one-square-mile clay settling areas. The modified design is pictured on the right demonstrating the treatment of an isolated section of the CSA.

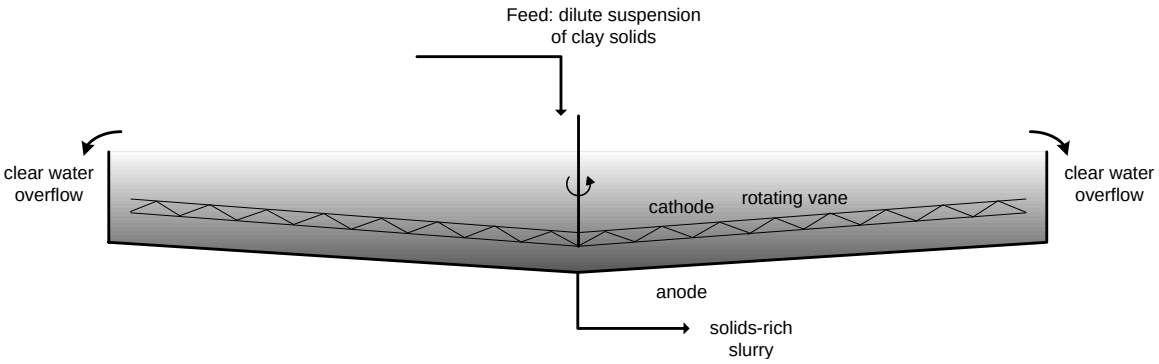

Figure 8-8. Schematic representation of thickener adapted for electrokinetically enhanced separation.

CHAPTER 9
CONCLUSIONS AND FUTURE WORK

This importance of this work originates from the world's growing demand for phosphate. Phosphate is used primarily as fertilizer to enhance the yield from food crops. As a result of phosphate mining, large amounts of dilute waste clays are formed which are stored in man-made enclosed retention ponds known as clay settling areas (CSAs). Over 100 square miles of the CSAs exist in Central Florida causing a major land storage issue. Due to the properties of the clays, it can take as much as 25 years for the CSAs to settle and dry to appropriate levels. This work involves application of an electric field to increase the rate of water removal to reduce the time required to consolidate the occupied land area. This chapter reviews the conclusions made from the bench-top experiments and simulations performed from this work. This discussion leads to the proposed next steps of this project. A new bench-top cell is proposed for future experiments and applications for scale-up demonstrations are discussed. While much work has been previously reported in the literature on electrokinetic dewatering of clays and other methods for water removal, the literature has not yet included development of parameters aimed towards large-scale design. The objective of this work was to use small-scale electrokinetic experiments to develop parameters that can be used for large-scale design. The development of simulations has been included to aid in large-scale projections in terms of power and energy requirements. This chapter proposes upcoming objectives for this project which build from the results and findings presented in this work.

9.1 Conclusions

A bench-top Plexiglas cell was used for application of an electric field to dewater waste clay slurries which arise due to phosphate mining in Central Florida. The waste clays are stored in large settling ponds in Central Florida which cover 100 square miles of land. These settling ponds, also known as clay settling areas (CSAs), take as much as 25 years to achieve an acceptable solids content of 40 wt%. A proof-of-concept bench-top experiment was performed at a cell potential of 80 V. After just 9 hours, the solids content approached 35 wt%. Therefore, from the bench-top cell, what typically takes 25 years through natural processes, was instead demonstrated to take only 9 hours from application of an electric field. This experiment demonstrated

conclusively that substantial water removal from phosphatic clays is achievable in the presence of an electric field.

A matrix of experiments were performed for different operating times and electric fields. Trends were demonstrated as the change in solids weight percent increased with increasing cell potential and operation time. The experimental results were used to develop constitutive relationships for both short and long operating times to predict the solids content of the clays for a given operating time. A maximum solids content was reached at long operation times. This maximum was a strong function of the electric field. For example, an electric field of 3 V/cm would give a maximum solids content of 30 wt% while an electric field of 0.1 V/cm would allow only 20 wt% to be reached. Therefore, a larger electric field is needed to reach an acceptable solids content.

Simulations were performed to calculate power and energy requirements for water removal of large-scale CSAs. The calculations included the use of the constitutive equations developed from the experimental work. The power and energy requirements were found to be extremely large. For example, to achieve a solids content of 25 wt% the power required was on the order of 10^7 kW and the energy required was on the order of 10^9 kW-h. This result suggests that alternative designs should be considered which scale down the amount of volume treated at a given time. This would reduce the number of electrodes needed and the power required to drive the separation of the water from the clays. The distance between electrodes would be smaller allowing a larger electric field and corresponding larger maximum solids content to be achieved.

Energy requirements from the bench-top experiments were calculated in terms of kW-h per kg of water removed. The results indicated that energy requirements were smallest at smaller electric fields. Experimental energy requirements were modeled separately on the basis of fundamental electrochemical relationships and equation (7–4). This comparison showed favorable agreement and verified the use of the constitutive relationship for long times (given as equation (7–4)) to characterize the experimental data.

9.2 Future Work

The results of the present work are used to propose additional steps for the continuation of this project. Collaborations with engineers from the project sponsor, Mosaic Fertilizer LLC, are proposed to involve discussions to develop designs for electrokinetic dewatering implementation.

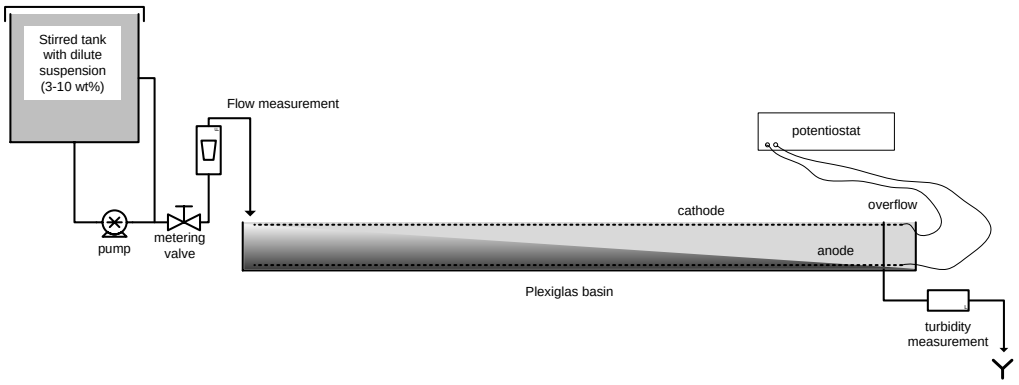

Figure 9-1. Schematic representation of bench-scale settling basin adapted for electrokinetically enhanced separation.

Discussions are proposed to include assessment of whether dewatering should take place within clay settling areas or as part of an in-line process dewatering unit.

Based upon the economic assessment presented in Section 8.2.2, further modeling and experimental verification is proposed for modified dewatering designs for clay settling areas as well as different in-line process dewatering units. The thickener, presented in Figure 8-8 would be best suited for model verification to explore its ability to for electrokinetically enhanced dewatering in combination with its existing features. Experimental verification of such a design would be proposed after the development of such a model.

Other work proposed involves a semi-batch operation as presented in Figure 9-1. This design would involve a continuous inlet feed stream of a dilute suspension of phosphatic clays with a continuous outlet stream of clear supernatant water. The inlet feed stream would originate directly from the phosphate beneficiation plant while the continuous outlet stream of clear supernatant water may be used for recycle back to the beneficiation plant. The solids removed from the incoming suspension would be accumulated within the basin. This type of design could be retrofitted to an existing clay settling area for remediation or it could be used as an in-line process operation. It may also be effective for treatment of an isolated section of a CSA as presented in Figure 8-7. Such a design could be studied through simulations, but would first involve the operation of a bench-top experiment. The results of the bench-top experiments would give insight to which type of implementation such a design would be best. The operation of the bench-top cell is proposed to explore the relationships among residence time, applied electric

field, and solids content of the effluent steam. Turbidity measurements will be implemented to allow real-time monitoring of effluent solids content. Upon completion of the bench-top experiments, it is proposed that a scale-up demonstration be built and operated on-site at Mosaic which would test the scalability of the electrokinetic design relationships established from this work.

REFERENCES

[1] D. Bloomquist, Centrifuge modeling of large strain consolidation phenomena in phosphatic clay retention ponds, Ph.D. thesis, University of Florida (1982).

[2] S. J. V. Kauwenbergh, J. B. Cathcart, G. H. McClellan, Mineralogy and alteration of the phosphate deposits of Florida, U.S. Geological Survey Bulletin 1914 (1990) 1–26.

[3] R. F. Craig, Soil Mechanics, 6th Edition, E & FN Spon, An Imprint of Chapman & Hall, London, UK, 1974.

[4] A. B. Fourie, D. G. Johns, C. J. F. P. Jones, Dewatering of mine tailings using electrokinetic geosynthetics, Can. Geotech. J. 44 (2007) 160–172.

[5] J. S. Newman, K. E. Thomas-Alyea, Electrochemical Systems, 3rd Edition, John Wiley & Sons, Hoboken, New Jersey, 2004.

[6] J. Morgan, Cathodic Protection, 2nd Edition, NACE International, Houston, TX, 1993.

[7] S. Speil, M. R. Thompson, Electrophoretic dewatering of clay, Trans. Electrochem. Soc. 81 (1942) 119–145.

[8] M. H. Stanczyk, I. L. Feld, Electro-dewatering tests of Florida phosphate rock slimes, Bu. Mines RI 6451.

[9] O. Terichow, A. May, Electrophoresis and coagulation studies of some Florida phosphate slimes, Bu. Mines RI 7816.

[10] H. J. Kelly, H. M. Harris, Electrical dewatering of dilute clay slurries, Bu. Mines RI 6479.

[11] S. Glendinning, C. J. F. P. Jones, R. C. Pugh, Reinforced soil using cohesive fill and electrokinetic geosynthetics, Int. J. Geomech. 5 (2005) 138–146.

[12] A. Fourie, Harnessing the power: opportunities for electrokinetic dewatering of mine tailings, Geotechnical News (June 2006).

[13] L. Yang, G. Nakhla, A. Bassi, Electro-kinetic dewatering of oily sludges, J. Hazard. Mater. B125 (2005) 130–140.

[14] J. Q. Shang, Electrokinetic dewatering of clay slurries as engineered soil covers, Can. Geotech. J. 34 (1997) 78–86.

[15] B. Paczkowska, Electroosmotic introduction of methacrylate polycations to dehydrate clayey soil, Can. Geotech. J. 42 (2005) 780–786.

[16] O. Larue, R. Wakeman, E. Tarleton, E. Vorobiev, Pressure electroosmotic dewatering with continuous removal of electrolysis products, Chem. Eng. Sci. 61 (2006) 4732–4740.

[17] J. Q. Shang, K. Y. Lo, Electrokinetic dewatering of a phosphate clay, J. Hazard. Mater. 55 (1997) 117–133.

[18] L. G. Bromwell, Physico-chemical properties of Florida phosphatic clays, Tech. rep., Florida Institue of Phosphate Research (1982).

[19] C. Barnett, Mine field, Florida Trend: The Magazine of Florida Business (May 2008).

[20] G. N. Anastassakis, Phosphates processing (chapter 2.4), TAILSAFE: Tailings Management Facilities - A State of the Art Report, editors: T. Meggyes, K. E. Roehl and D. Dixon-Hardy (2005).

[21] P. M. Tyler, W. H. Waggaman, Phosphatic slime a potential mineral asset, Industr. Eng. Chem. 46 (1954) 1049–1056.

[22] H. W. Long, D. P. Orne, Regional study of land use, planning, and reclamation, Tech. rep., Florida Institute of Phosphate Research (1990).

[23] B. M. Moudgil, Enhanced recovery of coarse particles during phosphate flotation, Tech. rep., Florida Institute of Phosphate Research (1992).

[24] S. R. Weaver, Evaluation of the use of geotextiles for capping phosphatic waste clay ponds, Master's thesis, University of Florida (1985).

[25] W. E. Pittman, J. W. Sweeney, State-of-the-art of phosphatic clay dewatering technology and disposal techniques (in two parts): 1. A review of phosphatic clay dewatering research, Tech. rep., Florida Institute of Phosphate Research (1983).

[26] H. El-Shall, P. Zhang, Process for dewatering and utilization of mining wastes, Miner. Eng. 17 (2004) 269–277.

[27] W. R. Reigner, C. Winkler, Reclaimed phosphate clay settling area investigation: Hydrologic model claibration and ultimate clay elevation prediction, Tech. rep., Florida Institute of Phosphate Research (2001).

[28] P. Zhang, Recovery of phosphate from Florida phosphatic clays, Tech. rep., Florida Institute of Phosphate Research (2001).

[29] P. Zhang, M. Bogan, Recovery of phosphate from Florida beneficiation slimes I. Reidentifying the problem, Miner. Eng. 8 (1995) 523–534.

[30] S. A. McClimans, Centrifugal model evaluation of the consolidation behavior of sand/phosphatic clay mixes, Master's thesis, University of Florida (1984).

[31] H. E. El-Shall, Development and evaluation of a rapid clay-dewatering process as a reclamation technique, Tech. rep., Florida Institute of Phosphate Research (1996).

[32] B. Scheiner, A. G. Smelley, D. Brooks, Large-scale dewatering of phosphatic clay waste from Central Florida, Bu. Mines 8611 (1981) 1–11.

[33] D. Znidarcic, A. N. Abu-Hejleh, T. Fairbanks, A. Robertson, Consolidation characteristics determination for phosphatic clays, Volume 1: Seepage induced consolidation test equipment description and users manual, Tech. rep., Florida Institute of Phosphate Research (1994).

[34] W. D. Carrier, Waste clay disposal in mine cuts, Tech. rep., Florida Institute of Phosphate Research (1982).

[35] K. Fa, V. K. Paruchuri, S. C. Brown, B. M. Moudgilc, J. D. Millera, The significance of electrokinetic characterization for interpreting interfacial phenomena at planar, macroscopic interfaces, Phys. Chem. Chem. Phys. 7 (2005) 678–684.

[36] A. Aysen, Soil Mechanics, A. A. Balkema Publishers, Lisse, The Netherlands, 2002.

[37] P. L. Berry, D. Reid, Introduction to Soil Mechanics, McGraw-Hill Book Company, London, UK, 1987.

[38] V. Mets, K. Amram, J. Ganor, Stoichiometry of smectite dissolution reaction, Geochim. Cosm. A. 69 (2005) 1755–1772.

[39] R. E. Grim, Clay Mineralogy, McGraw-Hill Book Company, 1968.

[40] A. McFarlane, K. Bremmell, J. Addai-Mensah, Improved dewatering behavior of clay minerals dispersions via interfacial chemistry and particle interactions optimization, J. Colloid Interf. Sci. 293 (2006) 116–127.

[41] K. Ma, A. C. Pierre, Clay sediment-structure formation in aqueous kaolinite suspensions, Clays Clay Miner. 47 (1999) 522–526.

[42] K. Ma, A. C. Pierre, Effect of interaction between clay particles and Fe3+ ions on colloidal properties of kaolinite suspensions, Clays Clay Miner. 45 (1997) 733–744.

[43] K. Ma, A. C. Pierre, Sedmentation behavior of a fine kaolinite in the presence of fresh Fe electrolyte, Clays Clay Miner. 40 (1992) 586–592.

[44] A. K. Helmy, S. G. de Bussetti, E. A. Ferreiro, The surface energy of palygorskite, Powder Technol. 171 (2007) 126–131.

[45] G. Prentice, Electrochemical Engineering Principles, Prentice Hall, Englewood Cliffs, NJ, 1991.

[46] D. Pletcher, F. C. Walsch, Industrial Electrochemistry, 2nd Edition, Chapman and Hall, 1990.

[47] D. Jones, Principles and Prevention of Corrosion, 2nd Edition, Prentice-Hall, Upper Saddle River, NJ, 1996.

[48] M. E. Orazem, B. Tribollet, Electrochemical Impedance Spectroscopy, John Wiley & Sons, Hoboken, NJ, 2008.

[49] A. J. Bard, L. R. Faulkner, Electrochemical Methods: Fundamentals and Applications, Wiley, New York, 1980.

[50] J. O. M. Bockris, A. K. N. Reddy, Modern Electrochemistry: Ionics, 2nd Edition, Vol. 1, Plenum Pub, New York, 1998.

[51] J. O. M. Bockris, A. K. N. Reddy, Modern Electrochemistry: Electrodics, 2nd Edition, Vol. 2, Plenum Pub, New York, 2000.

[52] J. Newman, K. E. Thomas-Alyea, Electrochemical Systems, 3rd Edition, John Wiley & Sons, Inc., Hoboken, NJ, 2004.

[53] A. J. Rutgers, M. D. Smet, Electrochemical Constants, National Bureau of Standards Circular 524, 1953, Ch. 25. Electrokinetic researches in capillary systems and in colloidal solutions, pp. 263–279.

[54] J. S. Newman, Electrochemical Systems, 2nd Edition, Prentice Hall, Englewood Cliffs, NJ, 1991.

[55] A. Klinkenberg, J. L. van der Minne, Electrostatics in the Petroleum Industry, Elsevier, Amsterdam, 1958.

[56] H. V. Olphen, An Introduction to Clay Colloid Chemistry, 2nd Edition, John Wiley & Sons, 1963.

[57] J. G. Sunderland, Electrokinetic dewatering and thickening. 1. Introduction and historical review of electrokinetic applications, J. App. Electrochem. 17 (1987) 889–898.

[58] P. C. Hiemenz, R. Rajagopalan, Principles of Colloid and Surface Chemistry, 3rd Edition, Marcel Dekker, Inc., New York, New York, 1997.

[59] D. H. Gray, J. K. Mitchell, Fundamental aspects of electro-osmosis in soils, J. Soil Mech. Found. Div., ASCE 93(6) (1967) 178–205.

[60] H. R. Kruyt, Colloid Science, Elsevier Publishing Company, New York, New York, 1952.

[61] K. R. Reddy, A. Urbanek, A. P. Khodadoust, Electroosmotic dewatering of dredged sediments: bench-scale investigation, J. Environ. Man. 78 (2006) 200–208.

[62] D. G. Buckland, J. Q. Shang, E. Mohamedelhassan, Electrokinetic sedimentation of contaminated Welland River sediment, Can. Geotech. J. 37 (2000) 735747.

[63] M. H. M. Raats, A. J. G. van Diemen, J. Lavèn, H. N. Stein, Full scale electrokinetic dewatering of waste sludge, Colloids Surf. A: Physicochem. Eng. Aspects 210 (2002) 231–241.

[64] H. Saveyn, G. Pauwels, R. Timmerman, P. V. der Meeren, Effect of polyelectrolyte conditioning on the enhanced dewatering of activated sludge by application of an electric field during the expression phase, Water Res. 39 (2005) 3012–3020.

[65] K. Lo, Electro-kinetic dewatering of Florida phosphate clays, Tech. rep., Florida Institute of Phosphate Research (1995).

[66] M. Y. Ho, G. Chen, Enhanced electro-osmotic dewatering of fine particle suspension using a rotating anode, Industr. Eng. Chem. Res. 40 (2001) 1859–1863.

[67] W. Jin, Z. Liu, F. Ding, Broth dewatering in a horizontal electric field, Separ. Sci. Technol. 38 (2003) 767–778.

[68] G. Maini, A. K. Sharman, C. J. Knowles, G. Sunderland, S. A. Jackman, Electrokinetic remediation of metals and organics from historically contaminated soil, J. Chem. Technol. Biotechnol. 75 (2000) 657–664.

[69] J. E. McLean, ECOPAC field test in Florida phosphate slime pond, Tech. rep., Monsanto Enviro-Chem (1986).

[70] M. K. A.-E. Rahman, Dewatering of phosphatic clay waste by flocculation, Chem. Eng. Technol. 23 (2000) 457–461.

[71] S. Mathur, P. Singh, B. Moudgil, Advances in selective flocculation technology for solid-solid separations, Int. J. Miner. Proc. 58 (2000) 201–222.

[72] A. G. Smelley, I. Feld, Flocculation dewatering of Florida phosphatic clay wastes, Bu. Mines 8349 (1979) 1–26.

[73] W. D. Carrier, Rapid clay dewatering phase II: Field-scale tests, Tech. rep., Florida Institute of Phosphate Research (2001).

[74] M. P. Hughes, AC electrokinetics: Applications for nanotechnology, Nanotechnol. 11 (2000) 124–132.

[75] J. Q. Shang, W. A. Dunlap, Improvement of soft clays by high-voltage electrokinetics, Journal of Geotechnical Engineering 122(4) (1996) 274–280.

[76] H. A. Pohl, Dielectrophoresis, Cambrige University Press, Cambridge, UK, 1978.

[77] M. Washizu, O. Kiurosawa, Electrostatic manipulation of DNA in microfabricated structures, IEEE Trans. Ind. Appl. 26(6).

[78] M. Bjelopavlic, P. K. Singh, H. El-Shall, B. M. Moudgil, Role of surface molecular architecture and energetics of hydrogen bonding sites in adsorption of polymers and surfactants, J. Colloid Interf. Sci. 226 (2000) 159–165.

[79] D. Cabrera-Guzman, The use of electrokinetics for hazardous waste site remediation, J. Air Waste Manag. Assoc. 40 (1990) 1670–1676.

[80] S. Dixit, R. Gombeer, J. D'hoore, The electrophoretic mobility of natural clays and their potential mobility within the pedon, Geoderma 13 (1975) 325–330.

[81] S. Gopalakrishnan, A. Mujumdar, M. Weber, Optimal off-time in interrupted electroosmotic dewatering, Separ. Technol. 6 (1996) 197–200.

[82] A. Neaman, A. Singer, The effects of palygorskite on chemical and physico-chemical properties of soils: A review, Geoderma 123 (2004) 297–303.

[83] B. D. Cullity, Elements of X-ray Diffraction, 3rd Edition, Prentice Hall, Upper Saddle River, New Jersey, 2001.

[84] J. P. McKinney, M. E. Orazem, Electrokinetic methods for dewatering of phosphatic clay slurries, ECS Trans. 19:26 (2009) 35–43.

[85] J. Q. Shang, K. Y. Lo, I. Inculet, Polarization and conduction of clay-water-electrolyte systems, J. Geotech. Eng. 121 (1995) 243–248.

[86] D. P. Riemer, M. E. Orazem, Modeling coating flaws with non-linear polarization curves for long pipelines, in: R. A. Adey (Ed.), Corrosion and Boundary Element Methods, Vol. 12 of Advances in Boundary Elements, WIT Press, Southampton, UK, 2005, pp. 225–259.

[87] D. P. Riemer, Modeling cathodic protection for pipeline networks, Ph.D. thesis, University of Florida (2000).

[88] J. P. McKinney, Evaluation of above-ground potential measurements for assessing pipeline integrity, Master's thesis, University of Florida (2006).

[89] M. E. Orazem, J. M. Esteban, K. J. Kennelley, R. M. Degerstedt, Mathematical models for cathodic protection of an underground pipeline with coating holidays: Part 1 - theoretical development, Corros. 53(4) (1997) 264–272.

[90] J. Morgan, Cathodic Protection, 2nd Edition, NACE International, Houston, TX, 1993.

[91] J. Wagner, Cathodic Protection Design I, NACE International, Houston, TX, 1994.

[92] A. W. Peabody, Control of Pipeline Corrosion, NACE International, Houston, TX, 1978.

[93] J. F. Yan, S. N. R. Pakalapati, T. V. Nguyen, R. E. White, R. B. Griffin, Mathematical modeling of cathodic protection using the boundary element method with a nonlinear polarization curve, J. Electrochem. Soc. 139(7) (1992) 1932–1936.

[94] K. J. Kennelley, L. Bone, M. E. Orazem, Current and potential distribution on a coated pipeline with holidays part i - model and experimental verification, Corros. 49(3) (1999) 199–210.

[95] C. Corfias, N. Pebere, C. Lacabanne, Characterization of a thin protective coating on galvanized steel by electrochemical impedance spectroscopy and a thermostimulated current method, Corros. Sci. 41(8) (1999) 1539–1555.

[96] I. Thompson, D. Campbell, Interpreting Nyquist responses from defective coatings on steel substrates, Corros. Sci. 36(1) (1994) 187–198.

[97] D. Diakow, G. V. Boven, M. Wilmott, Polarization under disbonded coatings: Conventional and pulsed cathodic protection compared, Mater. Perf. 37 (1998) 17–23.

[98] T. R. Jack, External corrosion of line pipe - a summary of research activities, Mater. Perf. 35 (1996) 18–24.

[99] J. A. Beavers, N. G. Thompson, Corrosion beneath disbonded pipeline, Mater. Perf. 36 (1997) 13–19.

[100] D. Riemer, M. Orazem, Development of mathematical models of cathodic protection of multiple pipelines in a right of way, in: Proceedings of the 1998 International Gas Research Conference, GRI, Chicago, 1998, p. 117, paper TSO-19.

[101] D. P. Riemer, M. E. Orazem, Cathodic protection of multiple pipelines with coating holidays, in: M. E. Orazem (Ed.), Procedings of the NACE99 Topical Research Symposium: Cathodic Protection: Modeling and Experiment, NACE International, Houston, TX, 1999, pp. 65–81.

[102] C. J. Geankoplis, Transport Processes and Unit Operations, 3rd Edition, Prentice Hall, Englewood Cliffs, New Jersey, 1993.

[103] W. L. McCabe, J. C. Smith, P. Harriot, Unit Operations of Chemical Engineering, 5th Edition, McGraw-Hill, Inc., 1993.

[104] R. H. Perry, C. H. Chilton, Chemical Engineer's Handbook, 5th Edition, McGraw-Hill Book Company, 1973.

[105] P. Kos, Gravity thickening of sludges, Ph.D. thesis, University of Massachusetts (1978).

BIOGRAPHICAL SKETCH

Patrick graduated from the University of South Carolina with a Bachelor of Science degree in chemical engineering in May of 2004. While at the University of South Carolina, Patrick developed an interest in electrochemistry by working on an undergraduate research project involving the characterization of a direct methanol fuel cell and by taking an undergraduate course in corrosion engineering. He entered graduate school in August of 2004 at the University of Florida and joined Professor Mark Orazem's research group which specializes in electrochemical engineering. In May of 2006, Patrick completed a Master of Science degree. Patrick's master's thesis involved simulations for cathodic protection of buried pipelines to improve prioritization of survey indications that locate corrosion causing coating defects. In the summer of 2006, Patrick was the NACE/CC Technologies Summer Internship Recipient. From this award, Patrick was sponsored by NACE (National Association of Corrosion Engineers) to intern at DNV Columbus (formerly CC Technologies). This internship allowed Patrick to participate in pipeline surveys which he had previously simulated in his master's research. In the fall of 2006, Patrick returned to the University of Florida where he began his doctoral research. Patrick has recently received and accepted a job offer from Intel, located in Hillsboro, Oregon. His employment at Intel will begin in July of 2010.